Advancing Acoustic Studies of Pelagic Fish and Zooplankton at the western Atlantic-Arctic Gateway

by

© Julian Andrzej Chawarski

A Thesis submitted to the school of Graduate Studies in partial fulfillment of the requirements for the degree of Doctor of Philosophy, Fisheries Science

Centre for Fisheries Ecosystem Research

Fisheries & Marine Institute at

Memorial University of Newfoundland and Labrador

St. John's, Newfoundland, Canada

May 2024

Abstract

The patterns of distribution among fish and zooplankton in the Arctic and their deep ocean habitats remain poorly described. Climatic disruptions to natural variability in temperature, light, and nutrient supply can modify species distributions, impacting the ecosystem at various levels. Across spatial and vertical domains, these environmental factors form complex relationships with species assemblages, which are challenging to measure with conventional sampling methods. Hydroacoustics is a promising approach to studying the distribution of organisms in hard-to-reach ecosystems. This thesis aims to advance new hydroacoustic methodologies for the study of pelagic fish and zooplankton and identify the structural drivers of their communities and distribution along the boundaries of Arctic-Atlantic modulated ecosystems. In my thesis, I used several emerging technologies, including lowered acoustic probes and broadband acoustic measurements, to assess the distributional patterns of pelagic fish and zooplankton at meter-level to ocean basin scales. I found that measurements of lanternfish inhabiting deep-scattering layers require detailed analysis that includes the identification and removal of anomalous signals, which can arise from a combination of physical and biological processes. To deal with this, I introduced a machine learning approach that helps identify anomalous signals and improves the precision of acoustic density measurements. When examining similar lanternfish dominated communities at the basin scale, I report that temperature-driven water mass boundaries act as a barrier to the dispersal of mesopelagic communities at high-latitudes, in both the northern and southern hemispheres. Furthermore, this same boundary appears to impact the vertical distribution of pelagic life, with likely impacts the vertical transport of nutrients and carbon. In the high Arctic, I report mixing processes in glacial fjord ecosystems can impact the vertical distribution of copepods and the morphological patterns of marine snow. This work highlights contrasting

conditions outside of two adjacent marine terminating glaciers, which each offer a glimpse of what future Arctic conditions may bring. Overall, my work contributes to a greater understanding of the structural drivers of Arctic pelagic communities and can be used to understand their sensitivities to future change.

Acknowledgments

I would like to thank my co-supervisor Dr. Maxime Geoffroy for affording me the opportunity to ask challenging questions in some of the most far flung reaches of the Arctic and for his support along the journey. Dr. Geoffroy has built an incredible research program in the Canadian Arctic and offered me generous access to his broad research network.

I would also like to thank Dr. David Coté for his steady guidance both in the field and during the writing of this thesis. His kind and generous disposition was helpful in getting through some of the most challenging times. I genuinely appreciate the additional responsibility he took on after Dr Louis Fortier's passing.

I am indebted to the late Dr. Louis Fortier, my co-supervisor and visionary behind the Amundsen Science program. His contributions to the fields of biological oceanography and Arctic science will never be forgotten.

I am also grateful for the impactful collaborations with the late Dr. Thor Klevjer. Thor was a supportive and encouraging collaborator who helped with several key aspects of this thesis, including the publication of my second research chapter. My deepest condolences go out to his family which lost him at far too young an age.

Many thanks to Toby Jarvis and the staff at Echoview software for getting me up to speed on broadband signal processing and troubleshooting analytical problems, Thibaud Dezutter for being one of the most fun and organized people I've ever worked with in the field, Adam Templeton for sharing your slice of Newfoundland with me, and Wendy Rose for keeping me grounded through some tough years.

I would also like to thank the captains, crew, and scientific support staff of the CCGS *Amundsen* and the Swedish icebreaker *Oden*. Without their skills, vision, and hard work none of this work would have taken place. Many thanks to the people of Qikiqtarjuaq, who welcomed me into their hometown on the sea-ice of Baffin Island. Their experience and knowledge of the land will stay with me forever.

To my parents, I thank you for supporting my curiosity and academic journey over the years. It's been a wandering, exhilarating, and at times lonesome, journey to the North Pole, but I would never have stepped foot in this realm without the sacrifices you've made for Szymon and I.

To Jasmin, your warmth, compassion, and support have made this journey all the more worth it. Thank you for guiding me toward new adventures and sitting shotgun during long journeys into wilderness. I'm proud of how far we've both grown, as individuals and as partners.

I acknowledge that the waters and lands where this PhD research was conducted are the ancestral and unceded territories of the of the Mi'kmaq and Beothuk (island of Newfoundland), the Inuit of Nunavut and Greenland, and of the Huu-ay-aht First Nation (Barkley Sound, British Columbia). I am grateful for their past and present stewardship of the life around us, and for the opportunity to learn and grow on their lands and waters.

Table of Contents

List of Tables

List of Figures

List of Common Abbreviations

ADCP	Acoustic Doppler Current Profiler
ANOSIM	Analysis of Similarity
APF	Antarctic Polar Front
AZOMP	Atlantic Zone Offshore Monitoring Program
CTD	Conductivity, Temperature, and Depth
CW	Continuous wave (in reference to narrowband acoustics)
dB	Decibel
DFO	Department of Fisheries & Oceans Canada
DSL	Deep Scattering Layer
DVM	Diel Vertical Migration
FFT	Fast Fourier Transform
FM	Frequency-modulated (in reference to broadband acoustics)
GIS	Greenland Ice Sheet
HDBSCAN	Hierarchical Density-Based Spatial Clustering of Applications with Noise
IKMT	Isaac Kidd Midwater Trawl
ISECOLD	Integrated Studies and Ecosystem Characterization of the Labrador Sea Deep Ocean
kHz	Kilohertz
KC-HB	Kennedy Channel – Hall Basin
LS	Lincoln Sea
nMDS	Non-Metric Multidimensional Scaling
PCA	Principal Component Analysis
PDF	Probability Distribution Function
PF	Petermann Fjord
SOF	Sherard Osborn Fjord
S_v	(Mean) Volume backscattering strength

s_v	volume backscattering coefficient
TS	Target Strength
UVP	Underwater Vision Profiler
WBAT	Wideband Autonomous Transceiver
$\bar{\sigma}_{bs}$	mean backscattering-cross section

Co-authorship Statement

The research displayed in this thesis was designed, conceptualized, and conducted by Julek Chawarski with guidance and support from Dr. Maxime Geoffroy and committee members Drs. David Coté and Louis Fortier. Following Dr. Fortier's passing, Dr. Tyler Eddy joined the committee and offered additional guidance in the final year of study. Julek Chawarski was responsible for field and laboratory data collection and analysis, with assistance from Drs. Maxime Geoffroy and David Coté. All chapters were written by Julek Chawarski, with intellectual and editorial input from Drs. Maxime Geoffroy, David Coté, and Tyler Eddy. An earlier version of Chapter 2 was submitted to ICES Journal of Marine Science and is pending re-submission. Chapter 3 has been published in Frontiers in Marine Science (see complete references below). Future publications in the primary literature based on work presented in this thesis will be co-authored by Julek Chawarski, Drs. Maxime Geoffroy and David Coté (Chapter 4), as well as members of the scientific team during the Ryder 2019 expedition.

Chawarski, J., Klevjer, T. A., Coté, D., & Geoffroy, M. (2022). Evidence of temperature control on mesopelagic fish and zooplankton communities at high latitudes. Frontiers in Marine Science, 9. https://doi.org/10.3389/fmars.2022.91798

Chapter 1.   Introduction

Understanding the interaction between organisms and their physical environment remains crucial for predicting how ecosystems will respond to climate change. Among some of the least studied marine ecosystems, the Arctic and deep ocean are already facing irreversible climate impacts (Polyakov et al., 2017, 2020; Brito-Morales et al., 2020; Rantanen et al., 2022). Disruptions to natural variability in temperature, light, and nutrient supply can modify critical global ecosystem services such as carbon cycling and biomass production (Boscolo-Galazzo et al., 2021; Ljungström et al., 2021; Ariza et al., 2022). The fundamental aspects of interactions between species and their ocean environments occur across two spatial domains: horizontal and vertical. The horizontal domain includes aspects of species distributions across latitudes and biogeography, with climate warming causing range shifts in lower latitude species towards more polar latitudes, which can lead to displacement or competition with endemic species (Perry et al., 2005; Kortsch et al., 2015; Dee et al., 2020). Along the vertical (depth) domain, physical gradients in temperature, light, and nutrients create distinct habitats at varying scales, such as static depth zones (e.g., epi and meso-pelagic) and narrow dynamic ranges like shifting particle and light fields that create transient vertical habitats for species as they move through water column (Lehodey et al., 2010; Aksnes et al., 2017; Gloeckler et al., 2018).

Together, these horizontal and vertical domains are of particular importance to pelagic, or open ocean, species like mesozooplankton and micronekton of size ranges from 0.2 mm to 20 cm (Vinogradov, 1962, 1997; Sutton et al., 2013; Netburn and Koslow, 2018; Romero-Romero et al., 2019). Pelagic species within these size ranges are characterized by their close connection to ocean

primary production, water mass properties, and their susceptibility to predation, making them a critical component of the ocean's biological pump (Hudson et al., 2014; Jones and Checkley, 2019; Koslow et al., 2019).

Oceanographic measurements can facilitate a better understanding of the physical characteristics of fish and zooplankton habitat in the ocean, yet the detection and measurement of organisms themselves remains challenging. Advances in remote sensing and autonomous data collection have significantly improved our understanding of these marine environments and the pressures they face with ongoing climate change. Through studies applying hydroacoustic technology, we have gained a greater understanding of the species that exist out of reach, such as those within the deep sound-scattering layers of the ocean (Irigoien et al., 2014; Klevjer et al., 2016; Proud et al., 2017). With steady advancements in the applicability of such technology come continuous opportunities to develop and improve existing methods to study pelagic organisms. By leveraging technological innovations such as broadband acoustics (Chu and Stanton, 1998; Ehrenberg and Torkelson, 2000) and autonomous lowered probes (Kloser, 1996; Kloser et al., 2016), this thesis aims to advance new methodologies for the study of pelagic fish and zooplankton and identify the structural drivers of their communities in some of the farthest-reaching Arctic ecosystems. The results of these studies can then be applied to broader ecosystem models and used to forecast the potential impacts of climate change, harvest pressure and sustainable resource management.

1.1 The shared waters of Canada and Greenland

Eastern Canada's and Western Greenland's rugged and glaciated coastlines extend north to the edge of the Central Arctic Ocean, where the Nares Strait links the North Atlantic basin of Baffin Bay with the Lincoln Sea, in the Arctic Ocean. Here, ca. 30-year-old Atlantic water that has circulated around the Arctic basins carries the last of its distinct temperature and salinity signal

from when it first entered the Arctic Ocean through the Fram Strait and the northern Barents Sea (Figure 1.1; Wefing et al., 2021). The last remnant of Atlantic water sheds its heat along Canada's and Greenland's northern coasts, contributing to basal melting of marine terminating glaciers (Straneo et al., 2012; Jakobsson et al., 2020b), thereby initiating a new journey for meltwater. The resultant glacial meltwater and terrestrial runoff form the beginnings of major south-flowing currents that reach as far south as the Gulf of Maine (Straneo and Saucier, 2008; Curry et al., 2014). Along Canada's eastern boundary, the ocean transitions from a cryosphere encased in sea-ice for up to 12 months of the year to the temperate and seasonally productive Northwest Atlantic Ocean (Greene et al., 2008; Pershing and Stamieszkin, 2020). Between Greenland and Labrador, another entry-point for warm Atlantic water occurs. Relatively warm, north-flowing water traveling along Greenland's southern coast encounters the sill-like structure of Davis Strait. The relatively shallow Strait channels most of the Atlantic water counterclockwise around the Labrador Sea. However, along the eastern margin of the Davis Strait, a portion of the coastal water moves along the Greenland coast, carrying the Atlantic water mass signal north into Baffin Bay (Figure 1.1; Curry et al., 2014). Simultaneously, buoyant south-flowing Arctic-origin water crosses the western margin of the Davis Strait, eventually joining water flowing from Hudson Bay to form the Labrador current (Haine et al., 2008; Straneo and Saucier, 2008). As it travels south along the North American continental shelf, the Labrador current supplies cold, oxygen-rich waters to the NW Atlantic ecosystem, which has supported some of the highest densities of the lipid-rich copepods *Calanus finmarchicus* and centuries of rich fishery harvests (Pershing et al., 2015; Pershing and Stamieszkin, 2020; Gonçalves Neto et al., 2021). In a similar fashion, Atlantic water from the Irminger Sea carries heat and nutrients north along the Greenland coast, enriching the

coastal ecosystem and contributing to the basal melting of the Greenland ice sheet (Wood et al., 2023)

When combined with atmospheric warming, climate-driven shifts in ocean circulation will impact these major currents, thereby altering the structure of Canada's Arctic, boreal and temperate marine ecosystems (Greene et al., 2008; Wilson et al., 2016; Peng et al., 2023). Along the latitudinal gradient of Arctic-Atlantic modulated ecosystems, the sensitivities of marine species, communities and populations to rapid warming remain largely unresolved. While some forage fish species are replacing others (Rose, 2005; Vihtakari et al., 2018), gelatinous plankton are taking on a larger role in the ecosystem (Geoffroy et al., 2018; Pettitt-Wade et al., 2020), and some species, such as polar bears, are developing specialized adaptations to sea-ice habitat loss (Laidre et al., 2022). In the absence of long-term observations, it is often along biogeographic (or oceanographic) boundaries where we can learn the most about the biological responses to climate change; such boundaries can indicate range limits of species and the environmental drivers that restrict them (Pinsky et al., 2020). As Atlantic water is the dominant water mass carrying the heat signature of atmospheric warming in the Arctic (Muilwijk et al., 2018), it plays a crucial role in structuring eastern Canada's pelagic ecosystem and its boundaries (Greene et al., 2008).

1.2 Canada's Eastern Subarctic – The Labrador Sea Ecosystem

Directly transected by the Arctic Circle (66° N), the Davis Strait is a geomorphological feature that separates the Labrador Sea from Baffin Bay (Figure 1.1). North of this point, the sun does not rise during days near the winter solstice. The extreme photoperiod above the Arctic Circle, governed by periods of prolonged winter darkness and prolonged summer sunlight, drives distinct adaptations to the daily and seasonal rhythms of feeding, growth, and reproduction of fish and plankton (Kaartvedt, 2008; Kaartvedt and Titelman, 2018). Acting almost as a sill, this relatively

4

shallow Strait also separates the cold bottom waters of Baffin Bay from the warmer Atlantic basin waters of the Labrador Sea and divides the north flowing Atlantic water along Greenland's coast into minor and major branches (Curry et al., 2014).

In the deepest parts of the Labrador Sea, away from the continental shelf, a complex and biodiverse pelagic ecosystem thrives (McKelvie and Haedrich, 1985; Sameoto, 1989; Pepin, 2013). Lanternfishes, of the family Myctophidae, are the dominant vertebrate component of the system and primary consumers of the lipid rich *Calanus* copepods (Sameoto, 1989; Pepin, 2013) Emerging in surface waters only at night to feed, these fish go largely unnoticed by humans. Yet, they are a vastly untapped protein source, despite being a major part of global ocean biomass. (Catul et al., 2011; Irigoien et al., 2014). Many species living in the darkness of the ocean's mesopelagic zone are notoriously difficult to sample for study (Kaartvedt et al., 2012; Proud et al., 2018). It is assumed that the near global distribution of mesopelagic fishes makes them an important component of the global carbon cycle (Davison et al., 2013; Belcher et al., 2019); however, many aspects of their relationship to the environment (e.g., physiological constraints) remain poorly documented (St. John et al., 2016). North of the Labrador Sea, the latitude of the Davis strait coincides with the Arctic circle (66° N), where the light-driven adaptations of globally distributed lanternfish species are theorized to reach their limit (Langbehn et al., 2022). However, as the northern Labrador Sea is constrained from Baffin Bay by basin-scale circulation patterns and winter sea-ice, it remains unclear how the environment in this region impacts the biogeography of lanternfish and other mesopelagic organisms. As interest in harvest potential of mesopelagic resources builds (Prellezo and Maravelias, 2019; Grimaldo et al., 2020), developing baseline estimates of abundance and distribution for sustainable management is crucial. Yet, due to the

many challenges of navigating fierce winter storms and seasonal sea-ice, the Labrador Sea remains a challenging pelagic ecosystem to study.
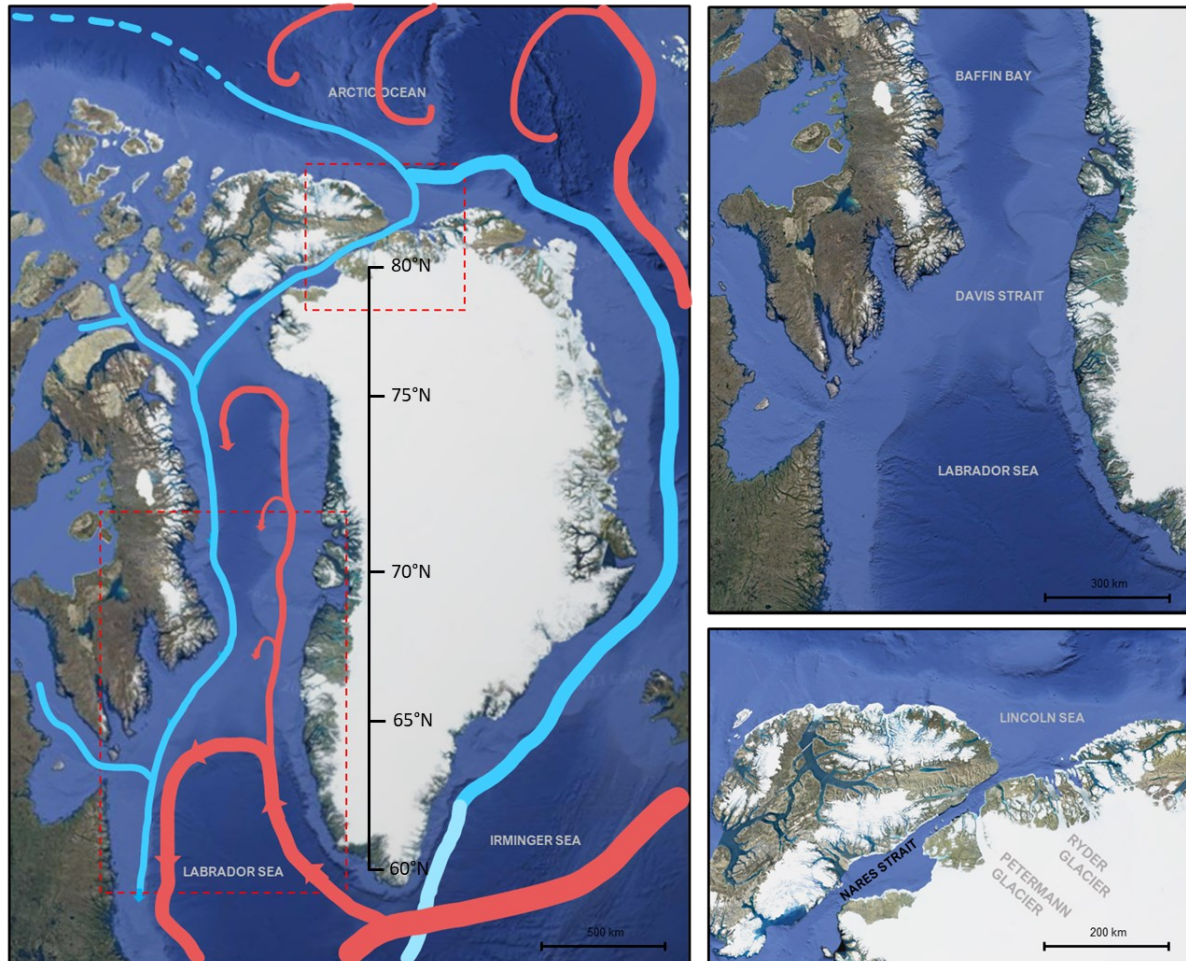
Figure 1.1 Ocean current pathways in the study area for Arctic (blue) and Atlantic (red) origin water (left). Northern Labrador Sea, Canada's southern Arctic-Atlantic gateway (top right), and Nares Strait region, Canada's northern Arctic-Atlantic gateway (bottom right). Image source: Google Earth ©.

1.3 The structure of subarctic mesopelagic ecosystems

Pelagic marine communities along the latitudinal gradient from temperate/sub-Arctic to Arctic waters are structured by both light and temperature (Aksnes et al., 2017; Ljungström et al., 2021). In lower latitudes across the world oceans, the ocean twilight zone supports rich communities of

fish and zooplankton, including lanternfish (family Myctophidae) and bristlemouth (family Gonostomatidae) species that feed on zooplankton and particles from the euphotic zone (Proud et al., 2017). Responding to daily changes in solar irradiance (i.e. day/night cycles), large portions of these communities rise in the water column to feed and rely on the cover of darkness to avoid predation, in a behavioral process known as diel vertical migration, or DVM (Brierley, 2014). In addition to abiotic factors, the structure and function of these communities is driven by complex trophic interactions and competing ontogenetic stages across taxa including arthropods, mollusks, fish, and marine mammals (Lehodey et al., 2010; Choy et al., 2016; Romero-Romero et al., 2019).

Given little is known about the complex biotic interactions of Arctic taxa, and how these interactions may change in the future, a first step towards understanding community responses to climate change is to leverage ecological theory that underpins species relationships with their physical environment. (Kaartvedt, 2008; Langbehn, 2017; Kaartvedt and Titelman, 2018; Ljungström et al., 2021). For instance, the photoperiod constraint hypothesis (Kaartvedt, 2008) poses that the population success of DVM performing lanternfish is limited by extreme photoperiod at high latitudes. However, few field studies have directly investigated their distributional patterns toward Arctic waters. At present, the highest biomass of twilight zone communities occurs at temperate latitudes (Irigoien et al., 2014; Hernández-León et al., 2020). However, because the oceanography of the mesopelagic zone is facing irreversible warming (Brito-Morales et al., 2020), this biomass may shift north, toward Arctic latitudes in the coming century (Ariza et al., 2022; Snoeijs-Leijonmalm et al., 2022).

1.4 Drivers of High Arctic ecosystems

At High-Arctic latitudes, which remain encased in sea ice for up to 12 months of the year, daily light-driven DVM behavior becomes less important (Longhurst et al., 1984; Fortier et al., 2001)

and seasonal impacts of light and temperature drive community assembly (Wassman and Reigstad, 2011). At high latitudes, both light and temperature are inherently connected to the presence of ice: it provides year-round habitat for sympagic ('ice-associated') algae, fish, and crustacean species (Søreide et al., 2006; Taylor et al., 2013; Koch et al., 2023) and acts as an insulator, regulating ocean temperature and downwelling light (Grenfell, 1979). Various freshwater sources, including ice melt, alter the thermohaline structure of the ocean, contributing to density differences of ocean layers in a process known as stratification (Aagaard et al., 1981; Yamamoto-Kawai et al., 2008). By trapping nutrients and algal cells in the euphotic zone, near-surface stratification helps initiate the process of phytoplankton blooms, regulating both the amplitude of production and the rate at which carbon reaches the seafloor (Tremblay et al., 2015; von Appen et al., 2021).

1.5 The Nares Strait Ecosystem

Far north of the Labrador Sea lies the High Arctic ecosystem surrounding the Nares Strait, a narrow waterway separating Canada's Ellesmere Island from the outlet glaciers of the Northern Greenland Icesheet. It is also the connection between productive open waters of the North Water Polynya (Sarvarjuaq) in the North Atlantic's Baffin Bay and the ice-packed Lincoln Sea in the Arctic Ocean. Here, both glacial ice and sea ice play a dominant role in structuring the marine ecosystem; the region is home to some of the largest marine terminating glaciers of the northern Greenland ice sheet (Johnson et al., 2011; Hogan et al., 2020) and the surrounding Lincoln Sea is known for the highest multiyear sea-ice concentration in the Arctic (Laxon et al., 2013). Atmospheric warming is accelerating melting of the Greenland ice sheet from above (Trusel et al., 2018), while the remnants of Atlantic water that has circulated the deep basins of the Central Arctic, sheds the last of its heat content in fjords, contributing to basal melting of glaciers (Straneo et al., 2012; Jakobsson et al., 2020b). The near-glacial marine ecosystems of the Greenland ice sheet face a

range of impacts from glacial meltwater, including increased freshwater, nutrient, and particle loading (Meire et al., 2017; Hopwood et al., 2020; Stuart-Lee et al., 2023). Together, these modifications to the marine ecosystem have unknown consequences to pelagic primary and secondary productivity, leaving uncertainty about future ecosystems.

Both the dominant *Calanus* copepod species *C. glacialis* and *C. hyperboreus* and their predator Arctic cod (*Boreogadus saida*) are adapted to the cold, low salinity meltwater and time their reproduction and feeding to coincide with phytoplankton blooms and seasonal patterns of ice formation and breakup (Daase et al., 2013; Mueter et al., 2016; Bouchard and Fortier, 2020; Søreide et al., 2022). By converting photosynthetically produced fatty acids to stable lipids, *Calanus* copepods of the High Arctic make energy available to higher trophic levels and contribute to the energetic balance of the ecosystem throughout winter months (Falk-Petersen et al., 2009; Søreide et al., 2010). Well-adapted to the extremes of the Arctic, they remain physiologically flexible to shifts in environmental conditions (Trudnowska et al., 2020; Hatlebakk et al., 2022). However, due to their vital role in the ecosystem, their risk of climate-driven displacement by lower latitude species has strong ecological implications for energy transfer through the ecosystem (Kaiser et al., 2022). Following a recent expedition to Ryder Glacier in 2019, we learned that glacial fjord environments of marine-terminating glaciers in the Nares Strait experience different levels of mixing based on their topography (Jakobsson et al., 2020b; Nilsson et al., 2023) and the ice-damming effects of the Lincoln Sea pack ice (Stranne et al., 2021). As these initial findings revealed distinct geomorphological drivers of ecosystem productivity, the conditions among two adjacent fjords presented as a unique mesocosm to study the effects of increasing stratification on particle production and *Calanus* copepods.

1.6 Remote sensing in the cold, deep ocean

In Canada's Arctic and deep ocean systems, where long-term observations are scarce, contemporary studies rely on remote sensing and opportunistic field sampling during interdisciplinary icebreaker expeditions (Doel et al., 2014). These expeditions are costly and leave significant spatio-temporal gaps in sampling, especially outside of summer months (Van Pelt et al., 2017). Remote sensing techniques, like hydroacoustics (Benoit-Bird and Lawson, 2016) are often used to fill these gaps. Hydroacoustics involves studying underwater sound propagation and its interaction with different mediums to measure targets and boundaries (MacLennan and Simmonds, 2004). Backscattering signatures, which relate to the size and properties of marine organisms, provide insights into organism distribution and behavior. For example, small zooplankton like copepods (2-8 mm) with fluid-like scattering properties due to their high lipid content are best detected at high frequencies (300-500 kHz) (Stanton and Chu, 2000). On the other hand, larger fish with gas-filled swim bladders produce geometric scattering signatures (Korneliussen et al., 2018). To study fish abundance and distribution, lower frequencies like 18, 38, and 70 kHz are used in standard acoustic fisheries surveys (Simmonds and MacLennan, 2005). Although species-specific scattering signatures are being developed using broadband acoustics, these simplified relationships between organisms and their scattering help fill knowledge gaps regarding their vertical and horizontal distribution (Benoit-Bird and Lawson, 2016).

Standardized acoustic-trawl surveys typically combine hull-mounted (down facing, mobile surveys) echosounders with biological sampling using trawl nets to obtain species identifications and abundance estimates (Simmonds and MacLennan, 2005). Recently, there has been increased interest in exploring a range of acoustic deployment types which can look at different aspects of organismal distribution at varying scales (Benoit-Bird and Lawson, 2016). For example, the recent

attention to the deep-scattering layer (DSL) as a hotspot for biodiversity and biomass, has led to novel acoustic approaches using lowered acoustic probes (Kloser et al., 2016; Bassett et al., 2020; Cotter et al., 2021b). By lowering autonomous echosounders to depth, scientists can take vertical measurements that extend beyond the range of hull-mounted instruments. For instance, the power of investigation using multi-frequency acoustics (i.e., transmitting multiple frequency signals simultaneously) is largely dependent on range from the receiver, which decreases with frequency due to seawater absorption loss (Francois and Garrison, 1982). These limitations have been met with new advancements in autonomous acoustic technology, whereby entire instrument packages (e.g., transducer & transceiver) can be lowered to the desired depth of study (Kloser et al., 2016). With the advancements, studies which could previously describe only the patterns of distribution of backscatter from the surface, can now measure individual targets at exceptionally high resolution throughout the water column (Bassett et al., 2020; Cotter et al., 2021b, 2021a).

The adoption of broadband (or frequency-modulated, FM) acoustic measurements vastly expands the volume of data collected, offering the potential promise of improving taxonomic or size detection of targets (Benoit-Bird and Waluk, 2020; Kubilius et al., 2020). Rather than using a continuous wave pulse, which transmits and measures the return pulse using a narrow frequency bandwidth, FM pulses are composed of a chirp that transmits a range of frequencies (Ehrenberg and Torkelson, 2000). FM returned pulses can contain distinguishing information along the frequency response about targets; however, they add to the considerable data volume of hydroacoustic data, which can slow processing time (Benoit-Bird and Waluk, 2020). With the commercial advancement of these new acoustic technologies come new scientific challenges that require merging the fields of signal processing, data science, physics, and biology. As such, lessons from other fields offer opportunities for novel applications of deep learning / machine learning for

sorting and filtering data to improve our understanding of species behavior and distribution (Lavery et al., 2017; Agersted et al., 2021; Cotter et al., 2021b).

1.7 Thesis overview

This thesis investigates the biogeographic and environmental drivers of fish and zooplankton assemblages in polar ecosystems, with a major focus on the western Atlantic-Arctic corridor. While this corridor broadly extends from the northeastern tip of the Canadian Arctic Archipelago to the northwest Atlantic Ocean, there are two focal points where the boundaries between water masses, or ice regimes, define how the ecosystem is structured: The Labrador Sea and Nares Strait. The Labrador Sea is widely recognized for its unique role in the physical oceanography of the global ocean, through deep water formation (Lilly et al., 1999). In light of recent proposals to expand Canada's marine protected areas, this region has been the focus of much biological research through the Integrated Studies and Ecosystem Characterization of the Labrador Sea Deep Ocean (ISECOLD) project. Through work with Fisheries & Oceans Canada (DFO), we embarked on several studies to characterize the biological components of the mesopelagic zone of the Labrador Sea. In the first set of studies, we developed eDNA methodology for the study of the mesopelagic fish and zooplankton and compared the detectability of organisms across functional groups with net sampling (Coté et al., n.d.; McClenaghan et al., 2020). Leveraging the broad spatial coverage of the ISECOLD expeditions in 2018 and 2019 in the Northwest Labrador Sea and transects extending into Baffin Bay, I developed two studies examining the vertical (Chapter 3) and horizontal (Chapter 2) distribution of lanternfishes near their biogeographic boundary. In 2019, I participated in the Ryder 2019 expedition to Northwest Greenland, aimed at geophysical mapping of Sherard Osborn Fjord, the terminus of the Ryder Glacier. Building upon the initial findings describing the unique physical oceanographic conditions in adjacent fjords, I developed a study

using a novel approach which combines optical and acoustic measurements to better understand the relationship between near-surface stratification, marine snow, and *Calanus* copepods.

There are several threads that tie this thesis together: 1) each study is among the first of its kind to use state-of-the-art acoustics tools in remote high Arctic regions; 2) each study required innovative applications of hull-mounted acoustics and/or lowered acoustic probes; and 3) each study deals with biogeographic regions that lie at the interface between Arctic and Atlantic waters.

Throughout this thesis, I leverage hydroacoustic tools to quantify and describe the distributions of fish and zooplankton within their environments. Much of the groundwork for this thesis involved designing and testing methodologies to obtain the highest quality acoustic data for comparison with a suite of other instrumentation and each chapter involves some iteration of a lowered acoustic probe. Specifically, hydroacoustic measurements are used primarily to infer how marine ecosystems are structured across horizontal and vertical scales. Chapters 3 and 4 focus on the distribution of backscatter in the vertical domain (Chapter 4) and a combination of both vertical and horizontal domains (Chapter 3). In Chapter 2, I measured individual fish within the mesopelagic deep scattering layer of the Northwest Labrador Sea, assessing their vertical distribution and density patterns. Chapter 2 uses broadband acoustic scattering to distinguish target signals, providing precise measurements of mesopelagic fish target strength (acoustic size) and estimates of their density within the DSL. As each approach has relevant applications in understudied systems in the deep ocean, this thesis combines several acoustic approaches to investigate pelagic organisms (Figure 1.2). Hydroacoustic data were used to measure patterns in backscatter across basin scales (1,000s of km) in Chapter 3, and individual targets at centimeter scales in Chapter 2. By combining two autonomous data streams, optical particle imaging with

high frequency acoustics, Chapter 4 advances the application of hydroacoustics on standard oceanographic sampling packages, such as the CTD rosette.
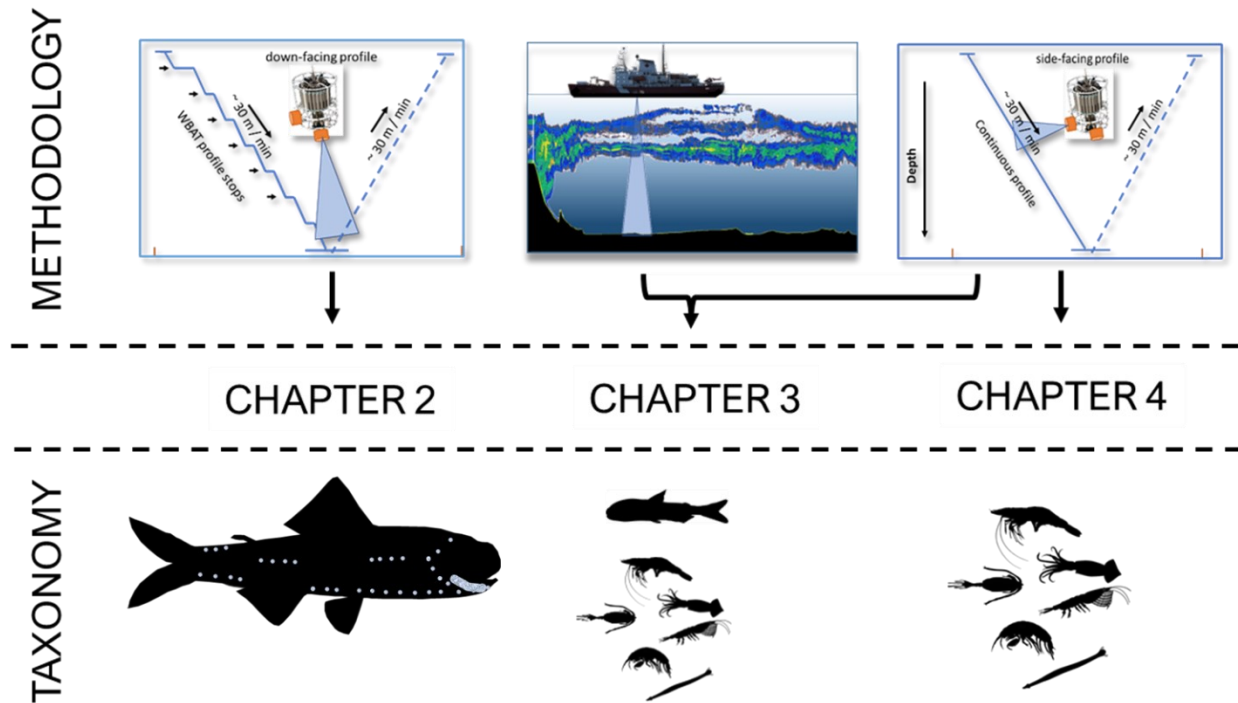
Figure 1.2 Overview of methodological approaches and broad taxonomic groups studied in each chapter. Chapter 3 uses both hull-mounted measurements (spatial) and lowered acoustic probes (vertical). Chapters 2 and 4 use lowered acoustic probes with vertical and horizontal oriented transducers, respectively.

Chapter 3 investigates how temperature boundaries influence the structure of meso- and bathy-pelagic ecosystems, by combining data collected from the Canadian Arctic with transects from the Southern Ocean. I used comparative transects to investigate why the deep-scattering layer weakens across frontal boundaries. In association with weakening backscatter towards the poles, we found evidence of a shift in the vertical structure of backscatter measured using lowered profilers, pointing to a broader change in ecosystem functioning and carbon cycling in the deep ocean.

Chapter 2 takes a finer scale look at the Northwest Labrador Sea, by investigating the vertical patterns of lanternfish distribution. This chapter introduces a new form of outlier detection used in machine learning to improve precision in target measurements within the broadband acoustic signal processing pipeline. I use these improved measurements to document target strength (i.e. acoustic size) patterns throughout the water column and estimate the density of organisms bearing gas-filled structure (i.e. swim bladders). There, I provide important estimates which can then be used in regionalized assessment of mesopelagic biomass and distributional patterns.

Chapter 4 focuses on the Nares Strait region of Northwest Greenland, an important Arctic-Atlantic throughflow which carries nutrient rich water into Baffin Bay (Jennings et al., 2011). Data for this chapter were collected during the 2019 Ryder Glacier cruise, a multi-disciplinary cruise led by Stockholm University to map Sherard Osborn Fjord in NW Greenland (Jakobsson et al., 2020a). During the cruise, the team uncovered key differences in the physical environments of these fjords, showing topographic control of ocean mixing by sea-ice and iceberg damming (Jakobsson et al., 2020b; Stranne et al., 2021). Chapter 4 expands on this geophysical research by investigating how amplified stratification impacts marine production and vertical distribution of copepods in the upper ocean. This chapter leverages a suite of optical, acoustic, and remote sensing tools to relate complex biogeophysical conditions of high Arctic fjords to the planktonic ecosystem.

1.8 References

Aagaard, K., Coachman, L. K., and Carmack, E. (1981). On the halocline of the Arctic Ocean. *Deep Sea Research Part A. Oceanographic Research Papers* 28, 529–545. doi: https://doi.org/10.1016/0198-0149(81)90115-1.

Agersted, M. D., Khodabandeloo, B., Liu, Y., Melle, W., and Klevjer, T. A. (2021). Application of an unsupervised clustering algorithm on in situ broadband acoustic data to identify different mesopelagic target types. *ICES Journal of Marine Science* 78, 2907–2921. doi: 10.1093/icesjms/fsab167.

Aksnes, D. L., Røstad, A., Kaartvedt, S., Martinez, U., Duarte, C. M., and Irigoien, X. (2017). Light penetration structures the deep acoustic scattering layers in the global ocean. *Sci Adv* 3, 1–6. doi: 10.1126/sciadv.1602468.

Ariza, A., Lengaigne, M., Menkes, C., Lebourges-Dhaussy, A., Receveur, A., Gorgues, T., et al. (2022). Global decline of pelagic fauna in a warmer ocean. *Nat Clim Chang* 12, 928–934. doi: 10.1038/s41558-022-01479-2.

Bassett, C., Lavery, A. C., Stanton, T. K., and Cotter, E. D. (2020). Frequency- and depth-dependent target strength measurements of individual mesopelagic scatterers. *J Acoust Soc Am* 148, EL153–EL158. doi: 10.1121/10.0001745.

Belcher, A., Saunders, R. A., and Tarling, G. A. (2019). Respiration rates and active carbon flux of mesopelagic fishes (Family Myctophidae) in the Scotia Sea, Southern Ocean. *Mar Ecol Prog Ser* 610, 149–162. doi: https://doi.org/10.3354/meps12861.

Benoit-Bird, K. J., and Lawson, G. L. (2016). Ecological Insights from Pelagic Habitats Acquired Using Active Acoustic Techniques. *Ann Rev Mar Sci* 8, 463–490. doi: 10.1146/annurev-marine-122414-034001.

Benoit-Bird, K. J., and Waluk, C. M. (2020). Exploring the promise of broadband fisheries echosounders for species discrimination with quantitative assessment of data processing effects. *J Acoust Soc Am* 147, 411–427. doi: 10.1121/10.0000594.

Boscolo-Galazzo, F., Crichton, K. A., Ridgwell, A., Mawbey, E. M., Wade, B. S., and Pearson, P. N. (2021). Temperature controls carbon cycling and biological evolution in the ocean twilight zone. *Science (1979)* 371, 1148–1152. doi: 10.1126/science.abb6643.

Bouchard, C., and Fortier, L. (2020). The importance of Calanus glacialis for the feeding success of young polar cod: a circumpolar synthesis. *Polar Biol*. doi: 10.1007/s00300-020-02643-0.

Brierley, A. S. (2014). Diel vertical migration. *Curr Biol* 24, R1074–R1076. doi: 10.1016/j.cub.2014.08.054.

Brito-Morales, I., Schoeman, D. S., Molinos, J. G., Burrows, M. T., Klein, C. J., Arafeh-Dalmau, N., et al. (2020). Climate velocity reveals increasing exposure of deep-ocean biodiversity to future warming. *Nat Clim Chang* 10, 576–581. doi: 10.1038/s41558-020-0773-5.

Catul, V., Gauns, M., and Karuppasamy, P. K. (2011). A review on mesopelagic fishes belonging to family Myctophidae. *Rev Fish Biol Fish* 21, 339–354. doi: 10.1007/s11160-010-9176-4.

Choy, C., Wabnitz, C., Weijerman, M., Woodworth-Jefcoats, P., and Polovina, J. (2016). Finding the way to the top: how the composition of oceanic mid-trophic micronekton groups determines apex predator biomass in the central North Pacific. *Mar Ecol Prog Ser* 549, 9–25. doi: 10.3354/meps11680.

Chu, D., and Stanton, T. K. (1998). Application of pulse compression techniques to broadband acoustic scattering by live individual zooplankton. *Journal of the Acoustical Society of America* 104, 39–55.

Coté, D., McClenaghan, B., Desforges, J., Fahner, N., Hajibabaei, M., Chawarski, J., et al. (2023). Comparing eDNA metabarcoding and conventional pelagic netting to inform biodiversity monitoring in deep ocean environments (in revision). *ICES Journal of Marine Science*.

Cotter, E., Bassett, C., and Lavery, A. (2021a). Comparison of mesopelagic organism abundance estimates using in situ target strength measurements and echo-counting techniques. *JASA Express Lett* 1, 040801. doi: 10.1121/10.0003940.

Cotter, E., Bassett, C., and Lavery, A. (2021b). Classification of broadband target spectra in the mesopelagic using physics-informed machine learning. *J Acoust Soc Am* 149, 3889–3901. doi: 10.1121/10.0005114.

Curry, B., Lee, C. M., Petrie, B., Moritz, R. E., and Kwok, R. (2014). Multiyear volume, liquid freshwater, and sea ice transports through Davis Strait, 2004-10. *J Phys Oceanogr* 44, 1244–1266. doi: 10.1175/JPO-D-13-0177.1.

Daase, M., Falk-Petersen, S., Varpe, Ø., Darnis, G., Søreide, J. E., Wold, A., et al. (2013). Timing of reproductive events in the marine copepod Calanus glacialis: A pan-Arctic perspective. *Canadian Journal of Fisheries and Aquatic Sciences* 70, 871–884. doi: 10.1139/cjfas-2012-0401.

Davison, P. C., Checkley, D. M., Koslow, J. A., and Barlow, J. (2013). Carbon export mediated by mesopelagic fishes in the northeast Pacific Ocean. *Prog Oceanogr* 116, 14–30. doi: 10.1016/j.pocean.2013.05.013.

Dee, L. E., Okamtoto, D., Gårdmark, A., Montoya, J. M., Miller, S. J., and Dee, L. E. (2020). Temperature variability alters the stability and thresholds for collapse of interacting species.

Doel, R. E., Friedman, R. M., Lajus, J., Sörlin, S., and Wråkberg, U. (2014). Strategic Arctic science: national interests in building natural knowledge – interwar era through the Cold War. *J Hist Geogr* 44, 60–80. doi: https://doi.org/10.1016/j.jhg.2013.12.004.

Ehrenberg, J. E., and Torkelson, T. C. (2000). FM slide (chirp) signals: a technique for significantly improving the signal-to-noise performance in hydroacoustic assessment systems. *Fish Res* 47, 193–199. doi: https://doi.org/10.1016/S0165-7836(00)00169-7.

Falk-Petersen, S., Mayzaud, P., Kattner, G., and Sargent, J. R. (2009). Lipids and life strategy of Arctic Calanus. *Marine Biology Research* 5, 18–39. doi: 10.1080/17451000802512267.

Fortier, M., Fortier, L., Hattori, H., Saito, H., and Legendre, L. (2001). Visual predators and the diel vertical migration of copepods under Arctic sea ice during the midnight sun. *J Plankton Res* 23, 1263–1278. doi: 10.1093/plankt/23.11.1263.

Francois, R., and Garrison, G. (1982). Sound absorption based on ocean measurments. Part II: boric acid contribution and equation for total absorption. *J. Acoust. Soc. Am* 72, 1879–1890.

Geoffroy, M., Berge, J., Majaneva, S., Johnsen, G., Langbehn, T. J., Cottier, F., et al. (2018). Increased occurrence of the jellyfish Periphylla periphylla in the European high Arctic. *Polar Biol*, 1–5. doi: 10.1007/s00300-018-2368-4.

Gloeckler, K., Choy, C. A., Hannides, C. C. S., Close, H. G., Goetze, E., Popp, B. N., et al. (2018). Stable isotope analysis of micronekton around Hawaii reveals suspended particles are an important nutritional source in the lower mesopelagic and upper bathypelagic zones. *Limnol Oceanogr* 63, 1168–1180. doi: 10.1002/lno.10762.

Gonçalves Neto, A., Langan, J. A., and Palter, J. B. (2021). Changes in the Gulf Stream preceded rapid warming of the Northwest Atlantic Shelf. *Commun Earth Environ* 2, 74. doi: 10.1038/s43247-021-00143-5.

Greene, C. H., Pershing, A. J., Cronin, T. M., and Ceci, N. (2008). Arctic climate change and its impacts on the ecology of the North Atlantic. *Ecology* 89, 24–38. doi: 10.1890/07-0550.1.

Grenfell, T. C. (1979). The Effects of Ice Thickness on the Exchange of Solar Radiation Over the Polar Oceans. *Journal of Glaciology* 22, 305–320. doi: DOI: 10.3189/S0022143000014295.

Grimaldo, E., Grimsmo, L., Alvarez, P., Herrmann, B., Møen Tveit, G., Tiller, R., et al. (2020). Investigating the potential for a commercial fishery in the Northeast Atlantic utilizing mesopelagic species. *ICES Journal of Marine Science*, 1:15. doi: 10.1093/icesjms/fsaa114.

Haine, T., Böning, C., Brandt, P., Fischer, J., Funk, A., Kieke, D., et al. (2008). "North Atlantic Deep Water Formation in the Labrador Sea, Recirculation Through the Subpolar Gyre, and Discharge to the Subtropics," in *Arctic–Subarctic Ocean Fluxes: Defining the Role of the Northern Seas in Climate*, eds. R. R. Dickson, J. Meincke, and P. Rhines (Dordrecht: Springer Netherlands), 653–701. doi: 10.1007/978-1-4020-6774-7_28.

Hatlebakk, M., Kosobokova, K., Daase, M., and Søreide, J. E. (2022). Contrasting Life Traits of Sympatric Calanus glacialis and C. finmarchicus in a Warming Arctic Revealed by a Year-Round Study in Isfjorden, Svalbard. *Front Mar Sci* 9. Available at: https://www.frontiersin.org/articles/10.3389/fmars.2022.877910.

Hernández-León, S., Koppelmann, R., Fraile-Nuez, E., Bode, A., Mompeán, C., Irigoien, X., et al. (2020). Large deep-sea zooplankton biomass mirrors primary production in the global ocean. *Nat Commun* 11, 6048. doi: 10.1038/s41467-020-19875-7.

Hogan, K. A., Jakobsson, M., Mayer, L., Reilly, B. T., Jennings, A. E., Stoner, J. S., et al. (2020). Glacial sedimentation, fluxes and erosion rates associated with ice retreat in Petermann Fjord and Nares Strait, north-west Greenland. *Cryosphere* 14, 261–286. doi: 10.5194/tc-14-261-2020.

Hopwood, M. J., Carroll, D., Dunse, T., Hodson, A., Holding, J. M., Iriarte, J. L., et al. (2020). Review article: How does glacier discharge affect marine biogeochemistry and primary production in the Arctic? *Cryosphere* 14, 1347–1383. doi: 10.5194/tc-14-1347-2020.

Hudson, J. M., Steinberg, D. K., Sutton, T. T., Graves, J. E., and Latour, R. J. (2014). Myctophid feeding ecology and carbon transport along the northern Mid-Atlantic Ridge. *Deep Sea Res 1 Oceanogr Res Pap* 93, 104–116. doi: 10.1016/j.dsr.2014.07.002.

Irigoien, X., Klevjer, T. A., Røstad, A., Martinez, U., Boyra, G., Acuña, J. L., et al. (2014). Large mesopelagic fishes biomass and trophic efficiency in the open ocean. *Nat Commun* 5, 1–10. doi: 10.1038/ncomms4271.

Jakobsson, M., Mayer, L. A., Farrell, J. F., and Ryder 2019 Scientific Party (2020a). Expedition report: SWEDARCTIC Ryder 2019.

Jakobsson, M., Mayer, L. A., Nilsson, J., Stranne, C., Calder, B., O'Regan, M., et al. (2020b). Ryder Glacier in northwest Greenland is shielded from warm Atlantic water by a bathymetric sill. *Commun Earth Environ* 1, 1–10. doi: 10.1038/s43247-020-00043-0.

Jennings, A., Sheldon, C., Cronin, T., Francus, P., Stoner, J., and Andrews, J. (2011). The Holocene History of Nares Strait: Transition from Glacial Bay to Arctic-Atlantic Throughflow. *Oceanography* 24, 26–41. doi: 10.5670/oceanog.2011.52.

Johnson, H. L., Münchow, A., Falkner, K. K., and Melling, H. (2011). Ocean circulation and properties in Petermann Fjord , Greenland. 116, 1–18. doi: 10.1029/2010JC006519.

Jones, W. A., and Checkley, D. M. (2019). Mesopelagic fishes dominate otolith record of past two millennia in the Santa Barbara Basin. *Nat Commun* 10. doi: 10.1038/s41467-019-12600-z.

Kaartvedt, S. (2008). Photoperiod may constrain the effect of global warming in arctic marine systems. *J Plankton Res* 30, 1203–1206. doi: 10.1093/plankt/fbn075.

Kaartvedt, S., Staby, A., and Aksnes, D. L. (2012). Efficient trawl avoidance by mesopelagic fishes causes large underestimation of their biomass. *Mar Ecol Prog Ser* 456, 1–6. doi: 10.3354/meps09785.

Kaartvedt, S., and Titelman, J. (2018). Planktivorous fish in a future Arctic Ocean of changing ice and unchanged photoperiod. *ICES Journal of Marine Science*. doi: 10.1093/icesjms/fsy077.

Kaiser, P., Hagen, W., Bode-Dalby, M., and Auel, H. (2022). Tolerant but facing increased competition: Arctic zooplankton versus Atlantic invaders in a warming ocean. *Front Mar Sci* 9. Available at: https://www.frontiersin.org/articles/10.3389/fmars.2022.908638.

Klevjer, T. A., Irigoien, X., Røstad, A., Fraile-Nuez, E., Benítez-Barrios, V. M., and Kaartvedt., S. (2016). Large scale patterns in vertical distribution and behaviour of mesopelagic scattering layers. *Sci Rep* 6, 1–11. doi: 10.1038/srep19873.

Kloser, R. J. (1996). Improved precision of acoustic surveys of benthopelagic fish by means of a deep-towed transducer. *ICES Journal of Marine Science* 53, 407–413. doi: 10.1006/jmsc.1996.0057.

Kloser, R. J., Ryan, T. E., Gordon, K., and Gershwin, L. (2016). Deep-scattering layer, gas-bladder density, and size estimates using a two-frequency acoustic and optical probe. *ICES Journal of Marine Science* 73, 2037–2048. doi: 10.1093/icesjms/fsv257.

Koch, C. W., Brown, T. A., Amiraux, R., Ruiz-Gonzalez, C., MacCorquodale, M., Yunda-Guarin, G. A., et al. (2023). Year-round utilization of sea ice-associated carbon in Arctic ecosystems. *Nat Commun* 14, 1964. doi: 10.1038/s41467-023-37612-8.

Korneliussen, R. J., Berger, L., Campanella, F., Chu, D., Demer, D., Fielding, S., et al. (2018). *Acoustic target classification*. doi: http://doi.org/10.17895/ices.pub.4567.

Kortsch, S., Primicerio, R., Fossheim, M., Dolgov, A. V, Aschan, M., and Kortsch, S. (2015). Climate change alters the structure of arctic marine food webs due to poleward shifts of boreal generalists. doi: 10.5061/dryad.73r6j.

Koslow, J. A., Davison, P., Ferrer, E., Jiménez Rosenberg, S. P. A., Aceves-Medina, G., Watson, W., et al. (2019). The evolving response of mesopelagic fishes to declining midwater oxygen concentrations in the southern and central California Current. *ICES Journal of Marine Science* 76, 626–638. doi: 10.1093/icesjms/fsy154.

Kubilius, R., Macaulay, G. J., and Ona, E. (2020). Remote sizing of fish-like targets using broadband acoustics. *Fish Res* 228. doi: 10.1016/j.fishres.2020.105568.

Laidre, K. L., Supple, M. A., Born, E. W., Regehr, E. v, Wiig, Ø., Ugarte, F., et al. (2022). Glacial ice supports a distinct and undocumented polar bear subpopulation persisting in late 21st-century sea-ice conditions. *Science (1979)* 376, 1333–1338. doi: 10.1126/science.abk2793.

Langbehn, T. J. (2017). Sea-ice loss boosts visual search: fish foraging and changing pelagic interactions in polar oceans. 5318–5330. doi: 10.1111/gcb.13797.

Langbehn, T. J., Aksnes, D. L., Kaartvedt, S., Fiksen, Ø., Ljungström, G., Jørgensen, C., et al. (2022). Poleward distribution of mesopelagic fishes is constrained by seasonality in light. *Global Ecology and Biogeography* 31, 546–561. doi: 10.1111/geb.13446.

Lavery, A. C., Bassett, C., Lawson, G. L., and Jech, J. M. (2017). Exploiting signal processing approaches for Broadband echosounders. *ICES Journal of Marine Science* 74, 2262–2275. doi: 10.1093/icesjms/fsx155.

Laxon, S. W., Giles, K. A., Ridout, A. L., Wingham, D. J., Willatt, R., Cullen, R., et al. (2013). CryoSat-2 estimates of Arctic sea ice thickness and volume. *Geophys Res Lett* 40, 732–737. doi: https://doi.org/10.1002/grl.50193.

Lehodey, P., Murtugudde, R., and Senina, I. (2010). Bridging the gap from ocean models to population dynamics of large marine predators: A model of mid-trophic functional groups. *Prog Oceanogr* 84, 69–84. doi: 10.1016/j.pocean.2009.09.008.

Lilly, J. M., Rhines, P. B., Visbeck, M., Davis, R., Lazier, J. R. N., Schott, F., et al. (1999). Observing Deep Convection in the Labrador Sea during Winter 1994/95. *J Phys Oceanogr* 29, 2065–2098. doi: https://doi.org/10.1175/1520-0485(1999)029<2065:ODCITL>2.0.CO;2.

Ljungström, G., Langbehn, T. J., and Jørgensen, C. (2021). Light and energetics at seasonal extremes limit poleward range shifts. *Nat Clim Chang* 11, 530–536. doi: 10.1038/s41558-021-01045-2.

Longhurst, A., Sameoto, D., and Herman, A. (1984). Vertical distribution of Arctic zooplankton in summer: eastern Canadian archipelago. *J Plankton Res* 6, 137–168. doi: 10.1093/plankt/6.1.137.

MacLennan, D. N., and Simmonds, E. J. (2004). Fisheries acoustics. *Rev Fish Biol Fish* 2, 339–341.

McClenaghan, B., Fahner, N., Coté, D., Chawarski, J., McCarthy, A., Rajabi, H., et al. (2020). Harnessing the power of eDNA metabarcoding for the detection of deep-sea fishes. 1–19. doi: 10.1101/2020.07.10.197012.

McKelvie, D. S., and Haedrich, R. L. (1985). Mesopelagic Fishes (excluding Myctophidae) from Research Surveys off Newfoundland and Labrador *. *NAFO Sci. Coun. Studies*, 67–76.

Meire, L., Mortensen, J., Meire, P., Juul-Pedersen, T., Sejr, M. K., Rysgaard, S., et al. (2017). Marine-terminating glaciers sustain high productivity in Greenland fjords. *Glob Chang Biol* 23, 5344–5357. doi: 10.1111/gcb.13801.

Mueter, F. J., Nahrgang, J., John Nelson, R., and Berge, J. (2016). The ecology of gadid fishes in the circumpolar Arctic with a special emphasis on the polar cod (Boreogadus saida). *Polar Biol* 39, 961–967. doi: 10.1007/s00300-016-1965-3.

Muilwijk, M., Smedsrud, L. H., Ilicak, M., and Drange, H. (2018). Atlantic Water Heat Transport Variability in the 20th Century Arctic Ocean From a Global Ocean Model and Observations. *J Geophys Res Oceans* 123, 8159–8179. doi: https://doi.org/10.1029/2018JC014327.

Netburn, A. N., and Koslow, J. A. (2018). Mesopelagic fish assemblages across oceanic fronts: A comparison of three frontal systems in the southern California Current Ecosystem. *Deep Sea Res 1 Oceanogr Res Pap* 134, 80–91. doi: 10.1016/j.dsr.2018.03.005.

Nilsson, J., van Dongen, E., Jakobsson, M., O'Regan, M., and Stranne, C. (2023). Hydraulic suppression of basal glacier melt in sill fjords. *Cryosphere* 17, 2455–2476. doi: 10.5194/tc-17-2455-2023.

Peng, Q., Xie, S.-P., Wang, D., Huang, R. X., Chen, G., Shu, Y., et al. (2023). Surface warming–induced global acceleration of upper ocean currents. *Sci Adv* 8, eabj8394. doi: 10.1126/sciadv.abj8394.

Pepin, P. (2013). Distribution and feeding of Benthosema glaciale in the western Labrador Sea: Fish-zooplankton interaction and the consequence to calanoid copepod populations. *Deep Sea Res 1 Oceanogr Res Pap* 75, 119–134. doi: 10.1016/j.dsr.2013.01.012.

Perry, A. L., Low, P. J., Ellis, J. E., and Reynolds, J. D. (2005). Climate Change and Distribution Shifts in Marine Fishes. *Science (1979)* 308, 1912–1915. doi: 10.1038/020493a0.

Pershing, A. J., Alexander, M. A., Hernandez, C. M., Kerr, L. A., le Bris, A., Mills, K. E., et al. (2015). Slow adaptation in the face of rapid warming leads to collapse of the Gulf of Maine cod fishery. *Science (1979)* 350, 809–812. doi: 10.1126/science.aac9819.

Pershing, A. J., and Stamieszkin, K. (2020). The North Atlantic Ecosystem, from Plankton to Whales. *Ann Rev Mar Sci* 12, 339–359. doi: 10.1146/annurev-marine-010419-010752.

Pettitt-Wade, H., Pearce, T., Kuptana, D., Gallagher, C. P., Scharffenberg, K., Lea, E. v., et al. (2020). Inuit observations of a tunicata bloom unusual for the amundsen gulf, western Canadian arctic. *Arct Sci* 6, 340–351. doi: 10.1139/as-2020-0018.

Pinsky, M. L., Selden, R. L., and Kitchel, Z. J. (2020). Climate-Driven Shifts in Marine Species Ranges: Scaling from Organisms to Communities. *Ann Rev Mar Sci* 12, 153–179. doi: 10.1146/annurev-marine-010419-010916.

Polyakov, I. V., Alkire, M. B., Bluhm, B. A., Brown, K. A., Carmack, E. C., Chierici, M., et al. (2020). Borealization of the Arctic Ocean in Response to Anomalous Advection From Sub-Arctic Seas. *Front Mar Sci* 7. doi: 10.3389/fmars.2020.00491.

Polyakov, I. V., Pnyushkov, A. V., Alkire, M. B., Ashik, I. M., Baumann, T. M., Carmack, E. C., et al. (2017). Greater role for Atlantic inflows on sea-ice loss in the Eurasian Basin of the Arctic Ocean. *Science (1979)* 356, 285–291. doi: 10.1126/science.aai8204.

Prellezo, R., and Maravelias, C. (2019). Exploring the economic viability of a mesopelagic fishery in the Bay of Biscay. *ICES Journal of Marine Science* 76, 771–779. doi: 10.1093/icesjms/fsy001.

Proud, R., Cox, M. J., and Brierley, A. S. (2017). Biogeography of the Global Ocean's Mesopelagic Zone. *Current Biology* 27, 113–119. doi: 10.1016/j.cub.2016.11.003.

Proud, R., Handegard, N. O., Kloser, R. J., Cox, M. J., and Brierley, A. S. (2018). From siphonophores to deep scattering layers: uncertainty ranges for the estimation of global mesopelagic fish biomass. *ICES Journal of Marine Science*. doi: 10.1093/icesjms/fsy037.

Rantanen, M., Karpechko, A. Yu., Lipponen, A., Nordling, K., Hyvärinen, O., Ruosteenoja, K., et al. (2022). The Arctic has warmed nearly four times faster than the globe since 1979. *Commun Earth Environ* 3, 168. doi: 10.1038/s43247-022-00498-3.

Romero-Romero, S., Choy, C. A., Hannides, C. C. S., Popp, B. N., and Drazen, J. C. (2019). Differences in the trophic ecology of micronekton driven by diel vertical migration. *Limnol Oceanogr* 64, 1473–1483. doi: 10.1002/lno.11128.

Rose, G. A. (2005). Capelin (Mallotus villosus) distribution and climate: A sea "canary" for marine ecosystem change. *ICES Journal of Marine Science* 62, 1524–1530. doi: 10.1016/j.icesjms.2005.05.008.

Sameoto, D. (1989). Feeding Ecology of the Lantern Fish Benthosema Glaciale in a Subarctic Region. *Polar Biol* 9, 167–178. doi: 10.1007/BF00297172.

Simmonds, E. J., and MacLennan, D. N. (2005). *Fisheries acoustics, 2nd edition*. London: Chapman and Hall.

Snoeijs-Leijonmalm, P., Flores, H., Sakinan, S., Hildebrandt, N., Svenson, A., Castellani, G., et al. (2022). Unexpected fish and squid in the central Arctic deep scattering layer. *Sci Adv* 8, 1–17. doi: 10.1126/sciadv.abj7536.

Søreide, J. E., Dmoch, K., Blachowiak-Samolyk, K., Trudnowska, E., and Daase, M. (2022). Seasonal mesozooplankton patterns and timing of life history events in high-arctic fjord environments. *Front Mar Sci* 9. doi: 10.3389/fmars.2022.933461.

Søreide, J. E., Hop, H., Carroll, M. L., Falk-Petersen, S., and Hegseth, E. N. (2006). Seasonal food web structures and sympagic-pelagic coupling in the European Arctic revealed by stable isotopes and a two-source food web model. *Prog Oceanogr* 71, 59–87. doi: 10.1016/j.pocean.2006.06.001.

Søreide, J. E., Leu, E., Berge, J., Graeve, M., and Falk-Petersen, S. (2010). Timing of blooms, algal food quality and Calanus glacialis reproduction and growth in a changing Arctic. *Glob Chang Biol* 16, 3154–3163. doi: https://doi.org/10.1111/j.1365-2486.2010.02175.x.

St. John, M. A., Borja, A., Chust, G., Heath, M., Grigorov, I., Mariani, P., et al. (2016). A dark hole in our understanding of marine ecosystems and their services: Perspectives from the mesopelagic community. *Front Mar Sci* 3, 1–6. doi: 10.3389/fmars.2016.00031.

Stanton, T. K., and Chu, D. (2000). Review and recommendations for the modelling of acoustic scattering by fluid-like elongated zooplankton: euphausiids and copepods. *ICES Journal of Marine Science* 57, 793–807. doi: 10.1006/jmsc.1999.0517.

Straneo, F., and Saucier, F. (2008). The outflow from Hudson Strait and its contribution to the Labrador Current. *Deep Sea Res 1 Oceanogr Res Pap* 55, 926–946. doi: 10.1016/j.dsr.2008.03.012.

Straneo, F., Sutherland, D. A., Holland, D., Gladish, C., Hamilton, G. S., Johnson, H. L., et al. (2012). Characteristics of ocean waters reaching Greenland's glaciers. *Ann Glaciol* 53, 202–210. doi: DOI: 10.3189/2012AoG60A059.

Stranne, C., Nilsson, J., Ulfsbo, A., O'Regan, M., Coxall, H. K., Meire, L., et al. (2021). The climate sensitivity of northern Greenland fjords is amplified through sea-ice damming. *Commun Earth Environ* 2, 4–11. doi: 10.1038/s43247-021-00140-8.

Stuart-Lee, A., Mortensen, J., Juul-Pedersen, T., Middelburg, J., Soetaert, K., Hopwood, M., et al. (2023). Influence of glacier type on bloom phenology in two Southwest Greenland fjords. *Estuar Coast Shelf Sci*, 108271. doi: 10.1016/j.ecss.2023.108271.

Sutton, T. T., Letessier, T. B., and Bardarson, B. (2013). Midwater fishes collected in the vicinity of the Sub-Polar Front, Mid-North Atlantic Ocean, during ECOMAR pelagic sampling. *Deep Sea Res 2 Top Stud Oceanogr* 98, 292–300. doi: 10.1016/j.dsr2.2013.08.001.

Taylor, P., Søreide, J. E., Carroll, M. L., Hop, H., Jr, W. G. A., Hegseth, N., et al. (2013). Sympagic-pelagic-benthic coupling in Arctic and Atlantic waters around Svalbard revealed by stable isotopic and fatty acid tracers. 37–41.

Tremblay, J.-É., Anderson, L. G., Matrai, P., Coupel, P., Bélanger, S., Michel, C., et al. (2015). Global and regional drivers of nutrient supply, primary production and CO2 drawdown in the changing Arctic Ocean. *Prog Oceanogr* 139, 171–196. doi: https://doi.org/10.1016/j.pocean.2015.08.009.

Trudnowska, E., Balazy, K., Stoń-Egiert, J., Smolina, I., Brown, T., and Gluchowska, M. (2020). In a comfort zone and beyond—Ecological plasticity of key marine mediators. *Ecol Evol* 10, 14067–14081. doi: https://doi.org/10.1002/ece3.6997.

Trusel, L. D., Das, S. B., Osman, M. B., Evans, M. J., Smith, B. E., Fettweis, X., et al. (2018). Nonlinear rise in Greenland runoff in response to post-industrial Arctic warming. *Nature* 564, 104–108. doi: 10.1038/s41586-018-0752-4.

Van Pelt, T. I., Huntington, H. P., Romanenko, O. V, and Mueter, F. J. (2017). The missing middle: Central Arctic Ocean gaps in fishery research and science coordination. *Mar Policy* 85, 79–86. doi: https://doi.org/10.1016/j.marpol.2017.08.008.

Vihtakari, M., Welcker, J., Moe, B., Chastel, O., Tartu, S., Hop, H., et al. (2018). Black-legged kittiwakes as messengers of Atlantification in the Arctic. *Sci Rep* 8, 1–11. doi: 10.1038/s41598-017-19118-8.

Vinogradov, M. E. (1962). Feeding of the Deep-Sea Zooplankton. *Rapp. Proc.-Verb.* 153, 114–120.

Vinogradov, M. E. (1997). "Some Problems of Vertical Distribution of Meso- and Macroplankton in the Ocean," in *Advances in Marine Biology*, eds. J. H. S. Blaxter, A. J. Southward, A. V Gebruk, E. C. Southward, and P. A. Tyler (Academic Press), 1–92. doi: https://doi.org/10.1016/S0065-2881(08)60015-2.

von Appen, W.-J., Waite, A. M., Bergmann, M., Bienhold, C., Boebel, O., Bracher, A., et al. (2021). Sea-ice derived meltwater stratification slows the biological carbon pump: results from continuous observations. *Nat Commun* 12, 7309. doi: 10.1038/s41467-021-26943-z.

Wassman, P., and Reigstad, M. (2011). Future Arctic Ocean seasonal ice zones and implications for pelagic-benthic coupling. *Oceanography* 24, 220–231.

Wefing, A.-M., Casacuberta, N., Christl, M., Gruber, N., and Smith, J. N. (2021). Circulation timescales of Atlantic Water in the Arctic Ocean determined from anthropogenic radionuclides. *Ocean Science* 17, 111–129. doi: 10.5194/os-17-111-2021.

Wilson, L. J., Fulton, C. J., Hogg, A. M., Joyce, K. E., Radford, B. T. M., and Fraser, C. I. (2016). Climate-driven changes to ocean circulation and their inferred impacts on marine dispersal patterns. *Global Ecology and Biogeography* 25, 923–939. doi: https://doi.org/10.1111/geb.12456.

Wood, M., Rignot, E., Fenty, I., An, L., Bjørk, A., van den Broeke, M., et al. (2023). Ocean forcing drives glacier retreat in Greenland. *Sci Adv* 7, eaba7282. doi: 10.1126/sciadv.aba7282.

Yamamoto-Kawai, M., McLaughlin, F. A., Carmack, E. C., Nishino, S., and Shimada, K. (2008). Freshwater budget of the Canada Basin, Arctic Ocean, from salinity, δ18O, and nutrients. *J Geophys Res Oceans* 113. doi: https://doi.org/10.1029/2006JC003858.

Chapter 2. Improved precision in target strength and density estimation of mesopelagic fish through detection of anomalous acoustic broadband signals

2.1 Abstract

Mesopelagic fish are widespread and abundant in the global oceans. They contribute to nutrient cycling via the biological carbon pump and may be a target of future fisheries. Estimating abundance of mesopelagic fish remains a challenge due to the limitations of ship-based echosounders and traditional trawling methods. Submersible broadband acoustic probes offer significant improvements to target measurements via increased range resolution and the possibility to use higher frequencies with expanded spectra; however, broadband measurements can introduce undesired signals into the data. Using an unsupervised outlier detection approach, we improved the precision of individual target measurements and density estimation of mesopelagic fish in the Labrador Sea. Consistently across the survey, we encountered a high variability in the frequency response of targets, both within the insonified volume and within distinct echo-traces. We apply an unsupervised outlier detection algorithm to identify unwanted target measurements based on their frequency response. We then use the target measurements of all frequency responses selected by the algorithm to estimate density of mesopelagic fish using echo-integration. We find that including anomalous signals positively skew density estimates of mesopelagic fish by up to 25%. Our approach reduces measurement error within echo-trace measurements and increases the precision of target strength and density estimations for mesopelagic targets within sound-scattering layers. This study provides new insight into the application of broadband echosounders for density estimation of mesopelagic resources.

2.2 Introduction

Mesopelagic fish are becoming increasingly recognized for their importance in biogeochemical cycling (St. John et al., 2016) and as a potential source of protein in future fisheries (Prellezo and Maravelias, 2019; Grimaldo et al., 2020). Hydroacoustic surveys are instrumental in revealing the distribution and biomass of mesopelagic sound-scattering organisms forming deep-scattering layers (DSLs) (Davison et al., 2015). However, biomass estimation across large spatial scales using echo-integration requires knowledge of the target strength distribution of organisms within sound scattering layers (Chu, 2011). Estimates of target strength using standard shipboard echosounders is limited due to beam spreading, poor range resolution, and a weakened signal-to-noise ratio at mesopelagic depths (Davison et al., 2015). Lowered acoustic platforms can facilitate measurements of individual organisms at depth and show promise in differentiating biological scatterers based on their frequency response characteristics at close range (Kloser et al., 2016; Bassett et al., 2020; Benoit-Bird and Waluk, 2020; Dias Bernardes et al., 2020; Agersted et al., 2021; Cotter et al., 2021b).

Recent adoption of broadband acoustic processing offers the advantage of pulse compression of frequency modulated (FM) signals which results in higher range resolution than available with narrowband signals (Chu and Stanton, 1998; Ehrenberg and Torkelson, 2000). This signal-processing approach allows for the detection of multiple impedance contrasts from body parts as well as constructive and destructive interference of echoes associated with movement (Kubilius et al., 2020). For these reasons, broadband scattering from individual fish is a complex signal that is dependent on the geometric, physical, biological characteristics of the target (Imaizumi et al., 2008; Forland et al., 2014).

For many species, swim-bladders are typically used to estimate the size and position of an organism in the water column due to their strong reflectance (Simmonds and MacLennan, 2005) and relative insensitivity to angle or orientation (Scoulding et al., 2015; Proud et al., 2018). Recent improvements in broadband model estimation of mesopelagic swim-bladders provide evidence that in-situ measurements can align with model projections (Agersted et al., 2021; Cotter et al., 2021b). However, to achieve precise measurements of target strength of swim-bladders within a given insonified volume requires the ability to differentiate signals produced by a range of stochastic biological and physical processes. In an individual fish, target strength can vary based on the combination of coherent and incoherent energy. Incoherent energy can add random components to the echo due to fish size exceeding the pulse wavelength and or inconsistencies from fish movement (i.e., swimming) (Stanton and Clay, 1986). The ratio of coherent and incoherent energy can be defined as a type of 'signal-to-noise' ratio (Demer and Conti, 2003; Kieser et al., 2005). Variations in this ratio can occur from overlapping echoes originating from different anatomical parts of an individual animal or from multiple fish within an aggregation (Demer et al., 2009). Depending on fish densities (individuals / volume), beam pattern effects can also play a strong role in ping-to-ping fluctuations in target strength (Stanton and Clay, 1986). Furthermore, the material properties of fish flesh, such as shear elastic viscosity, can lead to under or overestimation of target strength (Khodabandeloo et al., 2021) In addition to these challenges faced with single frequency measurements, current approaches to broadband processing can require additional parameterization that can impact the frequency response of a signal (Benoit-Bird and Waluk, 2020).

Following the widespread adoption of broadband (FM) capable instrumentation such as Simrad © EK80s on fisheries research vessels, the field of fisheries acoustics has been faced with new

challenges associated with data volume: broadband acoustic measurements can outsize previously collected narrowband datasets by several orders of magnitude. Because broadband analyses introduce additional signal complexity and large data volume, analytical approaches require automated steps to distinguish anomalous signals (e.g., from multiple organs or overlapping fish) from deterministic signals carrying information on the scattering properties of organisms, such as true reflections of gas-filled swimbladders. Unsupervised pattern recognition tools, such as clustering, offer a practical approach to classifying large wideband acoustic datasets (Malde et al., 2019; Agersted et al., 2021). Unsupervised cluster analysis assigns groups to untrained data without a universal definition for a cluster (Kaufman and Rousseeuw, 1990). Widely applied clustering algorithms like k-means and hierarchical clustering rely on assumptions about the data distribution, require parameterization, and are poorly designed to deal with noise (Macqueen, 1967; Kaufman and Rousseeuw, 1990; Xiao and Yu, 2012). Due to the complexity of ¬in-situ sound scattering within mesopelagic scattering layers we cannot rely on a priori assumptions about cluster shape or density. Instead, we rely on automated approach to detecting noise, or outliers in our data.

The aim of this study is to improve the precision of acoustic measurements of mesopelagic fish within deep sound-scattering layers. In the context of this study, the goal of precise measurements is to reduce the variation surrounding the mean value of target strength among individuals and identify any patterns of systematic bias at the survey level. The recent adoption of broadband echosounders offers a promising approach to improve target measurements, which requires further investigation into the source of frequency-dependent target measurements. Using lowered acoustic probe measurements, we demonstrate how the inclusion of anomalous target measurements within insonified volumes can impact target strength measurements and density estimation. We present a

detailed investigation into the potential sources of anomalous broadband target measurements, spotlighting an unsupervised approach to outlier detection in broadband spectral data.

2.3 Methods

2.3.1 Data Collection.

Data were collected aboard the CCGS *Amundsen* as part of the Integrated Studies and Ecosystem Characterization of the Labrador Sea Deep Ocean (ISECOLD) program. The survey was designed along three transects conducted over the northwest slope of the Labrador Sea (**Figure 2.1**).
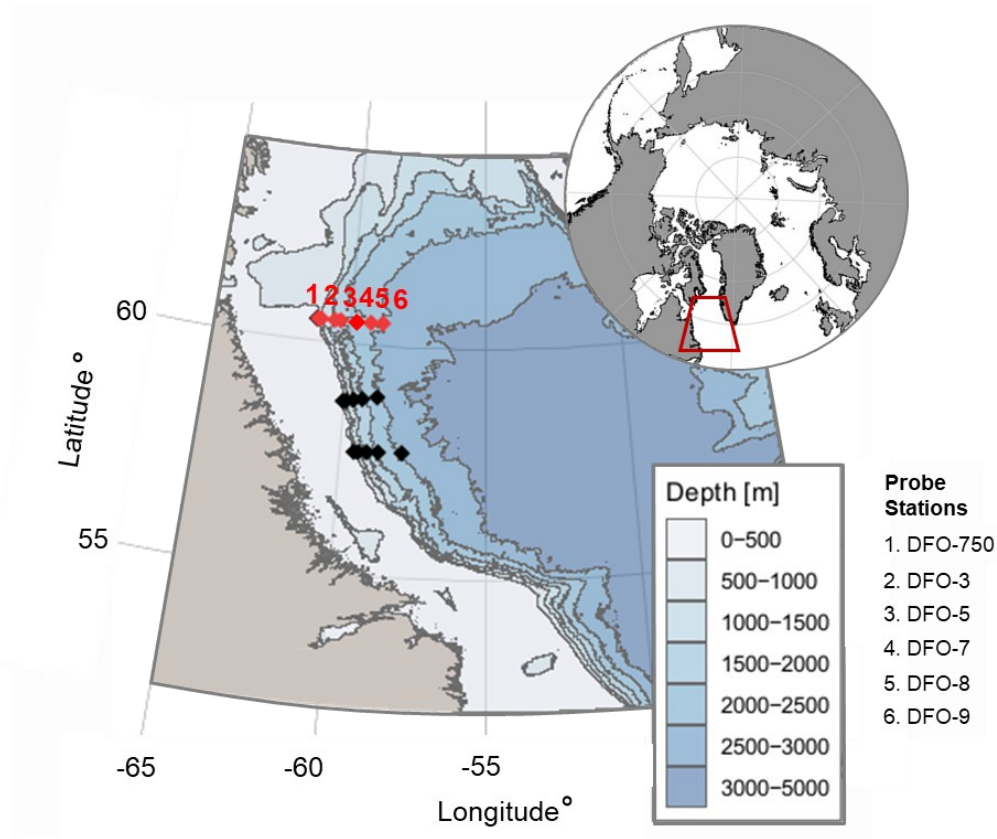
Figure 2.1 Sampling region and sites in the NW Labrador Sea. Data were collected during the ISECOLD expedition in July 2018 and 2019. Points on the map indicate mid-water trawl sampling sites (2019) and red points indicate sites where both the mid-water trawl and lowered acoustic probe were deployed (2018).

2.3.2 Biological Sampling

Biological samples were collected at 5 stations in 2018 and 10 stations in 2019 using a modified Isaac Kidd Midwater Trawl (IKMT). The net has a 9 m^2 rectangular opening with forward mesh size of 11 mm and a 5 mm codend. At each station, the net was lowered at 2 m s^{-1} to a target depth, as determined by real-time monitoring of acoustic backscatter from the hull-mounted EK60. Head-rope depth was monitored using a high precision acoustic positioning system (Kongsberg ®) while

the net was towed for 15-30 minutes at 1.5 to 2 m s^{-1} through the DSL depths ranging from 360 to 540 m, as seen on the ship's echosounder. An additional four tows were deployed *ad hoc* to < 100 m to confirm the presence/absence of migrating taxa. All biological samples were measured by their wet weight to within ±1 g.

Shipboard acoustic data were continuously collected with a 38 kHz hull-mounted (7 m ship's draft) EK60 split-beam echosounder operated at 1.204 ms pulse duration and 1000 W power at a 1000 m range. Ping rate was multiplexed with other acoustic systems to reduce interference and ranged from 0.3 to 1 Hz. The ship's transducers are calibrated annually following standard sphere methods (Demer et al., 2015).

A portion of the mesopelagic organisms of the Labrador Sea conduct diel vertical migration i.e. they ascend at dusk and descend at dawn (**Figure 2.1**). We thus classified the periods of the day using three broad categories: daytime, twilight, and nighttime. While any delineation of "biological day and night" related to solar angle is more or less arbitrary as organisms tend to track light levels rather than solar height (Kaartvedt et al., 2019), our observations of peak sound scattering layer migrations seen on the shipboard echosounder aligned well with the classic definition of 'civil twilight,' or when the solar angle falls below -6° from the horizon, henceforth defined as 'night'. Furthermore, we observed little to no vertical migration when the solar angle was greater than 6° above the horizon and used that threshold to define the 'day' period. The intervening period, during which organisms are visibly migrating, is defined as 'twilight'; however, no lowered probe measurements were made during this time.
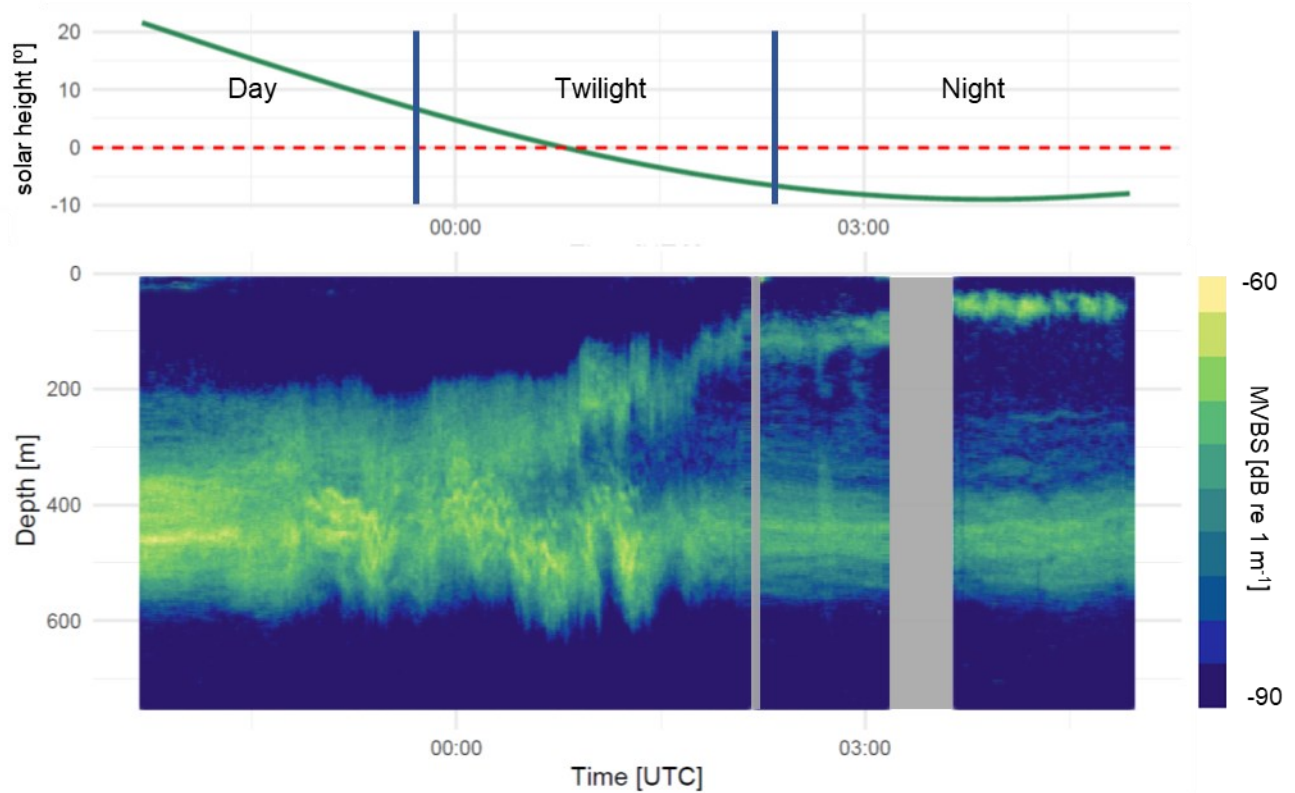
Figure 2.2 Relationship between solar altitude and DVM patterns observed in the Labrador Sea. The upper panel shows the estimated solar height angle based on the location and time of day, which is divided into three ecologically significant periods: Day (> 6°), Twilight (> -6°, < 6°), and Night (< -6°). The red dashed line corresponds to the horizon. The lower panel shows the mean volume backscatter strength calculated for 1-minute x 2.5 m cells. A -60 dB (upper) and -90 dB (lower) thresholds were applied to improve visualization of the dominant scattering layer. Vertical grey bars correspond to omitted data where CTD and net sampling operations took place.

2.3.3 Instrumentation Platform

In-situ broadband measurements were made with a wideband autonomous transceiver (WBAT, Kongsberg ©), equipped with a downward-facing 38 kHz (ES38-18DK) split-beam transducer. The echosounder package was mounted in a simple custom-built steel cage (dimensions 30 x 30 x 120 cm) and operated autonomously with a pre-programmed mission plan. The split-beam transducer transmitted frequency-modulated (FM) pulses in the 35-45 kHz bandwidth to a 200 m range. Each 1.024 ms pulse was transmitted at 450 W in 1 s intervals with an upward, linear

frequency sweep using a 'fast' taper at the beginning and end of the signal. The WBAT was calibrated at 30 m depth after the cruise using a 38.1 mm tungsten-carbide sphere following methods outlined by Stanton & Chu (2008) and Demer et al. (2015). Frequency-dependent gain, G(f), and beam-formation values were applied to raw acoustic data before further processing.

The probe was lowered at a rate of 80 m min^{-1} to approximately 10 m above scattering layers visible during real-time shipboard acquisition of the EK60. At each of the 6 stations, the probe stopped at four depths between 10-625 m (**Table 1**) and remained at each depth for an interval of 200-500 pings (4-8 minutes). CTD measurements were taken at each station using an SBE 911-plus ® and temperature and salinity profiles were used to calculate sound speed (Mackenzie, 1981) and the coefficient of absorption (Francois and Garrison, 1982).

2.3.4 Processing of *in-situ* data

Data was processed through a broadband signal processing pipeline (Figure 2.3). Band-pass filtered echoes from the WBAT were match-filtered (i.e. pulse compression) using the Echoview © post-processing software. Target processing was done using Echoview's wideband single target detection algorithm and echo-traces containing three or more target measurements across multiple pings, were automatically detected using the Echoview target tracking algorithm (see **Supplementary Table 1** for full single target detection and echo-trace selection settings). Echo-traces meeting detection criteria were selected from a range between 3 and 50 m from the transducer. In some cases, the effective measurement range was reduced due to high target densities causing an attenuation of the returned signal. At each depth, TS measurements were adjusted to compensate for depth and environmental dependent absorption values using CTD data. For each target within an echo-trace, the TS(f) spectrum, in dB re 1 m^2 was calculated using the following equation, as implemented in Cotter et al (2021a):

$$TS_{(f)} = 20 \log_{10} V_{targ} + 40 \log_{10}(r_{pk}) + 2\alpha(f)\, r_{pk} + 2G(f) + b(\phi, f) \qquad \text{(eq. 1)}$$

For $34 \le f \le 45$ kHz, where r_{pk} is the range to the peak in the power spectrum (V), $\alpha(f)$ is the frequency-dependent absorption coefficient, and b is the two-way beam pattern as a function of angle (ϕ) and frequency (f). V is calculated using a fast Fourier transform (FFT) with a 0.5 m window. Window size was selected based on the high level of classification accuracy found by Benoit-Bird & Waluk (2020) and applied for mesopelagic organisms by Bassett et al (2020). Prior to further analysis, TS(f) spectra were trimmed to omit 1 kHz portions at either end of the bandwidth to proactively reduce the influence of edge effects on the Fourier transform window (Benoit-Bird & Waluk, 2020). TS(f) curves were calculated for all target detections using 0.1 kHz frequency resolution.
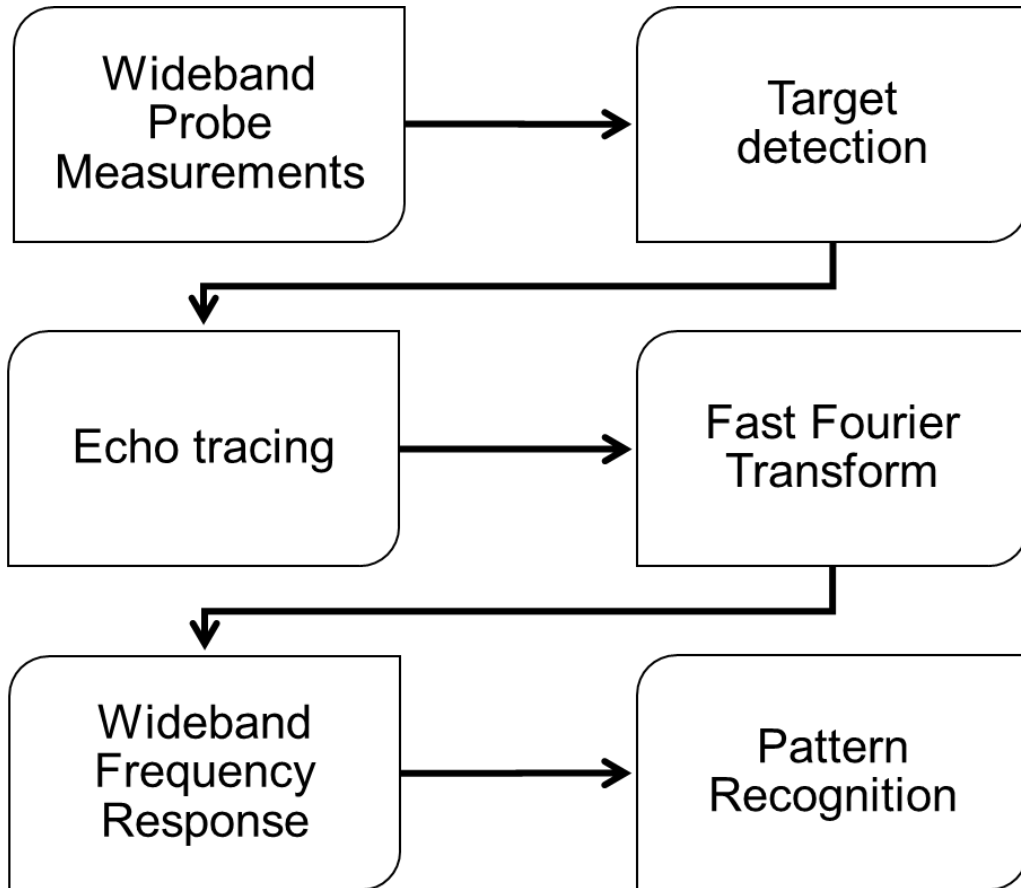
Figure 2.3 Flowchart indicating steps taken within the broadband signal processing pipeline.

2.3.5 Detection of anomalous signals

For the detection of anomalous frequency response signals within the TS(f) spectra dataset, we used hierarchical density-based spatial clustering of applications with noise (HDBSCAN, Campello et al 2015). HDBSCAN is a non-parametric approach for outlier detection that circumvents the need for determining a threshold based on the underlying distribution of the data and has been used to identify anomalous measurements across a range of applications (Lin et al., 2019; Wang et al., 2021; Ye et al., 2021). Embedded within the HBSCAN algorithm is a method called 'global-local outlier scores from hierarchies' (GLOSH), which is particularly effective for data that cannot be depicted in low-dimensional space. This is achieved by partitioning the data using a k-dimension tree and can be calculated in sub-linear time (Hahsler et al., 2019). Compared to other unsupervised outlier detection approaches, such as spectral and nearest-neighbor approaches, HBSCAN is a relatively low computation clustering method that is suitable for datasets containing up to 100 dimensions (Hahsler et al., 2019; ur Rehman and Belhaouari, 2021). Importantly, the algorithm can extract 'flat', or stable, clusters from a data corresponding to an infinite number of density thresholds in an unsupervised way (Campello et al., 2013). We therefore used this approach based on the hypothesis that outliers within our dataset had an unpredictable and stochastic distribution structure that arose from measurement errors that are inherent to *in-situ* and largely unfiltered target measurements. Furthermore, we made no prior assumptions about the amplitude or structure of the frequency response of targets. Due to the relatively narrow bandwidth (36-44 kHz) used in this study, we also assumed there was a low likelihood in distinguishing between taxa.

We implemented the HBSCAN algorithm on all the frequency response curves ($TS_{(f)}$ spectra) meeting basic echo-trace criteria (Supplementary Table 1). Due to the robustness of the HDBSCAN algorithm to large data volumes, we performed no prior feature selection on the data and saw no difference in performance when the data were normalized. Without making assumptions about cluster size, we used the maximum number of targets within in an echo-trace (20) to set the sole parameter of the algorithm—minPts—which represents the minimum cluster size and acts as a smoothing factor for the density estimates. All analysis was done on an Intel ® i9 8 core 2.5GHz CPU with 16 GB RAM running Windows 10. HDBCAN was performed using the implementation in the R package '*dbscan*' (Hahsler et al., 2019).

Sources of anomalous signals. We investigated the impact of variability of TS(f) within echo-trace measurements to assess the impact of measurement error due to weak signals or overlapping targets. To do this, we calculated the complex pulse envelope, $A(t)e^{-i\phi(t)}$ (m^2) of the analytical signal using the following equation as described in Lee & Stanton (2016):

$$A(t) = \sqrt{|f_R(t)|^2 + |f_I(t)|^2} \qquad \text{(eq. 2)}$$

whereby 'real' (R) and 'imaginary' (I) components are the coordinates representing the amplitude and phase of the FFT used to compute the frequency response, or TS(f), of each target.

2.3.6 Density Estimates

The volumetric density of mesopelagic organisms was calculated using an echo-integration approach (Simmonds and MacLennan, 2005). Due to the inherent challenges of echo-counting in high density scattering layers such as the DSL (Cotter et al., 2021), we combined our *in-situ* TS_{38} measurements with the volume backscattering coefficient (s_v, m^{-1}) from the hull-mounted EK60 echosounder. Concurrent mean volume backscattering (S_v, dB re 1 m^{-1}) was calculated at probe-

adjacent depths using the nearest post-deployment 5-minute interval. S_v was used to obtain the volume backscattering coefficient (s_v, m^{-1}) which are related by $S_v = 10 \log10 (s_v)$. Density (ρ_v, individuals / m^3) was calculated using the following equation:

$$\rho_v = \frac{S_v}{\bar{\sigma}_{bs}} \qquad \text{(eq. 3)}$$

Whereby, $\bar{\sigma}_{bs}$ is equal to the depth-dependent mean backscattering cross section (in m^2) at 38 kHz measured by the lowered probe. The mean backscattering cross-section was calculated from the depth-dependent linearly averaged Target Strength (dB re 1 m^2). The relationship between Target Strength and the backscattering cross-section can be expressed as:

$$TS = 10 \log_{10} \sigma_{bs} \qquad \text{(eq. 4)}$$

Anomalous TS measurements, as identified using outlier detection, were removed from echo-traces, and the resulting filtered TS$_{(f)}$ spectra (i.e., outlier removal), were used to calculate the linear average of TS at the nominal frequency, 38 kHz (TS$_{38}$). TS$_{38}$ was then calculated for each depth interval in which the lowered probe was deployed. Our density estimates were then compared with results from previous studies conducted in the Labrador Sea.

2.4 Results

During the expedition to the Labrador Sea, a distinct deep scattering layer was observed between 450 and 600 m, and the shipboard echosounder showed that this scattering layer migrated toward the surface during night and descended to mesopelagic depths during the day (Figure 2.2). The glacier lanternfish, *Benthosema glaciale*, was the dominant species captured by midwater trawl, comprising 97% of fish biomass and 53% of all catch biomass.

A total of 38,122 targets forming 6799 echo-traces were detected between ~40 m and 675 m depth during lowered probe deployments targeting scattering layers seen on the shipboard echosounder. Following implementation of the HDBSCAN algorithm, 64.81% of targets were grouped into a single coherent stable cluster (Figure 2.3). A small number of target spectra (87 targets, ~0.22%) were classified into their own discrete cluster; however, these were likely artefacts of the 'single-linkage' approach whereby objects lying in the sparser regions of the density-space did not fit within the stable cluster hierarchy. Thus, these targets were removed, and no further analyses of these spectra were performed.
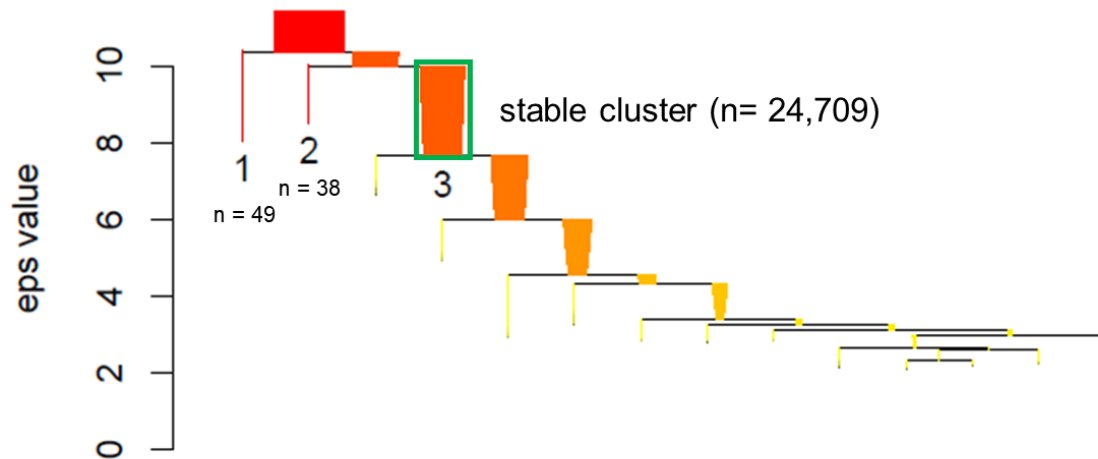
Figure 2.4 HDBSCAN hierarchy tree. This simplified tree shows cluster hierarchy, whereby eps (epsilon) value is equivalent to the radius associated with the density threshold. Cluster width shows cluster wide changes across the range of eps values. Only three clusters were identified The green box highlights the only coherent and stable TS(f) spectra among the three clusters found. By detecting a single stable cluster, the algorithm effectively acts as a de-noising algorithm. The frequency responses of this single stable cluster were later used to compute depth dependent TS_{38}. Subsequent branches on the tree indicate data groupings within cluster 3 with weak associations that were not identified as clusters.

In the outlier detection portion of the HDBSCAN algorithm, 35.2% of targets were identified as outliers, which we refer to as anomalous signals within the $TS_{(f)}$ spectrum. Within the entire

dataset, anomalous-labelled targets displayed a nearly 65 dB variation in TS$_{38}$, with stochastic nulls of varying magnitude occurring across the 36-44 kHz bandwidth (Figure 2.4)
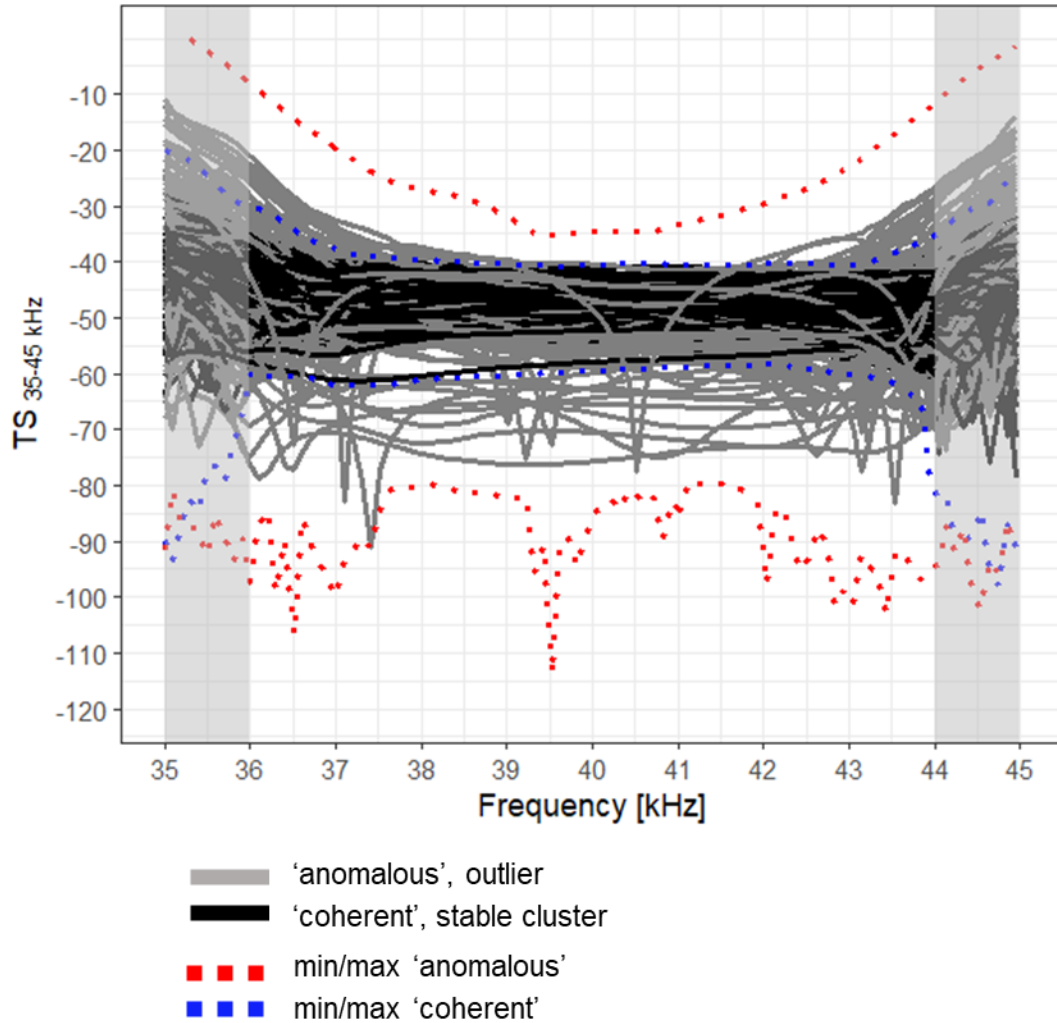
Figure 2.5 Representative TS(f) spectrum measurements for anomalous and coherent broadband signals. TS(f) spectra shown comprise a randomly sampled 1% of the total dataset. Dotted lines show the minimum and maximum values computed from the entire dataset for noise (red) and stable curves (blue). Grey bars indicate the portion of the bandwidth that was removed prior to classification due to known 'edge' effects from the fast Fourier transform.

Comparisons of TS(*f*) within echo-traces showed that both anomalous and coherent spectra were consistently found within individual echo-traces (Figure 2.5). Within the pings comprising an echo-trace, we observed several sources of measurement error which likely contributed to

anomalous TS(f) spectra. First, anomalous target spectra tended to occur within the first and last measurements of an echo-trace (Figure 2.5A). In many cases, anomalous spectra were a result of low amplitude in the frequency domain (i.e. frequency loss), such that anomalous signals were typically weaker than coherent signals (Figure 2.5B). In other cases, the source of anomalous signals appeared to occur when the pulse envelope of nearby targets was included in the analytical window used in the Fourier transform (0.5 m) (Figure 2.5C), thereby reducing the average TS$_{38}$ of an echo-trace. Overall, we observed consistent differences in the total variation of TS$_{38}$, whereby coherent target measurements (i.e. pings) varied by < 0.5 dB and anomalous target measurements varied by up to 5 dB or more over the whole spectrum (Figure 2.5D).
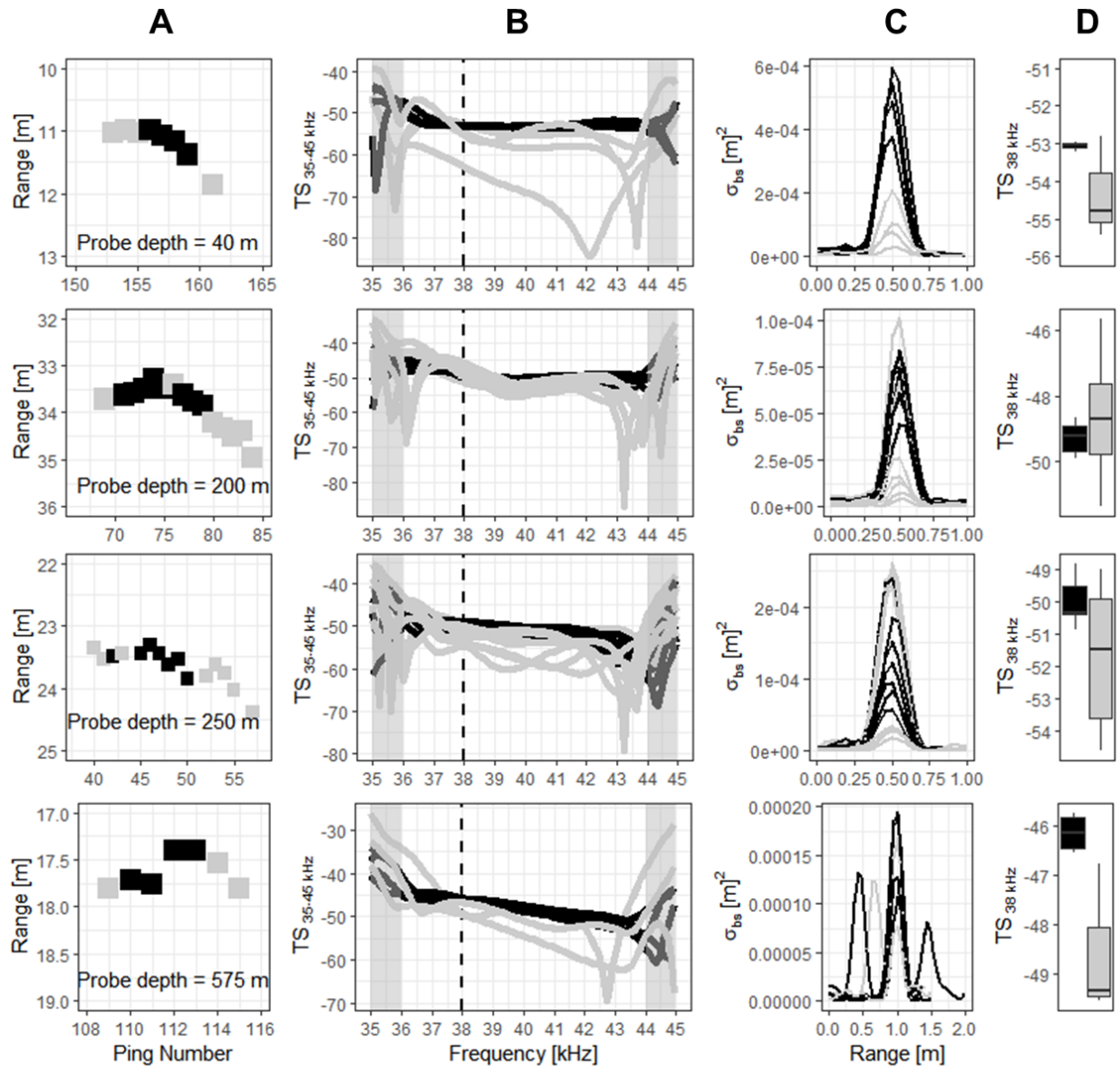
Figure 2.6 Examples of coherent and anomalous target measurement variation within echo-traces. Target position within echo-traces is displayed along the range axis, or distance from transducer of the lowered probe (**A**), echo-trace variation in TS_{35-44} (**B**), complex pulse envelope (σ_{bs}, m^2) (**C**), and TS_{38} distribution (**D**).

When comparing all TS measurements from the survey, we found that the difference in the linearly

averaged TS_{38} between targets that included all anomalous signals (-45.65 dB) and the averaged

TS_{38} of coherent signals only (-46.30 dB) values was relatively low (0.65 dB). However, when we compared the potential bias of including anomalous target measurements, we found differences in the depth distribution of this effect (Figure 2.6). During the day, averages of anomalous target spectra were up to 2.50 dB lower than coherent spectra at mesopelagic depths, and up to 2.80 dB higher at epipelagic depths. When compared to nighttime, we found a similar but less pronounced effect during nighttime, whereby average anomalous signals deviated from coherent signals by up to 1.20 dB.
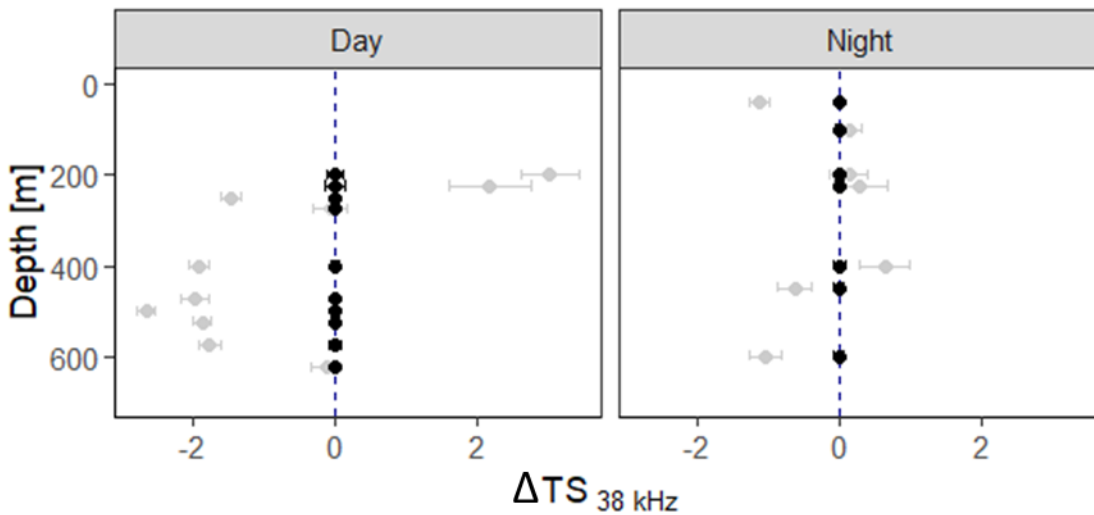
Figure 2.7 Difference of target strength between anomalous and coherent TS_{38} in relation to depth. Grey points indicate the linear average of TS_{38} for anomalous signals, relative to the linear average of TS_{38} for coherent spectra (ΔTS_{38}) +/- the standard error. Black points indicate the corresponding TS_{38} +/- the standard error after removing the anomalous signals.

Calculations at each lowered probe depth interval revealed a general pattern of decreasing target strength with depth. Linear averages of TS_{38} calculated from echo-traces with coherent TS(f) spectra ranged from -52.98 dB (40-90m; nighttime) to -44.40 dB (575-625 m; daytime) (Figure 2.7). Density estimation using echo-integration revealed the highest densities occurred within the DSL depths (400-600 m) during daytime (Figure 2.7). When compared to nighttime, densities in

the DSL decreased by 2.2 individual / 1000 m^3, representing approximately 85% decrease in organisms during the nighttime. Concurrently, densities in the upper water column during the night increased from 0 to up to 1.3 individuals / 1000 m^3 (Figure 7).
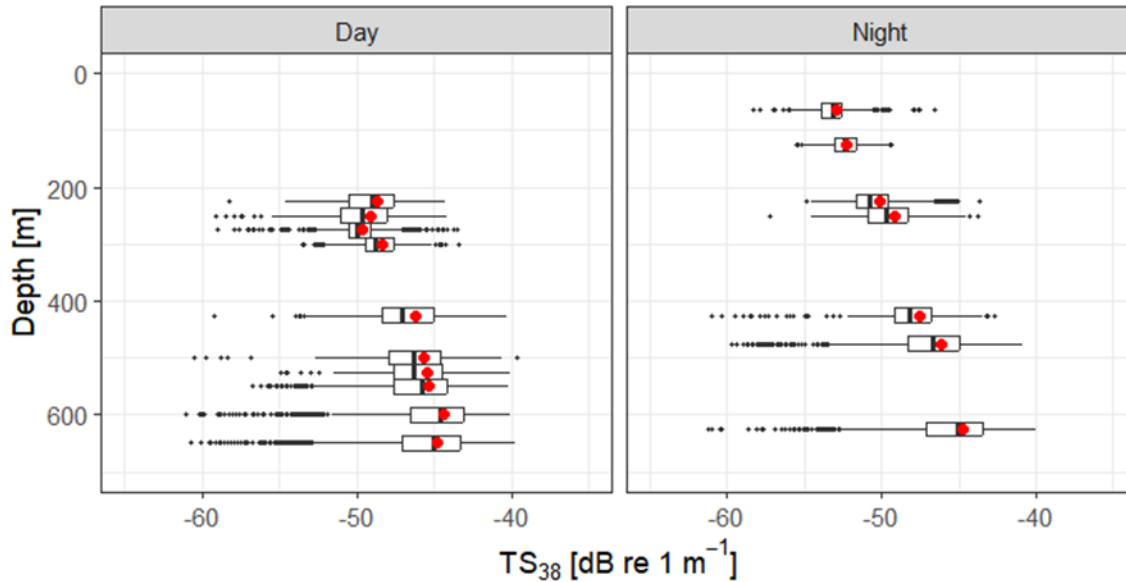
Figure 2.8 *In-situ* average Target Strength measurements (red dots) of coherent signals measured in day (left) and night (right) in relation to depth. Boxplots show maximum, minimum, and median values and boxes with 25th and 75th quartiles range.

Comparison of density estimates between using the linear average of all TS$_{38}$ values before and after anomalous signal detection yielded up to 25.9% bias of target densities during the day, and up to 10% during the night (Figure 2.8). Within the mesopelagic zone during the daytime, the presence of anomalous signals in the dataset would have consistently resulted in a 17-26% underestimation of target density. The two shallowest daytime profiles led to a 19-23% overestimation of target density. Overall, nighttime density estimates were less affected than daytime, where anomalous target bias would have led to a 0.5-10% difference in density.
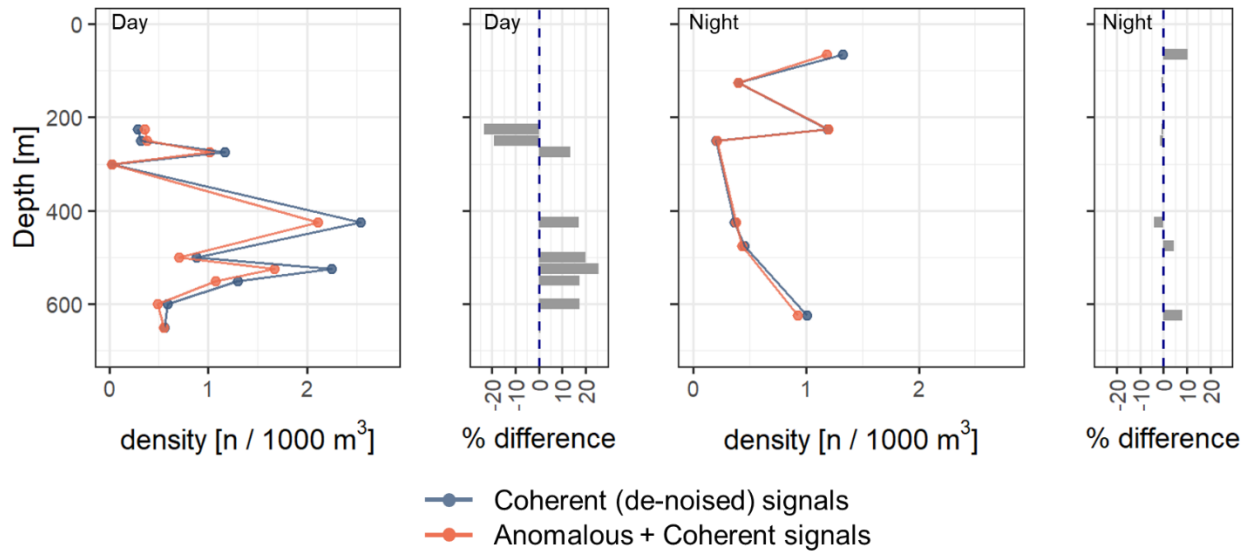
Figure 2.9 Corresponding density of organisms calculated using the depth-dependent linear TS values and the echo-integrated volume backscatter measured with the hull-mounted echosounder including outlier-detection filtered values (blue) vs raw valued calculated prior to outlier detection (orange). Percent (%) difference is calculated as the percent density difference between coherent and unfiltered (anomalous + coherent) targets.

2.4 Discussion

In acoustic studies assessing mesopelagic resources through echo-integration, measuring depth-dependent target strength is a critical component of estimating organism density and biomass (Davison et al., 2015; Bassett et al., 2020; Cotter et al., 2021). In our study, we found that inclusion of stochastic measurements in the target spectra, $TS_{(f)}$, increases dispersion and positively or negatively skews the probability distribution function (PDF) of TS_{38} within an echo-trace. Over the entire survey, the removal of anomalous target measurements had minimal impact on the global linear average of TS (0.65 dB); however, we observed both positive and negative bias within sound-scattering layers at discrete depths. We further demonstrate that the inclusion of anomalous spectra when calculating mean TS of broadband target measurements can result in up to 25% underestimation of organism density within the mesopelagic zone. Our approach, while requiring an understanding of measurement limitations, circumvents some of the challenges an analyst may

45

face when parameterizing broadband target measurements during fisheries survey of mesopelagic resources.

2.4.1 Comparison to other studies

Between the surface and 675 m, we found gas-bearing organism densities ranged between 0 - 2.5 individuals /1000 m^3. When compared to other studies in the NW Atlantic, we found that our density estimates through echo-integration fell within similar density ranges for gas-bearing organisms in the mesopelagic zone (Table 2.2). Along the latitudinal gradient of studies, our density estimates are lower than those seen further south along the North American continental slope (Sameoto, 1988; Pepin, 2013) but are similar to those estimated at nearby latitudes (Sameoto, 1989; Klevjer et al., 2020a) and using acoustic methods in the Arctic (Dias Bernardes et al., 2020). Therefore, these results may lend support to latitudinal impacts on the biogeography of myctophids, which are tied to both temperature and photoperiod (Chawarski et al., 2022; Langbehn et al., 2022). A comparison of nighttime measurements indicates that densities are highest near the surface, whereby a large proportion of the organisms rise to feed at night (i.e. DVM). Interestingly, the impact of TS measurement error on density estimation was reduced during nighttime, presumably due to a vertical dispersion of organisms corresponding to migratory feeding behavior. As concurrent measurements of organisms throughout the 24-cycle were not undertaken at a given site, any further quantitative analysis of vertical patterns may be impeded by spatial and temporal heterogeneity within the transect. However, based on our observations, the DSL of the Labrador Sea appears to contain gas-bearing scatterers at 38 kHz with different diel migration strategies that warrant further study.

2.4.2 The source and impact of anomalous signals

In studies using continuous wave (CW; single frequency) target measurements, TS of the individual is considered a stochastic process with PDF from which a mean can be estimated precisely (Korneliussen et al., 2018). In practice, this is achieved by calculating a linear average of multiple ensonified echoes of an organism (i.e., fish track, or echo-trace). Within an echo-trace, random TS error can be +/- 5-25% (Simmonds & McLennan 2005) due to the combined effect of coherent and incoherent signals (Stanton & Clay 1986). In sound scattering layers, where organisms are small and densities are high, measurement error can be difficult to account for, as there are varying sources of incoherent signals (Kieser et al., 2005). Frequency modulated (FM; broadband pules) signals can overcome some of the uncertainties around target measurements at high densities due to the increased range resolution that comes with matched-filtered processing (also known as pulse compression) (Chu and Stanton, 1998). Simultaneously, FM measurements can also add further complexity to the considerations needed for precise target measurements, through increased parameterization along the signal processing pipeline (Lavery et al., 2017). For instance, if the pulse envelope of the organism exceeds the window size of the fast Fourier transform, it can result in false estimates of the organism's frequency response (Benoit-Bird and Waluk, 2020). Matched-filtered signal processing can also introduce processing side lobes (Chu and Stanton, 1998), requiring an adjustment to the tapering of the transmit signal, which can also lead to loss of frequency content (Lavery et al., 2017). Furthermore, frequency-dependent beam patterns can impact the frequency content, if the beam compensation model is unable to account for target position along the edge of beam (Lavery et al., 2017).

While carrying some of the same error sources as CW measurements, our results suggest that some components of broadband TS(f) measurement error can be reduced by manually inspecting echo

envelopes, filtering off-axis targets, adjusting the fast Fourier transform (FFT) window, or adjusting the parameters of target detection and echo-tracing algorithms. We observed that incoherent TS(f) spectra within echo-traces can occur due to weak insonification of the target (i.e. low signal-to-noise ratio), or insufficient peak separation from nearby targets or residual ringing (Kieser et al., 2005). Typically, these occurred in the first and last measurements of the echo-trace, suggesting that frequency-dependent beam patterns effects may have also played a role. Manual approaches such as filtering off-axis targets can be an effective for measuring broadband TS(f) of single targets (Bassett et al., 2020), yet on the scale of large geographic surveys, can drastically increase the level of effort or yield low sample sizes when organisms are sparsely aggregated. As lowered probes at sound-scattering depths also carry additional measurement constraints, such as heave, drift, and changes in the incident angle of insonification, ideal in-situ measurements remain elusive.

We suggest that the outlier detection approach presented here can be effectively used to refine TS(f) spectra measurements of gas-bearing organisms at depth with a lowered broadband echosounder. While changes in fish orientation, or tilt-angle, can modify the frequency-response curve of fish (Forland et al., 2014), these appear to have little effect on the TS of myctophids in the 35-44 kHz frequency range (Scoulding et al., 2015), especially under the assumption of an air-filled swimbladder (Yasuma et al., 2010). Furthermore, model results suggest that TS for myctophids with small swimbladders (<0.5 mm radius) is driven by volume, rather than shape or orientation (Proud et al., 2018). This suggests that biological variation in the size or orientation of the swim-bladder is unlikely to be the dominant factor in generating incoherent target spectra. Therefore, the anomalous $TS_{(36\text{-}44\ kHz)}$ spectra likely originated from measurement of unwanted echoes.

2.4.3 Identity of scatterers

In the mesopelagic zone of the Labrador Sea, the dominant scattering group is composed of swim-bladdered fish which have a modelled resonance peak near 18-20 kHz (Kloser et al., 2002; Scoulding et al., 2015). Based on acoustic scattering models, it is unlikely that individual fluid-like, or "Rayleigh" scatterers, such as crustacean zooplankton species, would be detected as echo-traces at the 35-44 kHz bandwidth (Stanton et al., 2010). This study was part of a larger sampling program which found, based on trawl data, that glacier lanternfish *B. glaciale* represented 97% of this fish assemblage and 53% of total catch biomass. Based on these results and other acoustic studies in this region (Sameoto, 1989; Pepin, 2013; Klevjer et al., 2020b) and elsewhere (Kloser et al., 2016; Proud et al., 2018), we assume that gas-bearing organisms, namely fish, are the dominant source of target measurements. From our data it is unclear what proportion can be attributed to non-fish taxa, such as physonect siphonophores, which vary in size, distribution, and abundance across regions. Unfortunately, we could not confirm the presence nor absence of siphonophores because they rarely remain intact during trawling and are best observed using optical instrumentation (Warren et al., 2001; Kloser et al., 2016). The variation (up to 10 dB) we observed in coherent TS(f) spectra suggests that the measured organisms may experience resonance near our measured bandwidth, an observation which is consistent with previous studies for mesopelagic fish (Kloser et al., 2002; Scoulding et al., 2015); however, any further analysis of the identity of scatterers based on the $TS_{(f)}$ spectra is outside of the scope of this paper.

2.4.4 Vertical zonation and density of mesopelagic organisms

Following outlier detection and removal of anomalous TS(f) spectra, linear averages of TS_{38} ranged from -53.0 dB (40-90 m, nighttime) to -44.8 dB (575-625 m, daytime). Apart from daytime upper mesopelagic (200-250 and 250-300 m) sampling intervals, the general trend of increasing

TS with depth persisted throughout the water column (Figure 2.4). Probe measurements detected no echo-traces above 200 m during daytime, whereas a total of 479 echo- traces were detected <200m during nighttime (Figure 2.7). These findings are aligned with other studies, which find that daytime residency of myctophids is typically within sound scattering layers below 200 m (Proud et al., 2017; Klevjer et al., 2020a). As target strength provides a measure of acoustic size, the vertical patterns in TS may be related to size-depth relationships which have been reported for other pelagic species (Polloni et al., 1979; Smith and Brown, 2002; Geoffroy et al., 2016). A previous study in the North Atlantic has shown this pattern for *B. glaciale*, but results were limited to nighttime measurements in the upper 180 m (Halliday, 1970). We conducted some limited ad hoc sampling (3 trawl deployments) to depths <100 m during DVM and found a small but significant difference in median size *of B. glaciale* (0.3 mm smaller, t-test, p<0.005, n=846) when compared to integrated trawls between the surface and 500 m. At young stages, *B. glaciale* rely heavily on copepod prey, remaining near the surface before transitioning to deeper waters (Hudson et al., 2014). Therefore, the vertical zonation in TS observed in our study may be linked directly to ontogeny of feeding strategy. TS$_{(f)}$ differences may also be related to variation at the individual level (Proud et al., 2018) or due variation in swim-bladder morphology within the population (i.e. an ontogenetic shift from gas to lipid-filled) (Butler and Pearcy, 1972; Scoulding et al., 2015; Dornan et al., 2019). Furthermore, the ambient pressure at depth may increase swim-bladder density, thereby shifting the resonance region closer to the measured bandwidth (Godø et al., 2009). While we did not assess swim-bladder morphologies in this study, doing so could improve our understanding of the observed TS-depth relationships.

2.4.5 Limitations

After applying the best-known practices for broadband TS measurements, we used an outlier detection approach in $TS_{(f)}$ spectra of broadband mesopelagic targets. We did not perform a full investigation into the sources of anomalies in this data; however, based on the complexity of the signal processing pipeline, further investigations are strongly recommended, particularly in the context of mesopelagic sound-scatterers. Study of incoherent artefacts within the $TS_{(f)}$ spectrum is relatively new in the field of applied fisheries acoustics, and our data-driven approach may reduce the burden of analysis to achieve meaningful ecological data. Overall, the results of our study align well with target strength and density estimates from mesopelagic sound-scattering layers in the NW Atlantic. However, our study did not include a depth-dependent calibration of the echosounder which has been shown to overestimate TS by up to 0.5 dB at DSL depths (Haris et al., 2018). Whilst this level of error could impact the target strength and subsequent density estimates in our study, the effect on the positive TS-depth relationship should be negligible. We also did not account for amplifier linearity discrepancies, which may lead to underestimation of backscatter from echo-integration (De Robertis et al., 2019). Due to this and the potential impact of sound attenuation within the DSL, it is possible that density estimates at the lower depth ranges in our study may have been underestimated.

2.5 Conclusion

Acoustic studies have long dealt with varying sources of noise, including background noise and interference in the environments which can distort echograms (De Robertis and Higginbottom, 2007; Ryan et al., 2015; Wang et al., 2016). Based on our observations of broadband measurements within single echo-traces, our study focuses on incoherent data generated from unwanted echoes that manifest during the measurement of target $TS_{(f)}$ spectra. By removing anomalous spectra from

echo-traces, we reduced the influence of incoherent target measurements and increased the precision of TS_{38} measurements and density estimates of mesopelagic organisms. Using these methods, we observed that TS_{38} generally increased with depth, which suggests that lanternfishes in this region may be vertically structured by size to greater depths than previously observed. The correspondingly low TS values near the surface at nighttime also suggests that smaller *B. glaciale* comprise the dominant migrating signal seen on the hull-mounted echosounder. Our analytical approach bypasses the subjective and lengthy procedure of visually identifying curve shapes or filtering targets using pre-determined thresholds, such as range, target density, or beam position. Our resulting estimates of target strength and density align well with previous studies in the region and should be considered in regionalized biomass estimates in future investigations.

Table 2.1. Sampling domain and results of target strength and density estimates using the wideband acoustic probe. Reported TS values are equal to the linear average from echo-traces after removing anomalous signals. Empty cells correspond to depth ranges where no echo-traces were detected.

Station	Depth Range (m)	Time of Day	# targets	# pings	mean TS_{38} (dB re m^1)	density (10^{-3} m^3)
1. DFO750	10-60	Day	0	243	-	0.00
1. DFO750	100-150	Day	0	319	-	0.00
1. DFO750	250-300	Day	243	272	-49.11	0.32
1. DFO750	500-550	Day	1311	355	-45.43	2.24
2. DFO3	10-60	Day	0	230	-	0.00
2. DFO3	100-150	Day	0	255	-	0.00
2. DFO3	250-500	Day	998	260	-49.61	1.17
2. DFO3	500-550	Day	1730	467	-45.36	1.30
3. DFO5	40-90	Night	543	275	-52.98	1.32
3. DFO5	100-150	Night	248	364	-52.23	0.39
3. DFO5	250-300	Night	361	400	-50.12	1.19
3. DFO5	400-450	Night	326	216	-47.54	0.36
4. DFO7	20-70	Day	0	274	-	0.00
4. DFO7	200-250	Day	245	289	-48.64	0.29
4. DFO7	400-450	Day	1084	280	-46.21	2.54
4. DFO7	575-625	Day	1252	300	-44.40	0.59
5. DFO8	20-70	Day	0	290	-	0.00
5. DFO8	250-300	Day	523	414	-48.34	0.03
5. DFO8	475-525	Day	1137	363	-45.69	0.88
5. DFO8	625-675	Day	1317	410	-44.80	0.56
6. DFO9	20-70	Night	0	313	-	0.00
6. DFO9	200-250	Night	276	322	-49.14	0.20
6. DFO9	450-500	Night	797	380	-46.16	0.45
6. DFO9	600-650	Night	935	380	-44.79	1.01

Table 2.2. Comparison with myctophid densities estimated in other studies of the Northwest Atlantic and Labrador Sea. Ranges of estimates are due to vertical differences (this study), diel differences (Sameoto, 1988, 1989), geographic differences (Pepin, 2013), or the inclusion or exclusion of larger myctophids from estimates (Klevjer et al., 2020b).

Study	Region	Density [10^{-3} ind.·m^3]	Depth range [m]	Method
Sameoto (1988)	Nova Scotia Slope	5.8	0-1000	BIONESS vertical trawl
Sameoto (1989)	Davis Strait	1.7 - 1.8	0-1000	BIONESS vertical trawl
Pepin (2013)	SW slope of the Labrador Sea	3.9 - 12.9	0-750	Echo integration + Oblique trawl
Klevjer et al. (2020)	Central-Eastern Labrador Sea	1.15 - 7.5	0-1000	Oblique trawl
Cotter et al. (2021)	New England Continental Slope	0 - 5	0-800	*In-situ* TS and echo-integration
Bernardes et al. (2020)	Svalbard	0 - 2.5	0-600	*In-situ* TS and echo-integration
This study	NW slope of the Labrador Sea	0 - 2.5	0-675	*In-situ* TS and echo-integration

2.6 References

Agersted, M. D., Khodabandeloo, B., Liu, Y., Melle, W., and Klevjer, T. A. (2021). Application of an unsupervised clustering algorithm on in situ broadband acoustic data to identify different mesopelagic target types . *ICES Journal of Marine Science* 78, 2907–2921. doi: 10.1093/icesjms/fsab167.

Bassett, C., Lavery, A. C., Stanton, T. K., and Cotter, E. D. (2020). Frequency- and depth-dependent target strength measurements of individual mesopelagic scatterers. *J Acoust Soc Am* 148, EL153–EL158. doi: 10.1121/10.0001745.

Benoit-Bird, K. J., and Waluk, C. M. (2020). Exploring the promise of broadband fisheries echosounders for species discrimination with quantitative assessment of data processing effects. *J Acoust Soc Am* 147, 411–427. doi: 10.1121/10.0000594.

Butler, J. L., and Pearcy, W. G. (1972). Swimbladder Morphology and Specific Gravity of Myctophids off Oregon. *Journal of the Fisheries Research Board of Canada* 29, 1145–1150. doi: 10.1139/f72-170.

Campello, R. J. G. B., Moulavi, D., Zimek, A., and Sander, J. (2013). A framework for semi-supervised and unsupervised optimal extraction of clusters from hierarchies. *Data Min Knowl Discov* 27, 344–371. doi: 10.1007/s10618-013-0311-4.

Chawarski, J., Klevjer, T. A., Coté, D., and Geoffroy, M. (2022). Evidence of temperature control on mesopelagic fish and zooplankton communities at high latitudes. *Front Mar Sci* 9. doi: 10.3389/fmars.2022.917985.

Chu, D. (2011). Technology Evolution and Advances in Fisheries Acoustics. *J Mar Sci Technol* 19. doi: 10.51400/2709-6998.2188.

Chu, D., and Stanton, T. K. (1998). Application of pulse compression techniques to broadband acoustic scattering by live individual zooplankton. *Journal of the Acoustical Society of America* 104, 39–55.

Cotter, E., Bassett, C., and Lavery, A. (2021a). Comparison of mesopelagic organism abundance estimates using in situ target strength measurements and echo-counting techniques. *JASA Express Lett* 1, 040801. doi: 10.1121/10.0003940.

Cotter, E., Bassett, C., and Lavery, A. (2021b). Classification of broadband target spectra in the mesopelagic using physics-informed machine learning. *J Acoust Soc Am* 149, 3889–3901. doi: 10.1121/10.0005114.

Davison, P. C., Koslow, J. A., and Kloser, R. J. (2015). Acoustic biomass estimation of mesopelagic fish: backscattering from individuals, populations, and communities. *ICES Journal of Marine Science* 72, 1413–1424. doi: 10.1093/icesjms/fsv023.

De Robertis, A., Bassett, C., Andersen, L. N., Wangen, I., Furnish, S., and Levine, M. (2019). Amplifier linearity accounts for discrepancies in echo-integration measurements from two widely used echosounders. *ICES Journal of Marine Science* 76, 1882–1892. doi: 10.1093/icesjms/fsz040.

De Robertis, A., and Higginbottom, I. (2007). A post-processing technique to estimate the signal-to-noise ratio and remove echosounder background noise. *ICES Journal of Marine Science* 64, 1282–1291. doi: 10.1093/icesjms/fsm112.

Demer, D. A., Berger, L., Bernasconi, M., Bethke, E., Boswell, K. M., Chu, D., et al. (2015). *Calibration of acoustic instruments*. doi: http://dx.doi.org/10.25607/OBP-185.

Demer, D. A., and Conti, S. G. (2003). Validation of the stochastic distorted-wave Born approximation model with broad bandwidth total target strength measurements of Antarctic krill. *ICES Journal of Marine Science* 60, 625–635. doi: 10.1016/S1054.

Demer, D. A., Cutter, G. R., Renfree, J. S., and Butler, J. L. (2009). A statistical-spectral method for echo classification. *ICES Journal of Marine Science* 66, 1081–1090. doi: 10.1093/icesjms/fsp054.

Dias Bernardes, I., Ona, E., and Gjøsæter, H. (2020). Study of the Arctic mesopelagic layer with vessel and profiling multifrequency acoustics. *Prog Oceanogr* 182. doi: 10.1016/j.pocean.2019.102260.

Dornan, T., Fielding, S., Saunders, R. A., and Genner, M. J. (2019). Swimbladder morphology masks Southern Ocean mesopelagic fish biomass. *Proceedings of the Royal Society B: Biological Sciences* 286, 1–8. doi: 10.1098/rspb.2019.0353.

Ehrenberg, J. E., and Torkelson, T. C. (2000). FM slide (chirp) signals: a technique for significantly improving the signal-to-noise performance in hydroacoustic assessment systems. *Fish Res* 47, 193–199. doi: https://doi.org/10.1016/S0165-7836(00)00169-7.

Forland, T., Hobaek, H., Ona, E., and Korneliussen, R. J. (2014). Broad bandwidth acoustic backscatterings from sandeel - measurements and finite element simulations. *ICES Journal of Marine Science* 71, 1894–1903. doi: 10.1038/278097a0.

Francois, R., and Garrison, G. (1982). Sound absorption based on ocean measurments. Part II: boric acid contribution and equation for total absorption. *J. Acoust. Soc. Am* 72, 1879–1890.

Geoffroy, M., Majewski, A., LeBlanc, M., Gauthier, S., Walkusz, W., Reist, J. D., et al. (2016). Vertical segregation of age-0 and age-1+ polar cod (Boreogadus saida) over the annual cycle in the Canadian Beaufort Sea. *Polar Biol* 39, 1023–1037. doi: 10.1007/s00300-015-1811-z.

Godø, O. R., Patel, R., and Pedersen, G. (2009). Diel migration and swimbladder resonance of small fish: Some implications for analyses of multifrequency echo data. *ICES Journal of Marine Science* 66, 1143–1148. doi: 10.1093/icesjms/fsp098.

Grimaldo, E., Grimsmo, L., Alvarez, P., Herrmann, B., Møen Tveit, G., Tiller, R., et al. (2020). Investigating the potential for a commercial fishery in the Northeast Atlantic utilizing mesopelagic species. *ICES Journal of Marine Science*, 1:15. doi: 10.1093/icesjms/fsaa114.

Hahsler, M., Piekenbrock, M., and Doran, D. (2019). dbscan : Fast Density-Based Clustering with R. 91. doi: 10.18637/jss.v091.i01.

Halliday, R. G. (1970). Growth and Vertical Distribution of the Glacier Lanternfish, Benthosema glaciale , in the Northwestern Atlantic . *Journal of the Fisheries Research Board of Canada* 27, 105–116. doi: 10.1139/f70-011.

Haris, K., Kloser, R. J., Ryan, T. E., and Malan, J. (2018). Deep-water calibration of echosounders used for biomass surveys and species identification. *ICES Journal of Marine Science* 75, 1117–1130. doi: 10.1093/icesjms/fsx206.

Hudson, J. M., Steinberg, D. K., Sutton, T. T., Graves, J. E., and Latour, R. J. (2014). Myctophid feeding ecology and carbon transport along the northern Mid-Atlantic Ridge. *Deep Sea Res 1 Oceanogr Res Pap* 93, 104–116. doi: 10.1016/j.dsr.2014.07.002.

Imaizumi, T., Furusawa, M., Akamatsu, T., and Nishimori, Y. (2008). Measuring the target strength spectra of fish using dolphin-like short broadband sonar signals. *J Acoust Soc Am* 124, 3440–3449. doi: 10.1121/1.2990703.

Kaartvedt, S., Langbehn, T. J., and Aksnes, D. L. (2019). Food for Thought: Enlightening the ocean's twilight zone. *ICES Journal of Marine Science*, 1–10. doi: 10.1093/icesjms/fsz010.

Kaufman, L., and Rousseeuw, P. J. (1990). *Find Groups in Data: An Introduction to Cluster Analysis*. 2nd ed. Hoboken, NJ: John Wiley & Sons, Inc.

Khodabandeloo, B., Agersted, M. D., Klevjer, T. A., Pedersen, G., and Melle, W. (2021). Mesopelagic flesh shear viscosity estimation from in situ broadband backscattering measurements by a viscous–elastic model inversion. *ICES Journal of Marine Science* 78, 3147–3161. doi: 10.1093/icesjms/fsab183.

Kieser, R., Reynisson, P., and Mulligan, T. J. (2005). Definition of signal-to-noise ratio and its critical role in split-beam measurements. *ICES Journal of Marine Science* 62, 123–130. doi: 10.1016/j.icesjms.2004.09.006.

Klevjer, T. A., Knutsen, T., and Lorents, D. (2020a). Deep-Sea Research Part II Vertical distribution and migration of mesopelagic scatterers in four north Atlantic basins. doi: 10.1016/j.dsr2.2020.104811.

Klevjer, T., Melle, W., Knutsen, T., Strand, E., Korneliussen, R., Dupont, N., et al. (2020b). Micronekton biomass distribution, improved estimates across four north Atlantic basins. *Deep Sea Res 2 Top Stud Oceanogr* 180, 104691. doi: 10.1016/j.dsr2.2019.104691.

Kloser, R. J., Ryan, T. E., Gordon, K., and Gershwin, L. (2016). Deep-scattering layer, gas-bladder density, and size estimates using a two-frequency acoustic and optical probe. *ICES Journal of Marine Science* 73, 2037–2048. doi: 10.1093/icesjms/fsv257.

Kloser, R. J., Ryan, T., Sakov, P., Williams, A., and Koslow, J. A. (2002). Species identification in deep water using multiple acoustic frequencies. *Canadian Journal of Fisheries and Aquatic Sciences* 59, 1065–1077. doi: 10.1139/f02-076.

Korneliussen, R. J., Berger, L., Campanella, F., Chu, D., Demer, D., Fielding, S., et al. (2018). *Acoustic target classification*. doi: http://doi.org/10.17895/ices.pub.4567.

Kubilius, R., Macaulay, G. J., and Ona, E. (2020). Remote sizing of fish-like targets using broadband acoustics. *Fish Res* 228. doi: 10.1016/j.fishres.2020.105568.

Langbehn, T. J., Aksnes, D. L., Kaartvedt, S., Fiksen, Ø., Ljungström, G., Jørgensen, C., et al. (2022). Poleward distribution of mesopelagic fishes is constrained by seasonality in light. *Global Ecology and Biogeography* 31, 546–561. doi: 10.1111/geb.13446.

Lavery, A. C., Bassett, C., Lawson, G. L., and Jech, J. M. (2017). Exploiting signal processing approaches for Broadband echosounders. *ICES Journal of Marine Science* 74, 2262–2275. doi: 10.1093/icesjms/fsx155.

Lee, W.-J., and Stanton, T. K. (2016). Statistics of Broadband Echoes: Application to Acoustic Estimates of Numerical Density of Fish. *IEEE Journal of Oceanic Engineering* 41, 709–723. doi: 10.1109/JOE.2015.2476619.

Lin, C.-H., Hsu, K.-C., Johnson, K. R., Luby, M., and Fann, Y. C. (2019). Applying density-based outlier identifications using multiple datasets for validation of stroke clinical outcomes. *Int J Med Inform* 132, 103988. doi: https://doi.org/10.1016/j.ijmedinf.2019.103988.

Mackenzie, K. V. (1981). Nine-term equation for sound speed in the oceans. *J. Acoust. Soc. Am* 70, 807–812.

Macqueen, J. (1967). "Some methods for classification and analysis of multivariate observations," in *5th Berkeley Symp. Math. Statist. Prob.,* eds. L. Le Cam and J. Neyman, 281–297.

Malde, K., Handegard, N. O., Eikvil, L., and Salberg, A. (2019). Machine intelligence and the data-driven future of marine science. *ICES Journal of Marine Science*. doi: 10.1093/icesjms/fsz057.

Pepin, P. (2013). Distribution and feeding of Benthosema glaciale in the western Labrador Sea: Fish-zooplankton interaction and the consequence to calanoid copepod populations. *Deep Sea Res 1 Oceanogr Res Pap* 75, 119–134. doi: 10.1016/j.dsr.2013.01.012.

Polloni, P., Haedrich, R., Rowe, G., and Hovey Clifford, C. (1979). The Size-Depth Relationship in Deep Ocean Animals. *Internationale Revue der gesamten Hydrobiologie und Hydrographie* 64, 39–46. doi: 10.1002/iroh.19790640103.

Prellezo, R., and Maravelias, C. (2019). Exploring the economic viability of a mesopelagic fishery in the Bay of Biscay. *ICES Journal of Marine Science* 76, 771–779. doi: 10.1093/icesjms/fsy001.

Proud, R., Cox, M. J., and Brierley, A. S. (2017). Biogeography of the Global Ocean's Mesopelagic Zone. *Current Biology* 27, 113–119. doi: 10.1016/j.cub.2016.11.003.

Proud, R., Handegard, N. O., Kloser, R. J., Cox, M. J., and Brierley, A. S. (2018). From siphonophores to deep scattering layers: uncertainty ranges for the estimation of global mesopelagic fish biomass. *ICES Journal of Marine Science*. doi: 10.1093/icesjms/fsy037.

Ryan, T. E., Downie, R. A., Kloser, R. J., and Keith, G. (2015). Reducing bias due to noise and attenuation in open-ocean echo integration data. *ICES J. Mar. Sci.* doi: 10.1093/icesjms/fsv121.

Sameoto, D. (1988). Feeding of lantern fish Benthosema glaciale off the Nova Scotia Shelf. *Mar Ecol Prog Ser* 44, 113–129. doi: 10.3354/meps044113.

Sameoto, D. (1989). Feeding Ecology of the Lantern Fish Benthosema Glaciale in a Subarctic Region. *Polar Biol* 9, 167–178. doi: 10.1007/BF00297172.

Scoulding, B., Chu, D., Ona, E., and Fernandes, Paul. G. (2015). Target strengths of two abundant mesopelagic fish species. *J Acoust Soc Am* 137, 989–1000. doi: 10.1121/1.4906177.

Simmonds, E. J., and MacLennan, D. N. (2005). *Fisheries acoustics, 2nd edition*. London: Chapman and Hall.

Smith, K. F., and Brown, J. H. (2002). Patterns of diversity, depth range and body size among pelagic fishes along a gradient of depth. *Global Ecology & Biogeography* 11, 313–322.

St. John, M. A., Borja, A., Chust, G., Heath, M., Grigorov, I., Mariani, P., et al. (2016). A Dark Hole in Our Understanding of Marine Ecosystems and Their Services: Perspectives from the Mesopelagic Community. *Front Mar Sci* 3, 1–6. doi: 10.3389/fmars.2016.00031.

Stanton, T., and Clay, C. (1986). Sonar echo statistics as a remote-sensing tool: Volume and seafloor. *IEEE Journal of Oceanic Engineering* 11, 79–96. doi: 10.1109/JOE.1986.1145139.

Stanton, T. K., and Chu, D. (2008). Calibration of broadband active acoustic systems using a single standard spherical target. *J. Acoust. Soc. Am* 124, 128–136. doi: 10.1109/OCEANSKOBE.2008.4530923.

Stanton, T. K., Chu, D., Jech, J. M., and Irish, J. D. (2010). New broadband methods for resonance classification and high-resolution imagery of fish with swimbladders using a modified commercial broadband echosounder. *ICES Journal of Marine Science* 67, 365–378. doi: 10.1093/icesjms/fsp262.

ur Rehman, A., and Belhaouari, S. B. (2021). Unsupervised outlier detection in multidimensional data. *J Big Data* 8, 80. doi: 10.1186/s40537-021-00469-z.

Wang, L., Chen, P., Chen, L., and Mou, J. (2021). Ship AIS Trajectory Clustering: An HDBSCAN-Based Approach. *J Mar Sci Eng* 9. doi: 10.3390/jmse9060566.

Wang, X., Zhang, J., and Zhao, X. (2016). A post-processing method to remove interference noise from acoustic data collected from Antarctic krill fishing vessels. *CCAMLR Science* 23, 17–30.

Warren, J. D., Stanton, T. K., Benfield, M. C., Wiebe, P. H., Chu, D., and Sutor, M. (2001). In situ measurements of acoustic target strengths of gas-bearing siphonophores. *ICES Journal of Marine Science* 58, 740–749. doi: 10.1006/jmsc.2001.1047.

Xiao, Y., and Yu, J. (2012). Partitive clustering (K-means family). *Wiley Interdiscip Rev Data Min Knowl Discov* 2, 209–225. doi: 10.1002/widm.1049.

Yasuma, H., Sawada, K., Takao, Y., Miyashita, K., and Aoki, I. (2010). Swimbladder condition and target strength of myctophid sh in the temperate zone of the Northwest Paci c. *ICES Journal of Marine Science* 67, 135–144.

Ye, J. Y., Yu, C., Husman, T., Chen, B., and Trikala, A. (2021). Novel strategy for applying hierarchical density-based spatial clustering of applications with noise towards

spectroscopic analysis and detection of melanocytic lesions. *Melanoma Res* 31, 526–532. doi: 10.1097/CMR.0000000000000771.

2.6 Supplemental Tables & Figures

Supplementary Table 1. Single target and fish tracking settings used in Echoview.

Single Target Detection Settings	
TS threshold (dB)	-70
pulse length determination level (dB)	6
min. normalized pulse length	0.5
max. normalized pulse length	1.5
min. target separation (m)	0

Fish Tracking Settings	Major Axis	Minor Axis	Range
Alpha:	0.7	0.7	0.7
Beta:	0.5	0.5	0.5
Target Gates Exclusion Distance:			
	4	4	0.5
Maximum gap between pings =			1
Minimum number of targets in track=			3
Minimum number of pings in track=			3

Supplementary Table 2. Catch composition from 15 Isaac-Kidd Midwater trawl deployments conducted in 2018 and 2019.

Group	Order	Family	Species	Biomass (g)	Abundance (n)
Fish	Myctophiformes	Myctophidae	*Benthosema glaciale*	7529	4384
Fish	Stomiiformes	Gonostomatidae	*Cyclothone microdon*	10	38
Fish	Argentiniformes	Bathylagidae	*Bathylagus euryops*	140	22
Fish	Myctophiformes	Myctophidae	*Lampanyctus macdonaldi*	85	15
Fish	Myctophiformes	Myctophidae	*Lampadena speculigera*	184	12
Fish	Stomiiformes	Stomiidae	*Stomias boa*	65	9
Fish	Arctozenus risso	Paralepididae	*Arctozenus risso*	110	4
Fish	Anguilliformes	Nemichthyidae	*Nemichthys scolopaceus*	98	1
Fish	Scorpaeniformes	Liparidae	*Liparis fabricii*	1	1
Fish	Pleuronectiformes	Pleuronectidae	*Reinhardtius hippoglossoides*	1	2
Fish	Myctophiformes	Myctophidae	*Protomyctophum arcticus*	1	1
Fish	Stomiiformes	Stomiidae	*Borostomias antarcticus*	10	1
Crustacea	Euphausiacea	Euphausiidae	*Meganyctiphanes norvegica*	475	1410
Crustacea	Decapoda	Sergestidae	*Sergestes arcticus*	731	1133
Crustacea	Amphipoda	Hyperiidae	*Themisto sp.*	88	557
Crustacea	Decapoda	Sergestidae	*Sergia robusta*	238	403
Crustacea	Lophogastrida	Gnathophausiidae	*Gnathophausia zoea*	124	172
Crustacea	Decapoda	Acanthephyridae	*Acanthephyra pelagica*	274	93
Crustacea	Calanoida	Euchaetidae		1	51
Crustacea	Decapoda	Pasiphaeidae	*Pasiphaea multidentata*	7	30
Crustacea	unknown			1	5
Crustacea	Cypridinidae	Gigantocypris	*Gigantocypris muelleri*	2	1
Crustacea	Mysida	Mysidae	*Boreomysis tridens*	1	1
Molluscs	Oegopsida	Gonatidae	*Gonatus sp.*	143	58
Molluscs	Pteropoda	Clionidae	*Clione limacina*	10	33
Molluscs	Pteropoda	Limacinidae	*Limacina sp.*	1	8
Gelatinous	Aphragmophora	Sagittidae		1372	2407
Gelatinous	Cydippida	Pleurobrachidae		108	113
Gelatinous	unknown			583	110
Gelatinous	Beroida	Beroidae	*Beroe sp.*	50	30
Gelatinous	Coronatae	Periphyllidae	*Periphylla periphylla*	1632	15

Chapter 3. Evidence of temperature control on mesopelagic fish and zooplankton communities at high latitudes

This chapter formed the basis of the publication:

Chawarski, J., Klevjer, T. A., Coté, D., & Geoffroy, M. (2022). Evidence of temperature control on mesopelagic fish and zooplankton communities at high latitudes. Frontiers in Marine Science, 9. https://doi.org/10.3389/fmars.2022.917985

3.1 Abstract

Across temperate and equatorial oceans, a diverse community of fish and zooplankton occupies the mesopelagic zone, where they are detectable as sound-scattering layers. At high latitudes, extreme day-night light cycles may limit the range of some species, while at lower latitudes communities are structured by dynamic ocean processes, such as temperature. Using acoustic and oceanographic measurements, we demonstrate that latitudinal changes in mesopelagic communities align with polar boundaries defined by deep ocean temperature gradients. At the transition to cold polar water masses we observe abrupt weakening and vertical dispersion of acoustic backscatter of mesopelagic organisms, thereby altering the structure of the mesopelagic zone. In the Canadian Arctic, we used biological sampling to show that this boundary is associated with a significant change in the pelagic fish community structure. Rapid ocean warming projected at mesopelagic depths could shift these boundaries with far-reaching effects on ecosystem function and biogeochemical cycles.

3.2 Introduction

At mid-latitudes, the mesopelagic zone (i.e. depths ranging from 200 - 1000 m) houses communities of macrozooplankton and micronekton (Irigoien et al., 2014; Sutton et al., 2017) which occur in localized biomass peaks below the sunlit waters (Bianchi et al., 2013). As mid-trophic level organisms, many species in these communities link primary and microbial production with higher trophic levels, including megafauna (Lehodey et al., 2010; Choy et al., 2016; Bode et al., 2021; Schaber et al., 2022). Due to their nocturnal feeding migrations to surface waters, mesopelagic organisms also play an active role in the biological carbon pump (Davison et al., 2013; Irigoien et al., 2014). Global biomass estimates put mesopelagic fish resources between 2-20 gigatonnes, or roughly 100 times more than the annual catch of all other fisheries combined

(Hidalgo and Browman, 2019). For a large portion of the global oceans, this mesopelagic biomass, measured as deep sound-scattering layers (DSLs), is dominated by lanternfishes and other low light adapted species (Catul et al., 2011). However, at high latitudes extreme seasonal variation and productivity sustains mostly polar-adapted organisms with unique life-history strategies and migration behaviors (Knutsen et al., 2017; Geoffroy et al., 2019; Vedenin et al., 2020).

Toward the poles, marine ecosystems are heavily influenced by seasonality, with extreme variation of light and sea surface temperature over the year. While temperature has direct effects on physiological rates (Gillooly et al., 2001), light influences the ecology of vertically migrating plankton and fish, with critical impacts on their predation and survival (Kaartvedt, 2008; Ljungström et al., 2021). According to prevailing ecological theory, diel variation in light explains the horizontal distribution range of vertically migrating mesopelagic fish, such as lanternfish (family Myctophidae) (Langbehn et al., 2022). Under this theory, the extreme light regime presented at high latitudes, with periods of constant illumination and constant darkness, hinders the establishment of viable populations of mesopelagic fish toward the poles (Langbehn et al., 2022). Polar and equatorward mesopelagic communities should thus vary considerably in their structure and functioning along the gradient of seasonal light availability. Yet, observational challenges to studying mesopelagic systems at high latitudes leave it unclear if transitions in mesopelagic structure occur gradually across photoperiod gradients or are constrained by other ocean processes, such as temperature.

Temperature is a dynamic ocean variable that influences marine community structure on global scales (Hoegh-Guldberg and Bruno, 2010). In ectotherms, metabolism is universally temperature-dependent (Gillooly et al., 2001; Bruno et al., 2015), and because metabolism fuels all organism processes and activities, temperature constraints scale from individual processes to species

interactions (Rall et al., 2010) and ecosystems (López-Urrutia et al., 2006). Temperature thus shapes ecological communities and influences properties of the environment, including, for example, carbon remineralization depths (Boscolo-Galazzo et al., 2018, 2021). Temperature may also modulate both food demand and availability, altering the biological profile of the pelagic realm. As we currently lack comprehensive knowledge of the life-history of mesopelagic fishes (and their thermal tolerances), predictions of community-wide response to environmental change remains limited, particularly in poleward systems.

The relative importance of environmental gradients, such as photoperiod (Kaartvedt 2008) and temperature (Proud et al., 2017) or mesoscale features (Godø et al., 2012) to changes in mesopelagic community structure are uncertain. Acoustic measurements of backscatter enable mapping of the 'biological profile', revealing the distribution of pelagic macrozooplankton and micronekton throughout the water column (Benoit-Bird and Lawson, 2016). In this study, we use hull-mounted echosounders and ADCPs lowered in the water column along transects crossing polar fronts in both the Eastern Canadian Arctic and Southern Ocean to assess the impact of temperature boundaries on the distribution of mesopelagic organisms. We demonstrate that poleward dispersal of the globally coherent DSL is aligned with basin-scale mesopelagic temperature boundaries.

3.3 Materials & Methods

3.3.1 Acoustic Data

Shipboard acoustics were collected by two vessels during different sampling campaigns (Supplementary Fig. 1). In the Canadian Arctic, data were collected aboard the research icebreaker CCGS Amundsen during the Integrated Studies and Ecosystem Characterization of the Labrador Sea Deep Ocean (ISECOLD) cruise in July and August 2018. In the Southern Ocean, data were

collected in February 2008 along the 30ºE section aboard the Norwegian research vessel G.O. Sars. Shipboard measurements from both cruises were made using an EK60 38 kHz scientific echosounder calibrated using the standard-sphere method (Demer et al., 2015).

The lowered acoustic Doppler profilers (LADCP) were mounted on CTD-rosettes and lowered to within 5 m of the bottom. The 300 kHz LADCP data in the Canadian Arctic were collected aboard the CCGS Amundsen during the ISECOLD (2018 and 2019 cruise), the Department of Fisheries and Oceans Canada Atlantic Zone Offshore Monitoring Program (AZOMP) in 2019, and the Takuvik Green Edge expedition to Baffin Bay in 2016. Data for these expeditions were available from the Polar Data Catalogue hosted by the Canadian Cryospheric Information Network (CCIN) (Forest et al., 2020). LADCP data for the Southern Ocean were downloaded from the National Centers of Environmental Information (NCEI) database (Firing et al., 2019) and were available from sections in 2005, 2007, 2008, and 2014.

3.3.2 CTD profiles

Temperature and salinity profiles for the Canadian Arctic were collected from the CCGS Amundsen during the 2016, 2018 and 2019 campaigns using a Seabird © SBE 911+ deployed concurrently with the LADCP. Additional profiles from 2014 were downloaded from the Clivar & Carbon Hydrographic Data Office (CCHDO) database (Lee and Gobat, 2020). Temperature and salinity for the Southern Ocean from 2008 were also collected using a Seabird © SBE 911+ with concurrent LADCP measurements and were downloaded from the CCHDO database. (Speer, 2020)

3.3.3 Data processing

Backscatter from shipboard echosounders (S_v, dB re 1 m^{-1}) was calculated according to MacLennan et al. (2002). Sound-speed and absorption were calculated from CTD data

(Mackenzie, 1981) and applied to backscatter values. For display purposes, -60 to -87 dB range was applied to the data to highlight the dominant mesopelagic signal.

Backscatter from LADCP units was calculated according to Mullison (Mullison, 2017) (eq. 1) with factory supplied calibration constants per beam. Vertical profiles of sound-speed and absorption were calculated from the concurrent CTD profiles and were used when converting the LADCP counts to (relative) backscattering values.

$$S_{V(rel, dB)} = C + 10 \log 10 \left((T_X + 273.16) R^2 \right) - L_{DBM} - P_{DBW} + 2\alpha R + 10 \log 10 \left(10^{k_c(E - E_r)/10} - 1 \right)$$ (eq. 1)

where C is an instrument specific constant, T is the temperature at the transducer (in °K), R is the along-beam range to the measurement, L_{DBM} is $10 log_{10}$ transmit pulse length in meters, P_{DBW} is $10 log_{10}$ transmit power in watts, α is the acoustic absorption (in dB m^{-1}), E is the echo strength (in counts), E_r is received noise (in counts), and k_c is the Returned Signal Strength Indicator (RSSI) slope, a beam specific constant relating amplitude counts to the decibel scale. For Canadian Arctic data, we used factory supplied calibration constants and for the Southern Ocean data we used a generic instrument value of 0.45 dB count^{-1}. The high levels of sound-absorption at 300 kHz means that a hull-mounted transducer will have a very limited observational range before the signal from organisms drops below the noise-level. As backscatter is largely dependent on organism size; organisms much smaller than the wavelength (4.5 mm at 300 kHz and 1500 m s^{-1} sound speed) will give very little echo. Thus, the deployment of high-frequency acoustic equipment on a lowered platform, such as the CTD, enables observation of relatively small, weakly scattering animals at depths that surpass the range and vertical coverage of high frequency hull-mounted sounders.

The Gini index is a metric used to quantify resource inequalities (Gini Index, 2008), ranging from 0 for a perfectly evenly distributed resource to a value of 1 for maximum inequality. We here use

the Gini index to quantify the level of uniformity of backscatter within the vertical domain i.e., a high index will reflect that much of the backscatter strength originates from a discrete scattering layer. To minimize influence of changes stemming from diel vertical migration, nighttime data were omitted whereby only casts when the sun was >6 degrees above the horizon were used. Gini indices were calculated for each vertical profile using the R package 'ineq' (Zeileis, 2014).

3.3.4 Biological Sampling

Mesopelagic fish were captured at 26 stations aboard the CCGS *Amundsen* using an Isaac-Kidd midwater trawl (IKMT) in 2020-2021 (Supplementary Fig. 2). The net had a 13.5 m^2 (4.5 m x 3 m) aperture and was equipped with a 3/4 inch stretched forward mesh and a ½ inch stretched codend mesh. Tows were performed obliquely at a speed of 2-3 m/s to depths ranging between 100 and 800 m to match the depth of the acoustic scattering layers. Catch was sorted to species, where possible. No net data were available across the polar front in the Southern Ocean and hence, community analysis was restricted to the Canadian Arctic in this study.

3.3.5 Community Analysis

To compare the assemblage structures of adult fishes captured at mesopelagic depths on either side of the polar front, multivariate analysis was performed using the 'vegan' R package (Okansen et al., 2020). To reduce weighting of the dominant family Myctophidae, data was standardized using a Wisconsin double standardization and square root transformed. Similarity matrices of the abundance of mesopelagic fish across sites were then constructed using a Bray-Curtis Index (Bray and Curtis, 1957). In our final analysis, we used a family level taxonomy and omitted records containing singular occurrences of species, which were associated with coastal assemblages. An analysis of similarity (ANOSIM ; (Clarke, 1993) was performed on the resulting dissimilarity

matrix to statistically evaluate community differences on either side of the polar boundary. Non-metric multidimensional scaling (nMDS) was used to provide a two-dimensional visual representation of fish assemblage structure.

3.4 Results

3.4.1 Changes in fish communities across temperature boundaries

In both the northern and southern hemispheres, backscatter decreased by up to 97% when crossing the boundaries of distinct polar and subpolar water masses in the upper mesopelagic zone (Fig. 1). This pattern emerged from acoustic data, continuously recorded on transects crossing these boundaries, at 38 kHz, a frequency efficient at detecting swim-bladdered fish. In the Canadian Arctic, the disruption of the deep-scattering layer occurred in the Davis Strait ($\sim 66°$ N) at the interface between Arctic intermediate water and the West Greenland Irminger Current (Curry et al., 2014), known as the West Greenland Polar Front. Mesopelagic (200-1000m) temperatures in the Labrador Sea ranged from 4-5° C and decrease to 1-2° C in Baffin Bay. In the southern hemisphere, the disruption of the deep-scattering layer occurred along the Antarctic Polar front, where Antarctic intermediate water and upper circumpolar deep water converge (Orsi et al., 1995). Here, mesopelagic temperatures decreased more gradually with latitude and ranged from 2.5-3.5° C north of the polar front and dropped to approximately 2° C south of the front.
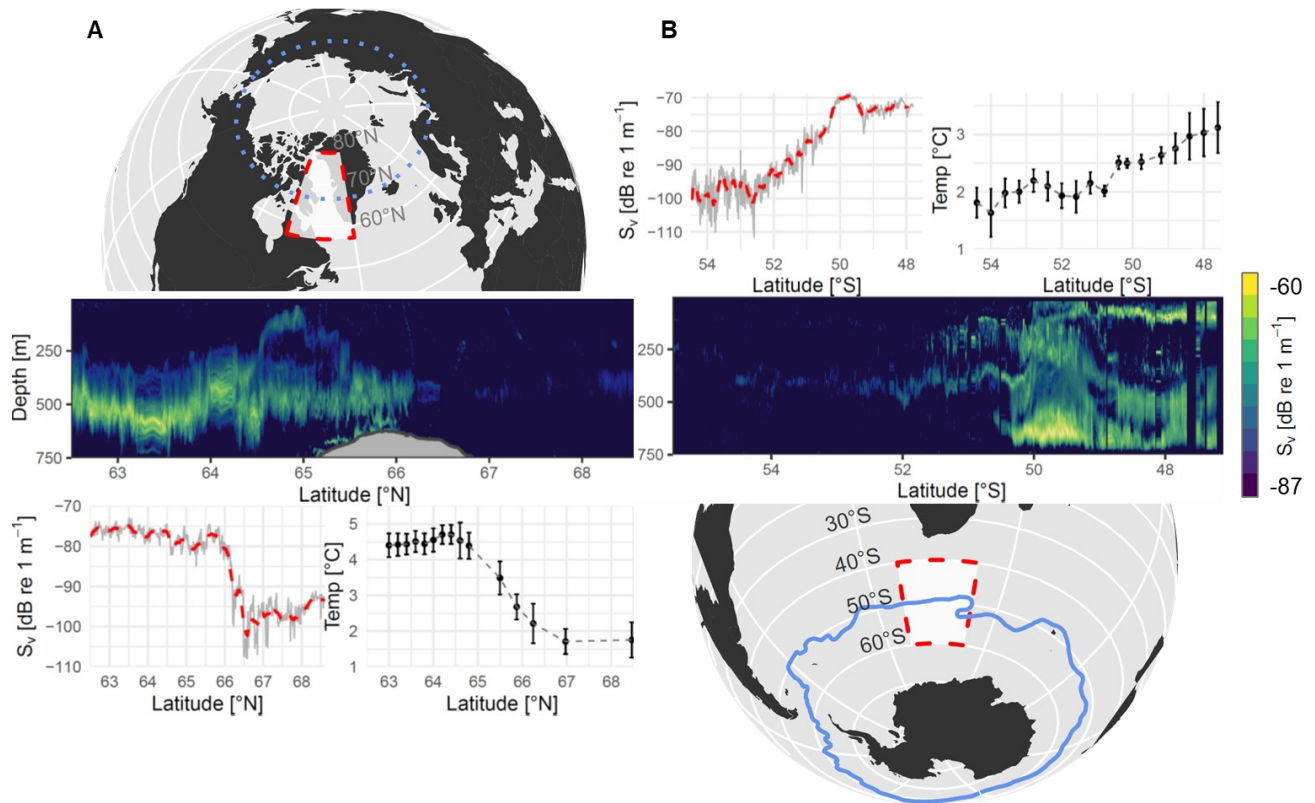
Figure 3.1 38 kHz acoustic backscatter across polar transition zones. Backscatter volume strength (S_v, db re 1 m^{-1}) collected during a latitudinal transect crossing the Arctic Circle in the Davis Strait (**A**) and the Antarctic sub-polar current (**B**). Echograms display acoustic backscatter calculated for 1 km long x 2.5 m deep intervals. Upper and lower thresholds of -87 to -60 dB were applied to facilitate visualization of the deep-scattering layers. Solid grey and red dashed lines represent S_v of upper water column (0-750 m) and a two-sided 25 km moving average, respectively. Temperature panels show mean +/- standard deviation of temperature in the mesopelagic zone (200-1000 m). Dotted blue line in left map panel indicates the position of the Arctic circle and solid blue line in right map panel indicates the Antarctic polar front.

A total of 1620 mesopelagic fish were captured in the Canadian Arctic in 2020-2021. The family-level community analysis showed that sites across the West Greenland polar front, distinguished by the deep water masses of the Labrador Sea and Baffin Bay, had significantly different fish communities (ANOSIM, R=0.67, p=0.001). P-value is based on 999 permutations. The resulting nMDS plot (Fig. 2) revealed all but one sites grouped according to their positions relative to the polar front. South of the front, the fish community in the Atlantic waters of the Labrador Sea was

characterized by a combination of four major fish families: Myctophidae (lanternfishes), Stomiidae (dragonfishes), Gonostomatidae (bristlemouths), and Bathylagidae (pencil-smelts). North of the front, the fish community in the Arctic waters of Baffin Bay was characterized by the families Gadidae (cods) and Liparidae (snailfishes). While there was a significant difference in overall community structure, a small number (n=40) of *Benthosema glaciale* were captured in the cold waters of Baffin Bay.
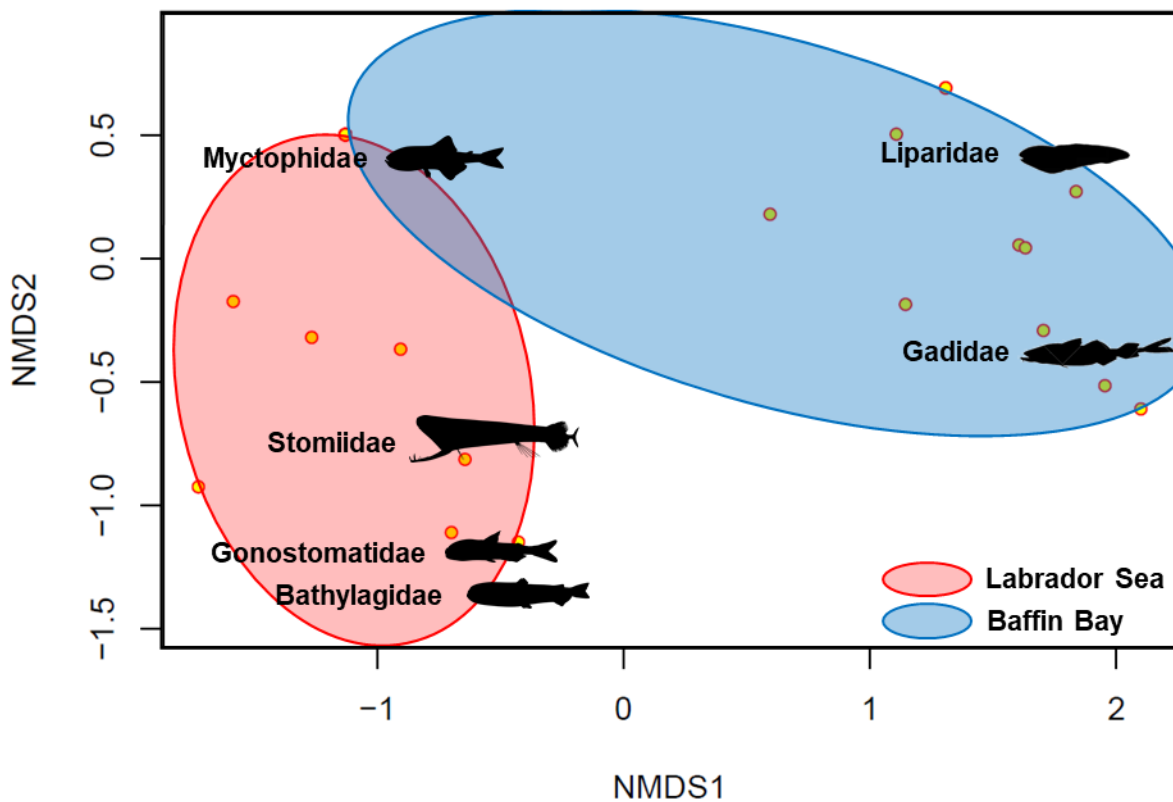
Figure 3.2 Family-level fish community response across the West Greenland Polar Front in the Canadian Arctic. Ordination plot using non-metric multidimensional scaling (nMDS, stress=0.057) of IKMT adult fish captured in the Canadian Arctic. Each sample (yellow) represents an individual site. Colored ellipses are computed to enclose all points along the boundary of groups representing fish families found in the Labrador Sea (red) and Baffin Bay (blue). Families (and representative images) are plotted as centroids and are computed as the weighted average scores in the ordination space.

3.4.2 Poleward changes in vertical structure of mesozooplankton

High frequency LADCP profiles, at frequencies suitable to detect mesozooplankton down to ~0.5-1 cm in size, revealed a similar poleward reduction in backscatter in the mesopelagic zone (Fig. 3A, B). These profiles further highlighted a concurrent shift in the dispersion of backscatter below the photic zone, through the meso- and bathy- pelagic water column (Fig 3 C, D). Using the Gini inequality index (Gini Index, 2008), which is independent of the coincident reduction in relative backscatter levels (S_v [rel, dB re $1m^{-1}$]), we found biological backscatter in subpolar waters to be concentrated within a deep-scattering layer (high inequality). In contrast, in polar waters we observed a consistently uniform distribution of organisms in the water column. In both hemispheres, our observations were strongly tied to water masses on either side of the polar front (Fig. 3.3 E, F).
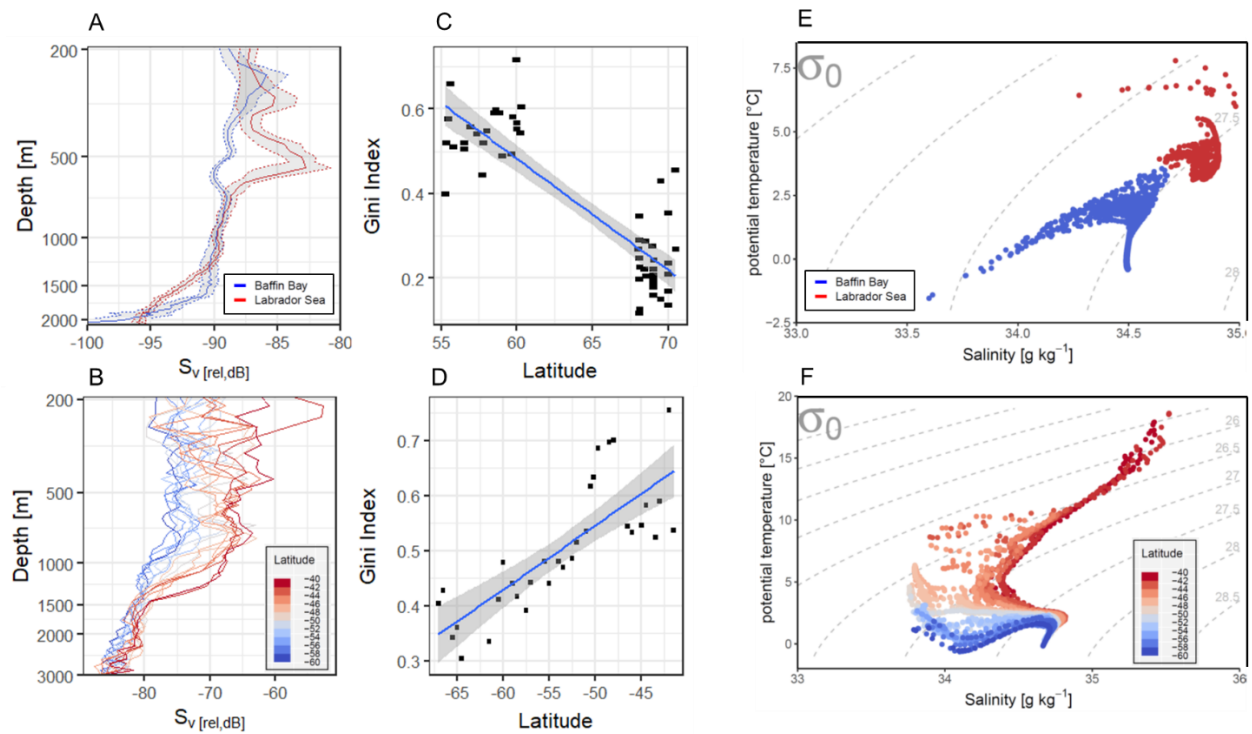
Figure 3.3 LADCP backscatter and Temperature-Salinity plots profiles across polar transition zones. 300 kHz LADCP profiles from the deep basins of the Labrador Sea in 2018 and 2019 and Baffin Bay in 2016 (A) and 150 kHz LADCP profiles along the southern transect (30°E line in 2008) across the Polar Frontal Zone (PFZ) (B). Vertical LADCP profiles in the Southern Ocean are presented as average backscatter per decimal degree. Vertical LADCP profiles in the Labrador Sea and Baffin Bay are presented as averages (solid lines) and 95% confidence intervals (dashed lines and grey shading). The corresponding Gini Index between 200 m depth and the seafloor for all stations deeper than 1500m along the northern transects (C) and corresponding Gini Index between 200-3000m for all stations in the Southern Ocean (D). Temperature-salinity diagrams from concurrent measurements in the Canadian Arctic (Baffin Bay/Labrador Sea) (E) and the Southern Ocean (F).

3.5 Discussion

The poleward dissolution of the deep-scattering layer (DSL) and subsequent dispersion over the water column clearly aligns with deep temperature boundaries (i.e., polar fronts) between basin-scale oceanographic regimes. In both hemispheres, the high-latitude change in mesopelagic

structure coincides with boundaries between previously defined biogeographical provinces (Longhurst, 2007; Sutton et al., 2017). In the northern hemisphere, changes in backscatter occurred near the Arctic circle (66° N) where photoperiod should begin to limit the success of low-light adapted lanternfishes (Kaartvedt, 2008; Ljungström et al., 2021), yet the boundary also occurred directly at the transition between warm and cold basin waters (Fig. 1). In the southern hemisphere, similar changes occurred along the Antarctic polar front, roughly 1700 km north of the Antarctic circle where photoperiod is presumed to constrain certain species. Together, these observations lend support to the idea that temperature plays a key role in structuring mesopelagic communities. We show that at high latitudes both the absolute levels of backscatter in DSLs, as well as the relative proportion of total mesopelagic backscatter found inside DSLs, are reduced. At lower latitudes, studies (Irigoien et al., 2014; Peña et al., 2014; Davison et al., 2015) implicitly suggest that a high proportion of pelagic biomass of micronekton and zooplankton are found within scattering layers, whereas our observations suggest that at high latitudes, the biomass is more evenly distributed over the water column (Fig. 3). We call this effect the vertical dispersion of biomass, and note that it is likely to result in very different vertical patterns of intra- and interspecific interactions, i.e. vertical patterns of ecology. It remains unclear if the observed correlation between temperature and vertical dispersion is due to an altered prey field or physiological limitations of certain species; however, the outcome likely yields a major shift in resource partitioning, active carbon export, and overall ecosystem function.

Among DSLs in mid to high-latitude oceanic systems, a large proportion of 38 kHz acoustic backscatter is attributed to swim-bladdered fish (Irigoien et al., 2014), but due to a potential shift in swim-bladder morphology, interpretations of weakening of mesopelagic backscatter as indicative of biomass decreases across such boundaries can be misleading (Dornan et al., 2019).

However, the same pattern observed here was also evident in higher frequency backscatter (300 and 150 kHz). Higher acoustic frequencies detect smaller components without air-inclusions, such as euphausiids and larger crustaceans, and are less prone to be affected by resonance effects that can bias density estimates (Stanton et al., 2010). The strong agreement between low and high-frequency acoustics suggests that the abrupt transition in total backscatter at the West Greenland Polar Front reflects a change in communities and/or a reduction in abundance of larger metazoans. This conclusion is supported by our catch data, which revealed that in the Canadian Arctic, the dispersion of the DSL is mirrored by a transition in the mesopelagic fish community. In the warmer waters of the Labrador Sea, the mesopelagic fish assemblage contains a variety of families, each with different adaptation to deep oceanic waters. Unlike single species dominated systems, the diversity of fish families present in the mesopelagic zone is likely to enhance community tolerance to environmental change (Lindegren et al., 2016).

The glacier lanternfish *Benthosema glaciale* (family Myctophidae) was the most abundant fish species in the Labrador Sea. Their populations are predicted to decrease steadily along a latitudinal photoperiod gradient (Langbehn et al., 2022). Since this species is a significant contributor to acoustic sound scattering throughout the northern hemisphere (Pepin, 2013; Klevjer et al., 2020b), we expected to see a similar gradual dissipation of the DSL with latitude. This prediction is somewhat in line with previous findings which document *Benthosemas*' occurrence above the Arctic circle, albeit in low numbers (Jensen, 1948; Jørgensen et al., 2005). However, our study rather demonstrates a drastic reduction in Myctophidae abundance north of the polar front, at least in the Canadian Arctic, which implicates other environmental drivers such as temperature. Moreover, the absence of larval specimens in previous surveys suggests that a component of its life-history may be inhibited by polar conditions, at least in the eastern Canadian Arctic (Sameoto,

1989). Nonetheless, there is evidence that pelagic physical boundaries (i.e., fronts) are frequently permeable to individual species. Due to their size and limited swimming capabilities, many lanternfishes are considered passive drifters, subject to advective dispersal in ocean currents (Kaartvedt et al., 2009). Therefore, their presence in small numbers in the Canadian Arctic is most likely due to the minor inflow of Atlantic-origin water entering Baffin Bay along Greenland's coast. In the European Arctic, where the volume of Atlantic water inflow is much higher, transient Atlantic origin DSLs have been observed in the Arctic Ocean (Geoffroy et al., 2019; Priou et al., 2021; Snoeijs-Leijonmalm et al., 2022). Despite growing documentation of these DSLs permeating the Artic water, there is little to suggest that boreal fish populations forming these scattering layers can sustain themselves long enough to considerably alter the mesopelagic ecosystem.

While many of the species of mesopelagic fish in the southern hemisphere differ from those in the northern hemisphere, a similar family-level assemblage forms the subpolar DSL (Escobar-Flores et al., 2020). Therefore, we suggest that the overall fish community function and its resulting sensitivity to temperature is similar to that seen in the north. A study highlighting latitudinal effects on body size of mesopelagic fish (following Bergmann's rule) found that the thermal range limit of small lanternfishes with a maximum size of ~50 mm is 2.5° C (Saunders and Tarling, 2018). Perhaps without coincidence, our observed backscatter boundary occurs at this same temperature in both hemispheres (Fig. 1). As body size is critical in both metabolic constraint and feeding behavior, certain large bodied lanternfish have seemingly overcome this temperature constraint by feeding on larger, energy rich prey such as krill (Saunders et al., 2019) whilst simultaneously relying on mass immigration from warmer waters to sustain their populations (Saunders et al., 2017). While the dissolution of the DSL in poleward waters has been previously reported in the

76

Southern Ocean (e.g., Escobar-Flores et al., 2020; Dornan et al., 2022); the relationship of this phenomenon to environmental variables and feeding guilds has remained uninvestigated. Furthermore, the similar shift in vertical structure of larger metazoans in both hemispheres lends further support to a significant shift in the 'biological profile' of the water column.

3.5.1 Enhanced connectivity in a warmer ocean and stability of temperature boundaries

Our estimates of the vertical distribution of zooplankton and fish using an LADCP offer clues to the overall functioning of the pelagic ecosystem (Ressler et al., 1998; Burd and Thomson, 2012). By using high frequency lowered acoustics, we captured a snapshot of the daytime vertical distribution of larger metazoans (down to ~0.5-1 cm in size). Differences in the biological profile of across water mass boundaries, such as reduced backscatter (lower S_v (rel, dB)) and increased dispersal (low Gini index) suggest important changes in organic flux pathways. For instance, high biomass within the mesopelagic zone can lead to increased recycling of particulate (Henson et al., 2012), and a greater depth and magnitude of carbon re-mineralization (Marsay et al., 2015). In addition to a shift in biomass distribution, different mesopelagic communities across the fronts can also modify the carbon export rate and transfer efficiency due to variation in size, ontogeny, and behavior (Vedenin et al., 2020; Saba et al., 2021). This shift in mesopelagic functioning is further supported by studies showing distinct biogeochemical signatures with different carbon export regimes across polar boundaries (Vichi et al., 2011; Fan et al., 2020).

These temperature boundaries where the backscatter and dispersion of mesopelagic organisms changed were located at different latitudes (and light regimes) in each hemisphere and the overall stability of these boundaries remains unclear. Our high frequency LADCP measurements suggest that the pattern of vertical distribution across the polar front was consistent over several years in the Southern Ocean (Supplementary Fig. S3). Using 38 kHz measurements from 2010, Escobar-

Flores et. al (2020) report a similar boundary seen at the Antarctic Polar front (APF) (~ 63° S) in the New Zealand sector of the Southern Ocean. Together, these findings suggest that temperature control in the mesopelagic zone may be a circumpolar phenomenon in the southern hemisphere. In the Indian Ocean sector, poleward displacement of the APF is linked to inter-annual changes in large-scale ocean circulation patterns (Kim and Orsi, 2014), such as the Southern Annular Mode (Gille, 2014). While the Antarctic circumpolar front is largely regulated by seafloor topography (Freeman et al., 2016), new evidence of past frontal movement may shift the existing paradigm of front stability (Civel-Mazens et al., 2021).

There have been considerably fewer investigations into variations in the West Greenland polar front; however, its stability will likely depend on the rate and volume of Atlantic water entering the Arctic through various gateways. In the European Arctic gateway, observations of northward shifts in boreal fish assemblage suggest that the movement of polar temperature boundaries are already underway (Fossheim et al., 2015) and a similar process is therefore possible in the northwest Atlantic. Overall, rapidly changing deep ocean temperature regimes (Brito-Morales et al., 2020) are likely to disrupt these boundaries, with far-reaching implications for ecosystem function and biogeochemical cycling.

3.5.2 Limitations

The study of deep-ocean pelagic communities at high latitudes using net sampling and acoustic measurements remains a major logistical challenge. In the absence of systematic assessments at high-latitude systems, we compiled opportunistic measurements across multiple years, survey platforms, and instruments. Based on previously published work, we are confident that distinct water masses exist across these boundaries and that their biological communities broadly show predictable changes in structure and functioning in the transition to polar waters. Since our

measurements are constrained to months that are ice-free and have warmer sea surface temperatures, we cannot ignore the possibilities that these boundaries may shift geographically or may be permeable under varying seasonal conditions. At lower-latitudes, mid-trophic mesopelagic biomass tends to respond to climate-atmospheric events (i.e. El Niño-Southern Oscillation) in 6 month lag intervals (Lehodey et al., 2010). Overall, observations of temporal response in poleward mesopelagic systems remain rare and our study provides a basis for further investigation.

Characterizing fish and zooplankton biomass and abundance remains a considerable challenge; net selectivity and avoidance behavior can play a large role in biasing catch composition (Kaartvedt et al., 2012). The unknown contribution of certain taxonomic groups to overall backscatter further inhibits our ability to make any conclusions regarding absolute abundance or biomass across these boundaries. For instance, smaller members of the family *Gonostomatidae* (e.g., *Cyclothone sp*.) may be excluded by larger mesh sizes, but bear swim-bladders that may resonate at lower frequencies, making significant contributions to backscatter (Peña et al., 2014). Unfortunately, we do not have biological data to match our acoustic measurements in the Southern Ocean and we therefore rely on the support of previous studies to assess how the micronekton communities may differ across these frontal boundaries.

Together, our acoustic and biological measurements offer a picture of the mesopelagic community transition in polar regions, which is abrupt and clearly aligns with a steep change in temperature between water masses. The change in mesopelagic communities across the West Greenland polar front suggests that community structures (and subsequent function) are altered by deep (>200 m) temperature gradients. The detailed mechanisms of how temperature drives highly complex mesopelagic assemblages remains outside of the scope of this paper. However, our study provides

a basis for future investigations into the functional biogeography of mesopelagic communities and their response to environmental forcing.

3.6 Conclusion

The high degree of similarity in both the northern and southern vertical profiles shows that the relationship between community structure and temperature is independent of the species present and suggests a major shift in the functioning of the upper ocean. While the change in vertical distribution of both micronekton and plankton is clearly associated with water mass transition, we lack a mechanistic understanding of the causes of the observed differences. Previous studies have suggested that mesopelagic fish biomass in high latitude systems are restricted by latitudinal light gradients (Kaartvedt, 2008; Ljungström et al., 2021), but empirical studies have found that while backscatter typically drops off across these gradients (Norheim et al., 2016; Escobar-Flores et al., 2020)), biomass of mesopelagic fish does not follow the same patterns (Escobar-Flores et al., 2020; Klevjer et al., 2020a; Dornan et al., 2022). The front between Austral and Antarctic mesopelagic structure, however, starts much closer to the equator than the front in the northern hemisphere, suggesting that photoperiod is unlikely to be the only limitation to DSL forming fish communities in polar waters. The tight coupling with temperature documented in our data suggests that global warming will affect vertical structure and functioning of high-latitude marine ecosystems, including at mesopelagic depths.

3.7 References

Benoit-Bird, K. J., and Lawson, G. L. (2016). Ecological Insights from Pelagic Habitats Acquired Using Active Acoustic Techniques. *Ann. Rev. Mar. Sci.* 8, 463–490. doi:10.1146/annurev-marine-122414-034001.

Bianchi, D., Stock, C., Galbraith, E. D., and Sarmiento, J. L. (2013). Diel vertical migration: Ecological controls and impacts on the biological pump in a one-dimensional ocean model. *Global Biogeochem. Cycles* 27, 478–491. doi:10.1002/gbc.20031.

Bode, A., Olivar, M. P., and Hernández-León, S. (2021). Trophic indices for micronektonic fishes reveal their dependence on the microbial system in the North Atlantic. *Sci. Rep.* 11, 1–10. doi:10.1038/s41598-021-87767-x.

Boscolo-Galazzo, F., Crichton, K. A., Barker, S., and Pearson, P. N. (2018). Temperature dependency of metabolic rates in the upper ocean: A positive feedback to global climate change? *Glob. Planet. Change* 170, 201–212. doi:10.1016/j.gloplacha.2018.08.017.

Boscolo-Galazzo, F., Crichton, K. A., Ridgwell, A., Mawbey, E. M., Wade, B. S., and Pearson, P. N. (2021). Temperature controls carbon cycling and biological evolution in the ocean twilight zone. *Science (80-.).* 371, 1148–1152. doi:10.1126/science.abb6643.

Bray, J. R., and Curtis, J. T. (1957). An Ordination of the Upland Forest Communities of Southern Wisconsin. *Ecol. Monogr.* 27, 325–349. doi:https://doi.org/10.2307/1942268.

Brito-Morales, I., Schoeman, D. S., Molinos, J. G., Burrows, M. T., Klein, C. J., Arafeh-Dalmau, N., et al. (2020). Climate velocity reveals increasing exposure of deep-ocean biodiversity to future warming. *Nat. Clim. Chang.* 10, 576–581. doi:10.1038/s41558-020-0773-5.

Bruno, J. F., Carr, L. A., and O'Connor, M. I. (2015). Exploring the role of temperature in the ocean through metabolic scaling. *Ecology* 96, 3126–3140. doi:10.1890/14-1954.1.

Burd, B. J., and Thomson, R. E. (2012). Estimating zooplankton biomass distribution in the water column near the Endeavour Segment of Juan de Fuca Ridge using acoustic backscatter and concurrently towed nets. *Oceanography* 25, 269–276. doi:http://dx.doi.org/10.5670/oceanog.2012.25.

Catul, V., Gauns, M., and Karuppasamy, P. K. (2011). A review on mesopelagic fishes belonging to family Myctophidae. *Rev. Fish Biol. Fish.* 21, 339–354. doi:10.1007/s11160-010-9176-4.

Choy, C., Wabnitz, C., Weijerman, M., Woodworth-Jefcoats, P., and Polovina, J. (2016). Finding the way to the top: how the composition of oceanic mid-trophic micronekton groups determines apex predator biomass in the central North Pacific. *Mar. Ecol. Prog. Ser.* 549, 9–25. doi:10.3354/meps11680.

Civel-Mazens, M., Crosta, X., Cortese, G., Michel, E., Mazaud, A., Ther, O., et al. (2021). Antarctic Polar Front migrations in the Kerguelen Plateau region, Southern Ocean, over the past 360 kyrs. *Glob. Planet. Change* 202, 103526. doi:10.1016/j.gloplacha.2021.103526.

Clarke, K. R. (1993). Non-parametric multivariate analyses of changes in community structure. *Aust. J. Ecol.* 18, 117–143. doi:https://doi.org/10.1111/j.1442-9993.1993.tb00438.x.

Curry, B., Lee, C. M., Petrie, B., Moritz, R. E., and Kwok, R. (2014). Multiyear volume, liquid freshwater, and sea ice transports through Davis Strait, 2004-10. *J. Phys. Oceanogr.* 44, 1244–1266. doi:10.1175/JPO-D-13-0177.1.

Davison, P. C., Checkley, D. M., Koslow, J. A., and Barlow, J. (2013). Carbon export mediated by mesopelagic fishes in the northeast Pacific Ocean. *Prog. Oceanogr.* 116, 14–30. doi:10.1016/j.pocean.2013.05.013.

Davison, P. C., Koslow, J. A., and Kloser, R. J. (2015). Acoustic biomass estimation of

mesopelagic fish: backscattering from individuals, populations, and communities. *ICES J. Mar. Sci.* 72, 1413–1424. doi:10.1093/icesjms/fsv023.

Demer, D. A., Berger, L., Bernasconi, M., Bethke, E., Boswell, K. M., Chu, D., et al. (2015). Calibration of acoustic instruments. *ICES Coop. Res. Rep.* 326, 1–133. doi:http://dx.doi.org/10.25607/OBP-185.

Dornan, T., Fielding, S., Saunders, R. A., and Genner, M. J. (2019). Swimbladder morphology masks Southern Ocean mesopelagic fish biomass. *Proc. R. Soc. B Biol. Sci.* 286, 1–8. doi:10.1098/rspb.2019.0353.

Dornan, T., Fielding, S., Saunders, R. A., and Genner, M. J. (2022). Large mesopelagic fish biomass in the Southern Ocean resolved by acoustic properties. *Proc. R. Soc. B Biol. Sci.* 289, 1–10. doi:10.1098/rspb.2021.1781.

Escobar-Flores, P. C., O'Driscoll, R. L., Montgomery, J. C., Ladroit, Y., and Jendersie, S. (2020). Estimates of density of mesopelagic fish in the Southern Ocean derived from bulk acoustic data collected by ships of opportunity. *Polar Biol.* 43, 43–61. doi:10.1007/s00300-019-02611-3.

Fan, G., Han, Z., Ma, W., Chen, S., Chai, F., Mazloff, M. R., et al. (2020). Southern Ocean carbon export efficiency in relation to temperature and primary productivity. *Sci. Rep.* 10, 1–11. doi:10.1038/s41598-020-70417-z.

Firing, E., Hummons, J. M., Thurnerr, A. M., and Visbeck, M. (2019). Ocean currents from lowered acoustic Doppler profilers (LADCP) from the Climate Variability (CLIVAR) project from 2003 to 2014 assembled at the University of Hawaii and Lamont-Doherty Earth Observatory, Columbia University. R/V Roger Revelle cruise KNOX14. Available at: https://www.ncei.noaa.gov/archive/accession/CLIVAR-LADCP.

Forest, A., Guillot, P., Linkowski, T., and Morriset, S. (2020). LADCP data collected by the CCGS Amundsen in the Canadian Arctic. *LADCP data Collect. by CCGS Amundsen Can. Arct.* doi:https://doi.org/10.5884/12714.

Fossheim, M., Primicerio, R., Johannesen, E., Ingvaldsen, R. B., Aschan, M. M., and Dolgov, A. V. (2015). Recent warming leads to a rapid borealization of fish communities in the Arctic. *Nat. Clim. Chang.* 5, 673–677. doi:10.1038/nclimate2647.

Freeman, N. M., Lovenduski, N. S., and Gent, P. R. (2016). Temporal variability in the Antarctic Polar Front (2002-2014). *J. Geophys. Res. Ocean.* 121, 7263–7276. doi:10.1002/2016JC012145.

Geoffroy, M., Daase, M., Cusa, M., Darnis, G., Graeve, M., Hernández, N. S., et al. (2019). Mesopelagic sound scattering layers of the high Arctic: Seasonal variations in biomass, species assemblage, and trophic relationships. *Front. Mar. Sci.* 6. doi:10.3389/fmars.2019.00364.

Gille, S. T. (2014). Meridional displacement of the Antarctic Circumpolar Current. *Philos. Trans. R. Soc. A Math. Phys. Eng. Sci.* 372, 1–13. doi:10.1098/rsta.2013.0273.

Gillooly, J. F., Brown, J. H., West, G. B., Savage, V. M., and Charnov, E. L. (2001). Effects of Size and Temperature on Metabolic Rate. *Science (80-.).* 293, 2248–2251.

doi:10.1126/science.1061967.

Gini Index (2008). in *The Concise Encyclopedia of Statistics* (New York, NY: Springer New York), 231–233. doi:10.1007/978-0-387-32833-1_169.

Godø, O. R., Samuelsen, A., Macaulay, G. J., Patel, R., Hjøllo, S. S., Horne, J., et al. (2012). Mesoscale eddies are oases for higher trophic marine life. *PLoS One* 7, 1–9. doi:10.1371/journal.pone.0030161.

Henson, S. A., Sanders, R., and Madsen, E. (2012). Global patterns in efficiency of particulate organic carbon export and transfer to the deep ocean. *Global Biogeochem. Cycles* 26, 1–14. doi:10.1029/2011GB004099.

Hidalgo, M., and Browman, H. I. (2019). Developing the knowledge base needed to sustainably manage mesopelagic resources. *ICES J. Mar. Sci.* 76, 609–615. doi:10.1093/icesjms/fsz067.

Hoegh-Guldberg, O., and Bruno, J. F. (2010). The impact of climate change on the world's marine ecosystems. *Science (80-.).* 328, 1523–1528. doi:10.1016/s0262-4079(10)61509-6.

Irigoien, X., Klevjer, T. A., Røstad, A., Martinez, U., Boyra, G., Acuña, J. L., et al. (2014). Large mesopelagic fishes biomass and trophic efficiency in the open ocean. *Nat. Commun.* 5, 1–10. doi:10.1038/ncomms4271.

Jensen, A. S. (1948). Contributions to the ichthyofauna of Greenland, 8-24. *Skr. Udbiget Univ. Zool. Mus. Kobenhavn* 9, 1–182.

Jørgensen, O. A., Hvingel, C., Møller, P. R., and Treble, M. A. (2005). Identification and mapping of bottom fish assemblages in Davis Strait and southern Baffin Bay. *Can. J. Fish. Aquat. Sci.* 62, 1833–1852. doi:10.1139/f05-101.

Kaartvedt, S. (2008). Photoperiod may constrain the effect of global warming in arctic marine systems. *J. Plankton Res.* 30, 1203–1206. doi:10.1093/plankt/fbn075.

Kaartvedt, S., Røstad, A., Klevjer, T. A., and Staby, A. (2009). Use of bottom-mounted echo sounders in exploring behavior of mesopelagic fishes. *Mar. Ecol. Prog. Ser.* 395, 109–118. doi:10.3354/meps08174.

Kaartvedt, S., Staby, A., and Aksnes, D. L. (2012). Efficient trawl avoidance by mesopelagic fishes causes large underestimation of their biomass. *Mar. Ecol. Prog. Ser.* 456, 1–6. doi:10.3354/meps09785.

Kim, Y. S., and Orsi, A. H. (2014). On the variability of antarctic circumpolar current fronts inferred from 1992-2011 altimetry. *J. Phys. Oceanogr.* 44, 3054–3071. doi:10.1175/JPO-D-13-0217.1.

Klevjer, T. A., Melle, W., Knutsen, T., and Aksnes, D. L. (2020a). Vertical distribution and migration of mesopelagic scatterers in four north Atlantic basins. *Deep Sea Res. Part II Top. Stud. Oceanogr.* 180, 1–11. doi:10.1016/j.dsr2.2020.104811.

Klevjer, T., Melle, W., Knutsen, T., Strand, E., Korneliussen, R., Dupont, N., et al. (2020b). Micronekton biomass distribution, improved estimates across four north Atlantic basins. *Deep Sea Res. Part II Top. Stud. Oceanogr.* 180, 1–11. doi:10.1016/j.dsr2.2019.104691.

Knutsen, T., Wiebe, P. H., Gjøsæter, H., Ingvaldsen, R. B., and Lien, G. (2017). High Latitude Epipelagic and Mesopelagic Scattering Layers—A Reference for Future Arctic Ecosystem Change. *Front. Mar. Sci.* 4, 1–21. doi:10.3389/fmars.2017.00334.

Langbehn, T. J., Aksnes, D. L., Kaartvedt, S., Fiksen, Ø., Ljungström, G., Jørgensen, C., et al. (2022). Poleward distribution of mesopelagic fishes is constrained by seasonality in light. *Glob. Ecol. Biogeogr.* 31, 546–561. doi:10.1111/geb.13446.

Lee, C., and Gobat, J. (2020). CTD data from Cruise 316N20130914, exchange version. Accessed from CCCHDO. doi:10.7284/900550.

Lehodey, P., Murtugudde, R., and Senina, I. (2010). Bridging the gap from ocean models to population dynamics of large marine predators: A model of mid-trophic functional groups. *Prog. Oceanogr.* 84, 69–84. doi:10.1016/j.pocean.2009.09.008.

Lindegren, M., Checkley, D. M., Ohman, M. D., Koslow, J. A., and Goericke, R. (2016). Resilience and stability of a pelagic marine ecosystem. *Proc. R. Soc. B Biol. Sci.* 283, 1–9. doi:10.1098/rspb.2015.1931.

Ljungström, G., Langbehn, T. J., and Jørgensen, C. (2021). Light and energetics at seasonal extremes limit poleward range shifts. *Nat. Clim. Chang.* 11, 530–536. doi:10.1038/s41558-021-01045-2.

Longhurst, A. (2007). *Ecological Geography of the Sea*. London: Academic Press Inc. (London) Ltd.

López-Urrutia, Á., Martin, E. S., Harris, R. P., and Irigoien, X. (2006). Scaling the metabolic balance of the oceans. *Proc. Natl. Acad. Sci.* 103, 8739–8744. doi:10.1073/pnas.0601137103.

Mackenzie, K. V. (1981). Nine-term equation for sound speed in the oceans. *J. Acoust. Soc. Am* 70, 807–812.

Maclennan, D. N., Fernandes, P. G., and Dalen, J. (2002). A consistent approach to definitions and symbols in fisheries acoustics. *ICES J. Mar. Sci.* 59, 365–369. doi:10.1006/jmsc.2001.1158.

Marsay, C. M., Sanders, R. J., Henson, S. A., Pabortsava, K., Achterberg, E. P., and Lampitt, R. S. (2015). Attenuation of sinking particulate organic carbon flux through the mesopelagic ocean. *Proc. Natl. Acad. Sci. U. S. A.* 112, 1089–1094. doi:10.1073/pnas.1415311112.

Mullison, J. (2017). Backscatter Estimation Using Broadband Acoustic Doppler Current Profilers - Updated. *ASCE Hydraul. Meas. Exp. Methods Conf.* 031, 1–6.

Norheim, E., Klevjer, T. A., and Aksnes, D. L. (2016). Evidence for light-controlled migration amplitude of a sound scattering layer in the Norwegian Sea. *Mar. Ecol. Prog. Ser.* 551, 45–52. doi:10.3354/meps11731.

Okansen, J., Blanchet, G., Friendly, M., Kindt, R., Legendre, P., McGlinn, D., et al. (2020). vegan: Community Ecology Package.

Orsi, A. H., Whitworth, T., and Nowlin, W. D. (1995). On the meridional extent and fronts of the

Antarctic Circumpolar Current. *Deep. Res. Part I* 42, 641–673. doi:10.1016/0967-0637(95)00021-W.

Peña, M., Olivar, M. P., Balbín, R., López-Jurado, J. L., Iglesias, M., Miquel, J., et al. (2014). Acoustic detection of mesopelagic fishes in scattering layers of the Balearic Sea (western Mediterranean). *Can. J. Fish. Aquat. Sci.* 71, 1186–1197. doi:10.1139/cjfas-2013-0331.

Pepin, P. (2013). Distribution and feeding of Benthosema glaciale in the western Labrador Sea: Fish-zooplankton interaction and the consequence to calanoid copepod populations. *Deep. Res. Part I Oceanogr. Res. Pap.* 75, 119–134. doi:10.1016/j.dsr.2013.01.012.

Priou, P., Nikolopoulos, A., Flores, H., Gradinger, R., Kunisch, E., Katlein, C., et al. (2021). Dense mesopelagic sound scattering layer and vertical segregation of pelagic organisms at the Arctic-Atlantic gateway during the midnight sun. *Prog. Oceanogr.* 196, 102611. doi:10.1016/j.pocean.2021.102611.

Proud, R., Cox, M. J., and Brierley, A. S. (2017). Biogeography of the Global Ocean's Mesopelagic Zone. *Curr. Biol.* 27, 113–119. doi:10.1016/j.cub.2016.11.003.

Rall, B. C., Vucic-Pestic, O., Ehnes, R. B., Emmerson, M., and Brose, U. (2010). Temperature, predator–prey interaction strength and population stability. *Glob. Chang. Biol.* 16, 2145–2157. doi:https://doi.org/10.1111/j.1365-2486.2009.02124.x.

Ressler, P. H., Biggs, D. C., and Wormuth, J. H. (1998). Acoustic estimates of zooplankton and micronekton biomass using an ADCP. in *The Journal of the Acoustical Society of America*, 2167–2168. doi:10.1121/1.421730.

Saba, G. K., Burd, A. B., Dunne, J. P., Hernández-León, S., Martin, A. H., Rose, K. A., et al. (2021). Toward a better understanding of fish-based contribution to ocean carbon flux. *Limnol. Oceanogr.* 66, 1639–1664. doi:10.1002/lno.11709.

Sameoto, D. (1989). Feeding Ecology of the Lantern Fish Benthosema Glaciale in a Subarctic Region. *Polar Biol.* 9, 167–178. doi:10.1007/BF00297172.

Saunders, R. A., Collins, M. A., Stowasser, G., and Tarling, G. A. (2017). Southern Ocean mesopelagic fish communities in the Scotia Sea are sustained by mass immigration. *Mar. Ecol. Prog. Ser.* 569, 173–185. doi:10.3354/meps12093.

Saunders, R. A., Hill, S. L., Tarling, G. A., and Murphy, E. J. (2019). Myctophid Fish (Family Myctophidae) Are Central Consumers in the Food Web of the Scotia Sea (Southern Ocean). *Front. Mar. Sci.* 6, 1–22. doi:10.3389/fmars.2019.00530.

Saunders, R. A., and Tarling, G. A. (2018). Southern ocean mesopelagic fish comply with Bergmann's rule. *Am. Nat.* 191, 343–351. doi:10.1086/695767.

Schaber, M., Gastauer, S., Cisewski, B., Hielscher, N., Janke, M., Peña, M., et al. (2022). Extensive oceanic mesopelagic habitat use of a migratory continental shark species. *Sci. Rep.* 12, 1–14. doi:10.1038/s41598-022-05989-z.

Snoeijs-Leijonmalm, P., Flores, H., Sakinan, S., Hildebrandt, N., Svenson, A., Castellani, G., et al. (2022). Unexpected fish and squid in the central Arctic deep scattering layer. *Sci. Adv.* 8, 1–17. doi:10.1126/sciadv.abj7536.

Speer, K. (2020). CTD data from Cruise 33RR20080204, exchange version. Accessed from CCHDO. doi:10.7284/903752.

Stanton, T. K., Chu, D., Jech, J. M., and Irish, J. D. (2010). New broadband methods for resonance classification and high-resolution imagery of fish with swimbladders using a modified commercial broadband echosounder. *ICES J. Mar. Sci.* 67, 365–378. doi:10.1093/icesjms/fsp262.

Sutton, T. T., Clark, M. R., Dunn, D. C., Halpin, P. N., Rogers, A. D., Guinotte, J., et al. (2017). A global biogeographic classification of the mesopelagic zone. *Deep. Res. Part I Oceanogr. Res. Pap.* 126, 85–102. doi:10.1016/j.dsr.2017.05.006.

Vedenin, A., Kulagin, D., Musaeva, E., and Vereshchaka, A. (2020). The Southern Polar Front as a key to mesoplankton migratory behavior. *Sci. Rep.* 10, 1–14. doi:10.1038/s41598-020-70720-9.

Vichi, M., Allen, J. I., Masina, S., and Hardman-Mountford, N. J. (2011). The emergence of ocean biogeochemical provinces: A quantitative assessment and a diagnostic for model evaluation. *Global Biogeochem. Cycles* 25, 1–17. doi:10.1029/2010GB003867.

Zeileis, A. (2014). ineq: Measuring inequality, concentration, and poverty. Available at: https://cran.r-project.org/package=ineq.

3.8 Supplemental Figures
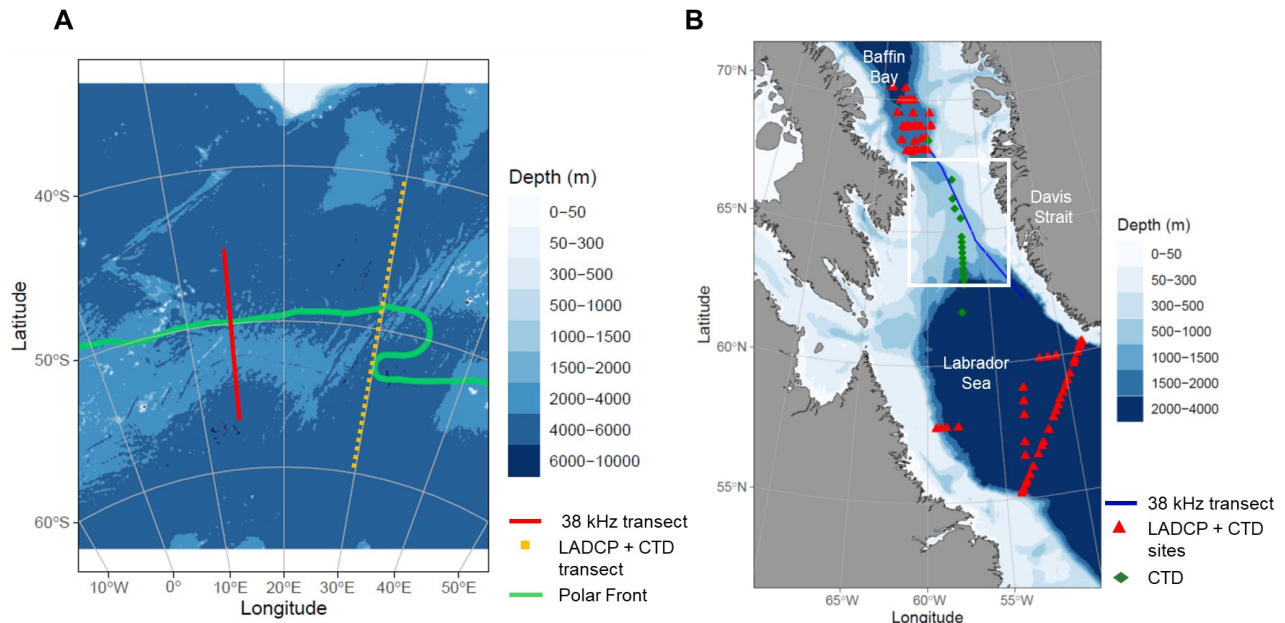
S1. Acoustic and hydrographic sampling locations. The Southern Ocean between 0° and 40° E in the Southern Ocean (**A**) and the Canadian Arctic-Atlantic gateway between Baffin Bay and the Labrador Sea (**B**).
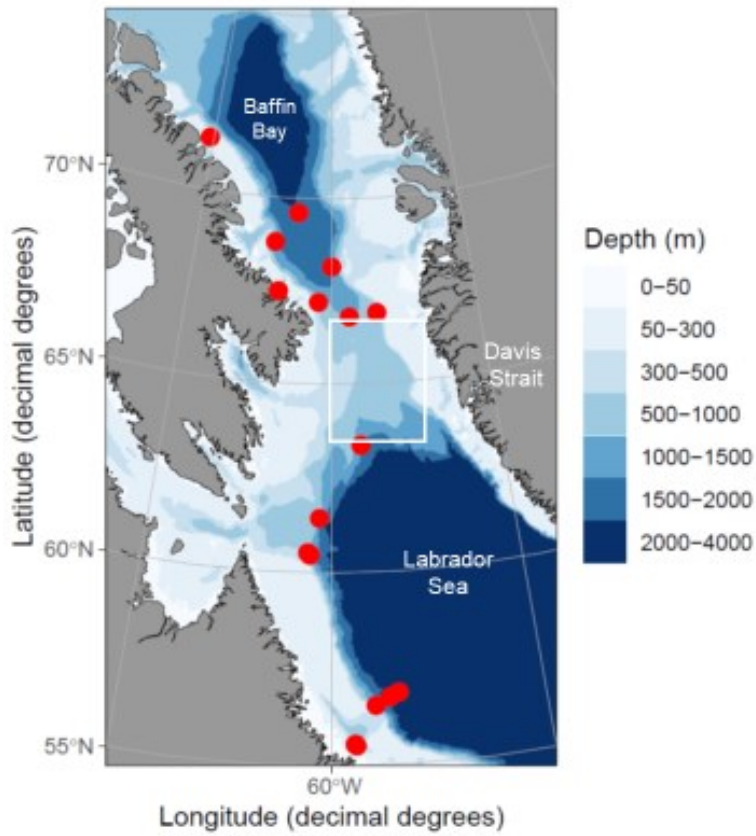
S2. IKMT sampling locations in the Canadian Arctic. Trawling sites from 2020-2021 are shown in red and include only sites that were sampled in water depth >500 m.

A. February 2005 - Longitude: 150°W – 150 kHz LADCP
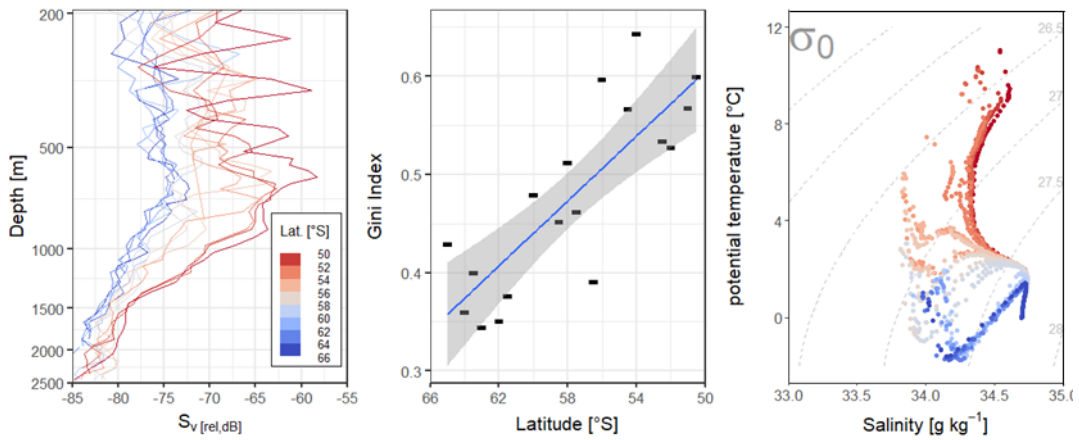
B. February-March 2007 - Longitude: 82-95 °W – 300 kHz LADCP
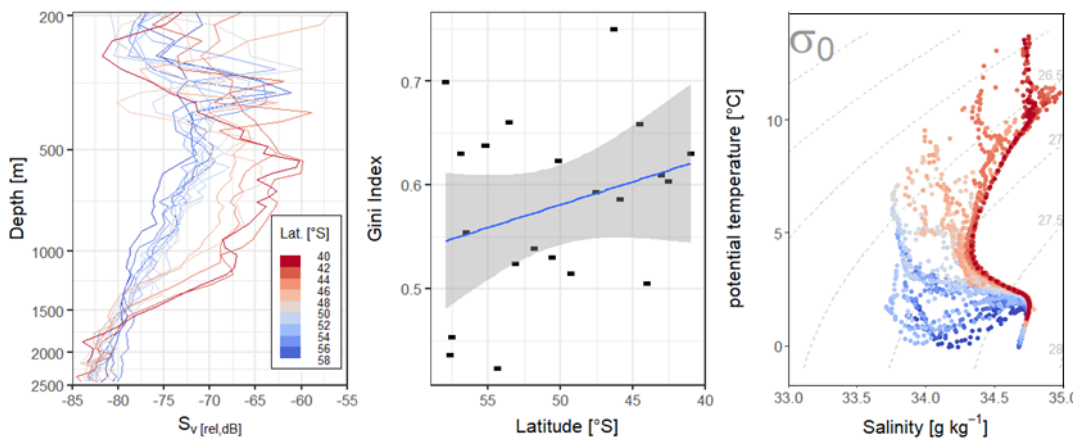
C. February 2008 - Longitude: 103 °W – 150 kHz LADCP
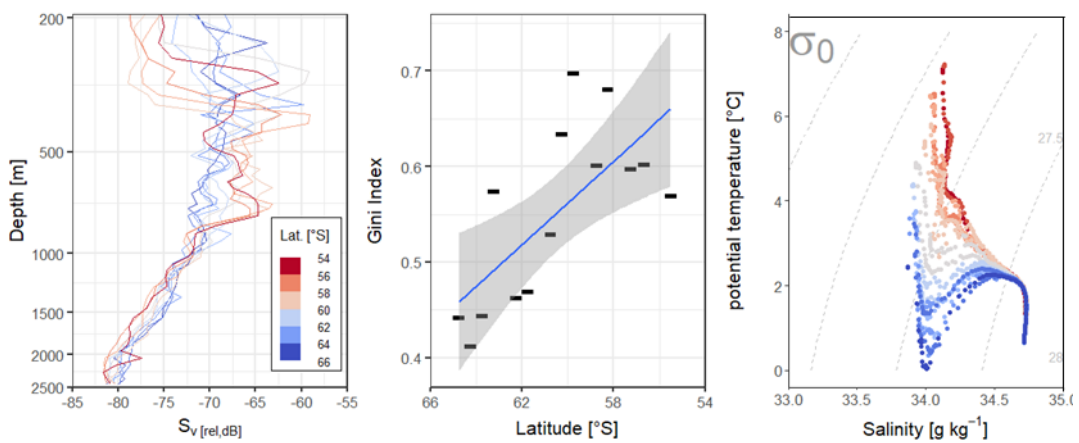
D. April 2014 - Longitude: 150 °W – 150 kHz LADCP
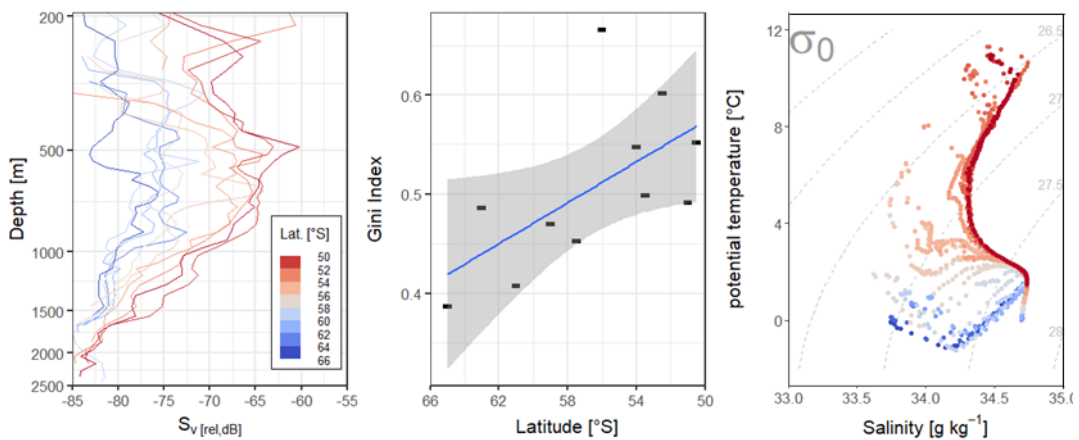
S3. Additional LADCP backscatter profiles, Gini index calculations, and TS diagrams. The patterns seen in the Atlantic sector of the Southern Ocean polar transition zone are consistent across years and locations (**A-D**).

Chapter 4. Mixing of glacial surface water increases marine snow production and alters copepod vertical distribution

4.1 Abstract

Glacial meltwater is a major contributor to stratification in polar waters. The volume of meltwater exported from glacial fjord ecosystems depends on glacier type, fjord topography, and circulation patterns. Stratification from glacial meltwater input in estuaries impacts both light and nutrient availability, altering the timing and magnitude of phytoplankton blooms. Ice conditions surrounding the fjords of northwest Greenland can impede near-surface circulation and trap low-density meltwater plumes, amplifying stratification. Whilst stratification is a critical process in the initiation of phytoplankton blooms, reduced mixing can impede production, altering the formation processes of marine snow. Here, using a combination of optical and acoustical instrumentation, we investigated how oceanographic conditions in two adjacent fjords (Petermann Fjord and Sherard Osborn Fjord) impacted the vertical distribution of two key components of Arctic pelagic ecosystems: marine snow and copepods. We show that the amplified stratification, caused by ice-damming outside Sherard Osborn Fjord, is associated with low quantities and qualities of marine snow. By contrast, the adjacent well-mixed surface waters of the Petermann Fjord ecosystem are characterized by high quality, abundant marine snow. We also find that copepod vertical distribution coincides with the marine snow profiles, whereby, copepods are more evenly distributed through a well-mixed water column and shifted toward the surface during stratification. As ocean stratification is expected to increase in high latitude glacial ecosystems in the future, impacts on marine snow production and grazing behavior of copepods will likely impact pelagic predators and benthic-pelagic coupling.

4.2 Introduction

Stratification is a key process initiating primary production because it impacts vertical gradients in nutrient supply and phytoplankton cells (Aagaard et al., 1981). In the upper waters of Arctic fjords, the accumulation of buoyant glacial meltwater increases stratification during warm summer months, impacting coastal marine productivity (Hopwood et al., 2020). Depending on volume and level of mixing, meltwater can either enhance or diminish primary production through the transport of nutrients and sediments (Meire et al., 2017; Hopwood et al., 2020; Stuart-Lee et al., 2023). Furthermore, the contribution of primary production to the overall biological productivity depends not only on the level of primary production, but on the quality of sinking biogenic particulates (Buesseler, 1998; Jackson and Checkley, 2011). Marine snow forms when living and dead biogenic particles aggregate and are modified by a combination of biophysical processes including microbial digestion, remineralization, and grazing (Alldredge and Silver, 1988; De La Rocha and Passow, 2007).

While studies have begun to elucidate how marine snow abundance and morphology are tied to environmental Arctic conditions such as sea ice break up and melting (Szeligowska et al., 2021; Trudnowska et al., 2021), little is known about their impact on pelagic grazers. As key mediators of energy in marine ecosystems, copepods are intrinsically linked to marine snow through their consumption, production, and breakdown of biogenic particles (Long et al., 2007; Jackson and Checkley, 2011; Toullec et al., 2019). During productive summer months, copepods aggregate in the euphotic zone, where their vertical distribution is often described as a compromise between predator avoidance and optimal feeding depth, modulated by light and primary productivity (Longhurst, 1976). However, at fine vertical scales the relationship between copepods and sinking marine snow is likely to vary depending on the quantity and quality of particles. For instance,

processes such as meltwater stratification can lead to retention of particulate in surface waters, effectively slowing particle sinking rates (von Appen et al., 2021). Within glacial fjord systems, the additional mechanism of ice-damming, due to build up of sea-ice outside the fjord, can trap buoyant meltwater and enhance stratification with unknown consequences to sinking particulate (Stranne et al., 2021). As melting of the Greenland ice sheet increases the freshwater flux into the ocean, high Arctic fjord ecosystems are becoming more stratified (Trusel et al., 2018; Ardyna and Arrigo, 2020). The investigation of the impact of such conditions may provide early insights of how future ocean ecosystems may respond to climate change.

Because different fjord systems experience varying degrees of freshwater influx today, due to contrasting physical characteristics, space-for-time substitution enables insights into the impacts of stratification on plankton dynamics. Archetypal fjords for the study of glacier-ocean interactions are typically restricted to lower latitude Greenlandic fjords, and around Svalbard, where Atlantic inflow water is a large contributor to basal melting and ecosystem regulation (Hegseth and Tverberg, 2013; Weydmann-Zwolicka et al., 2021; Szeligowska et al., 2022). By contrast, fjord systems in NW Greenland remain relatively isolated from the warm Atlantic water mass but are strongly influenced by a dense accumulation of multi-year sea ice in the Lincoln Sea and glacier ice (icebergs) originating from the northern Greenland Ice Sheet. Two of the largest marine-terminating glaciers of the northern Greenland Ice Sheet, Petermann and Ryder glaciers, face contrasting magnitudes of glacial melting due to differences in their exposure to open ocean conditions. Sherard Osborn Fjord (SOF), home to the marine terminating Ryder Glacier, is one of the few large outlet glaciers of the GIS which remains relatively isolated from horizontal exchange due to the combination of bathymetry and ice damming (Jakobsson et al., 2020b; Stranne et al., 2021). In 2019, the combined effect of unusually high atmospheric temperatures and sea-ice and

iceberg damming process at the opening of SOF led to an amplified surface water stratification regime (Stranne et al., 2021). In the neighboring Petermann Fjord (PF), the export of sea ice and surface water into Nares Strait resulted in a well-mixed upper water column (i.e., 0-100 m), with high near-surface fluorescence (Stranne et al., 2021). These strongly contrasting conditions between two adjacent fjords provided a unique opportunity to further our understanding of plankton dynamics in a virtually unstudied pelagic ecosystem (Kalenitchenko et al., 2019).

Increasing ocean stratification associated with rapid climate warming has growing potential to alter productivity in Arctic waters (Wassman and Reigstad, 2011). For example, in open Arctic seas there is growing evidence that meltwater from sea-ice can amplify stratification enough to negatively impact aspects of ecosystem production, including the functioning of the particle pump (von Appen et al., 2021). In glacial fjords, impacts to productivity from melting glaciers are challenging to generalize; interacting fjord dynamics such as glacier type, circulation, turbidity, and light can be attributed to both drastic positive and negative effects on primary productivity and planktonic organisms (Meire et al., 2017; Szeligowska et al., 2021, 2022; Weydmann-Zwolicka et al., 2021; Stuart-Lee et al., 2023). Particle production is a key proxy of the relationship between glacial dynamics and pelagic productivity (Szeligowska et al., 2021, 2022; Trudnowska et al., 2021). Recent advances in particle imaging show that particle size and shape are directly related to Arctic bloom stages and attenuation depth, or depth where particles are consumed or re-mineralized (Durkin et al., 2021; Trudnowska et al., 2021). Because sinking biogenic particles are the primary source of food for secondary producers, such as copepods, differences in their morphology can alter producer-to-consumer coupling and flux. In high Arctic environments, the underlying drivers of different production/particle-flux states remain poorly understood.

Copepods respond to changes in their environment by modifying their vertical distribution in the water column (Vinogradov, 1997). The short-term responses of copepods to their environment are associated with tradeoffs between feeding success and predator avoidance (Vinogradov, 1962; Basedow et al., 2010). At latitudes >80°, predator avoidance strategies, such as diel vertical migration, are considered less important in open waters due to low variability in ambient light during summer months (Longhurst et al., 1984; Fortier et al., 2001). Therefore, during months when primary productivity is highest, Arctic copepods will typically aggregate in the euphotic zone where feeding opportunities are highest (Sameoto, 1984; Kosobokova and Hirche, 2000; Blachowiak-Samolyk et al., 2007). At finer vertical scales, however, drivers of vertical distribution are poorly understood, particularly in Arctic environments (Trudnowska et al., 2015). Within the euphotic zone, the combination of biological and physical processes can alter chemical and optical cues, structuring zooplankton habitats at meter level scales (Long et al., 2007; Szeligowska et al., 2021, 2022). Despite the reliance of Arctic calanoid copepods on phytoplankton, the level of primary productivity is not always synonymous with food quality, due to the process of particle aggregation (Jackson and Checkley, 2011) and variation in feeding strategies among Arctic copepods (Trudnowska et al., 2020). Consequently, grazers move toward their preferred food, such as the particle concentration maximum, rather than the shallower production maximum (Napp et al., 1988).

In this study, we investigated the ecological significance of vertical stratification on particle production and the subsequent impact on the vertical distribution of copepods in the upper 100 m of the water column in two adjacent glacial fjords. Building upon the extensive knowledge gained about the physical environments in SOF and PF (Jakobsson et al., 2020b; Stranne et al., 2021), the goals of this study are to investigate 1) how amplified stratification influences marine snow particle

quantity and quality, and 2) how different particle states (i.e., particle shape and size) among fjords impact the vertical distribution of copepods. To meet our objectives, we leveraged optical and acoustic sampling tools to characterize marine snow and copepod distributions in the upper water column. We hypothesize that amplified stratification reduces particle production, impacting the distribution of detritivorous copepods. We expect differences in particle production and morphology, leading to variation in the quality of particulate available to feeding copepods. In waters with low particulate levels, we expect copepods to aggregate near the surface, where the biogenic particle density maximum typically lies.

4.3 Materials & Methods

4.3.1 Study Area

The study area was located north of 80° N, between the Nares Strait and the Lincoln Sea with the primary sampling program focused on Petermann and Sherard Osborn Fjords (Figure 4.1). The oceanography and geomorphology of these two fjords are described in detail elsewhere (Jakobsson et al., 2020b; Stranne et al., 2021). In brief, both fjords reach maximum depths exceeding 800 m+ and are home to marine terminating glaciers with floating ice tongues. Surface and subglacial meltwater contribute to the outflowing current above 200 m and remnants of circulated Atlantic water from the Central Arctic Ocean flow inward at depths below 400 m in each fjord.
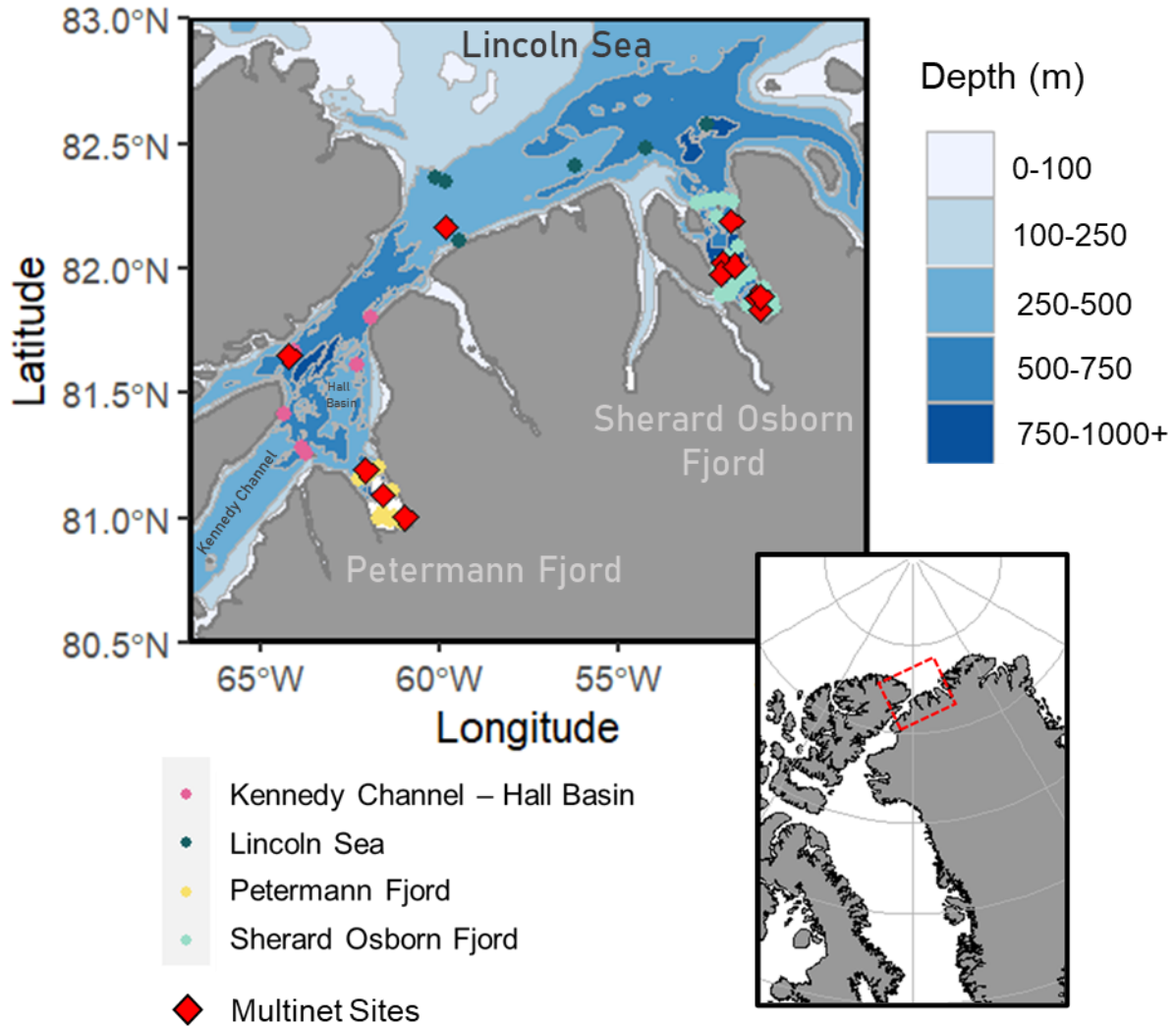
Figure 4.1 Study area and sampling sites in NW Greenland. Inset shows Northwest Greenland, with the red box outlining the study region (Petermann and Sherard Osborn Fjords). Colored dots show the locations of optical and acoustic sampling using the CTD-rosette, and red diamonds show the locations of multinet sampling sites. All sampling was conducted between August 5 – September 10th, 2019 as part of the Ryder Glacier cruise.

4.3.2 Data Collection

Sampling stations (Figure 4.1) were located in Kennedy Channel – Hall Basin (KC-HB), Sherard Osborn Fjord (SOF), the Lincoln Sea (LS), and Petermann Fjord (PF) during the Ryder Glacier 2019 cruise (August 5 – September 10th, 2019) on the icebreaker Oden led by Stockholm University (Jakobsson et al., 2020a). At each sampling station, optical (particle imaging), acoustic,

and biological (zooplankton) data were collected. The seasonal progression of ice conditions in the region was qualitatively assessed using satellite imagery (MODIS Characterization Support Team (MCST), 2017) downloaded on 01/16/23 from https://worldview.earthdata.nasa.gov/. Using these satellite images, we describe surface sea ice extent at approximately 2-week intervals during the cruise period.

4.3.3 Optical Data

Particle images were collected using an Underwater Vision Profiler (UVP5, Hydroptic ©) mounted to the water sampler rosette. The UVP5 system detects and counts all objects larger than ~100 μm in a ~1 L volume illuminated with a digital camera (Picheral et al., 2010). The system automatically detects objects and stores vignettes of objects >80 pixels (from approximately 500 μm to a maximum of 200 mm). For this study, the UVP5 was mounted onto the rosette water sampler that also carried conductivity, temperature, and depth sensors (CTD; SBE 911plus, Seabird Scientific, Bellevue, WA, USA). The acquisition frequency reached up to 8 Hz. The rosette was lowered with an average descent speed of up to 0.5 ms−1; however, speeds varied considerably during challenging ice conditions. Due to the high levels of turbidite particle entrainment in subglacial plumes, the UVP5 was unable to quantify particle distributions with any consistency below 100 m; therefore, our analyses are restricted to the upper 100 m of the water column.

4.3.4 Acoustic Data

Acoustic data (volume backscattering strength S_v in dB re 1 m^{-1}) for the measurement of mesozooplankton distribution were collected using a rosette-mounted wideband autonomous transceiver (WBAT, Simrad ©), equipped with an ES333 split-beam transducer that was mounted horizontally relative to the rosette frame. Data were collected to 50 m range using a 0.5 s sampling interval. Pulses were transmitted in broadband (also known as frequency modulated, FM) mode

using a 320-420 kHz bandwidth pulse and a transmitted pulse duration of 1.024 ms and 200 W power. Acoustic data containing biological backscatter were mostly limited to 25-100 m depth due to inherent challenges in the sampling environment: above 25 m, measurements were contaminated by backscatter from nearby icebergs and the air-water interface. Below 100 m, much of the mesozooplankton data were masked by strongly scattering particulate entrained in subglacial turbidity plumes. Each profile was smoothed using a missing value imputation and moving average with a 30-ping window. Ping-depth intervals varied between 0.2 to 0.8 m, depending on the rosette speed during lowering.

4.3.5 Zooplankton Data

Zooplankton samples were collected using a multinet (Hydrobios ©) deployed at 12 sampling stations after the CTD cast to collect zooplankton at discrete depth intervals (Suppl. Figure 1). The multinet is comprised of five nets, each with an opening of 0.25 m^2 and 200 μm mesh that terminates in a PVC net cup during retrieval, each net opening is closed at the desired depth by an arrangement of spring-loaded levers which are triggered by a motor unit. An integrated pressure sensor allows for continuous supervision of the operating depth indicated on the display of the deck command unit. After retrieval, the net was returned to the deck, rinsed with fresh seawater, and samples were collected from each net cup for subsequent processing in the laboratory. Zooplankton samples were preserved in borax-buffered 2% formalin-seawater solution and later taxonomically identified using microscopy. Samples were taken at 12 stations throughout SOF, KC-HB, LS, and PF: seven in SOF, one in KC-HB, one in LS, and two in PF.

4.3.6 Data Analysis

Morphological analysis of marine snow. A key component to understanding the fate of particulate carbon and food availability to higher trophic levels (i.e., copepods) involved a

quantitative image analysis of marine snow particles in each fjord and region. Using the UVP5 image dataset for the upper 100 m of the water, images were individually classified using the EcoTaxa web application (https://ecotaxa.obsvlfr.fr/), using machine learning classifiers trained on the GreenEdge 2016 expedition dataset from Baffin Bay (Bruyant et al., 2022) Several iterations of subset validation and re-prediction were performed to improve automated classification. All images in the upper 100 m were manually validated. Following methodology developed in Trudnowska et al. (2022) and using non-living particles from the 'detritus' category, we selected similar morphological features which are subdivided into four groups of key ecological descriptors: size, shape, brightness, and structure (Supplemental Table 1). For each morphological feature extreme feature values (0.1%) were trimmed, and those with highly skewed distributions were normalized using log-transformation. Next, the feature dataset was scrutinized for cross-correlation using a similarity matrix built using the Morpheus software (Suppl. Figure 2) and any features with a Pearson correlation coefficient greater than or equal to 0.97 were removed from the dataset. In some cases, highly correlated features (e.g. area & major axis) were retained to maintain balance among four key ecological descriptors of marine snow (Trudnowska et al., 2021).

The final optical dataset included 6245 images of detrital particles. These images and their features were then used in a principal component analysis (PCA). This method was used to hierarchize and discretize the features into a lower-dimensional space to facilitate interpretation. The first 4 principal components, accounting for 83% of morphological variance, were then used to distinguish discrete morphotypes via k-means clustering. The number of clusters was identified using an optimization procedure, whereby varying values of k were used to compute within-cluster sum of squares (also known as the 'elbow- method; Thorndike 1953). All analyses were performed using R Statistical Software (v4.2.0; R Core Team 2022). PCA and k-means clustering were

performed using the 'FactorMineR' (Lê et al., 2008) and base R statistical packages. Data wrangling and visualization was done using the 'tidyverse' group of R packages (Wickham et al., 2019).

To calculate particle concentrations of marine snow for each depth profile, the sampled volume for each 5 m interval was calculated using the image acquisition rate and descent speed of the instrument. Because no depth trends were observed in the particle density within individual profiles, concentrations for each profile were then integrated by dividing the total particle count by the total sampled volume in each 100 m profile.

Acoustic Analysis. Following the expedition, the echosounder was calibrated *ex-situ* at the Kongsberg testing facility using a 22 mm copper sphere and following standard spherical calibration methods (Demer et al., 2015). Based on calibration results, data were subsampled using a 350-380 kHz bandpass filter to avoid resonant and noisy portions of the bandwidth. Acoustic profiles of broadband S_v backscatter were manually cleaned for noise and interference in Echoview 11 (Echoview Software Pty Ltd, Hobart, Australia), which manifested as horizontal banding, most likely due to crosstalk interference with the 300 kHz LADCP. Corrections to sound speed, absorption and range were made using S_v-range matrices that were temporally aligned with CTD measurements. Finally, depth profiles of mean volume backscatter at the center frequency (365 kHz) were calculated to assess the vertical distribution of copepods. Statistical metrics of the vertical distribution, Centre of Mass and Equivalent Area, were calculated following methods developed in Urmy et al (2012). The suitability of this data for the measurement of the vertical distribution of copepods was based on the acoustic wavelength at this bandwidth (~3.8-4.2 mm), which corresponds to the typical size ranges of the dominant Arctic copepod: *Calanus* spp.

Zooplankton samples. Zooplankton sampled in the shallowest depth interval (0 - 50 m) were split twice using a Folsom splitter. Samples were then sieved from preservative formalin solution and rinsed in freshwater, before being manually sorted into taxonomic groups. Copepods were sorted into three major size classes: large copepods, small copepods, and nauplii. Large copepods included the three major Calanoid copepods *C. glacialis, C. hyberboreus,* and *C. finmarchicus* as well as *Metridia sp* and *Euchaeta sp*. Small copepods included *Oithona sp., Microcalanus sp.* The nauplii group contained nauplii of all copepods. Gelatinous plankton such as siphonophores were unable to be counted due to poor preservation.

4.4 Results

4.4.1 Seasonal Ice Conditions

During the 2019 sampling season, sea-ice break up in Petermann and Sherard Osborn Fjords occurred on similar timescales (Figure 4.2). Beginning in mid-July, fissures began to form at the glacial tongues and localized ocean circulation drove ice outward toward the opening of each fjord. In Petermann Fjord, ice was eventually exported into the Kennedy Channel – Hall Basin region by August 14th. By contrast, the large icebergs and fractured sea-ice in Sherard Osborn Fjord remained entrapped within the fjord, staying in circulation throughout the short open-water season (Figure 4.2).
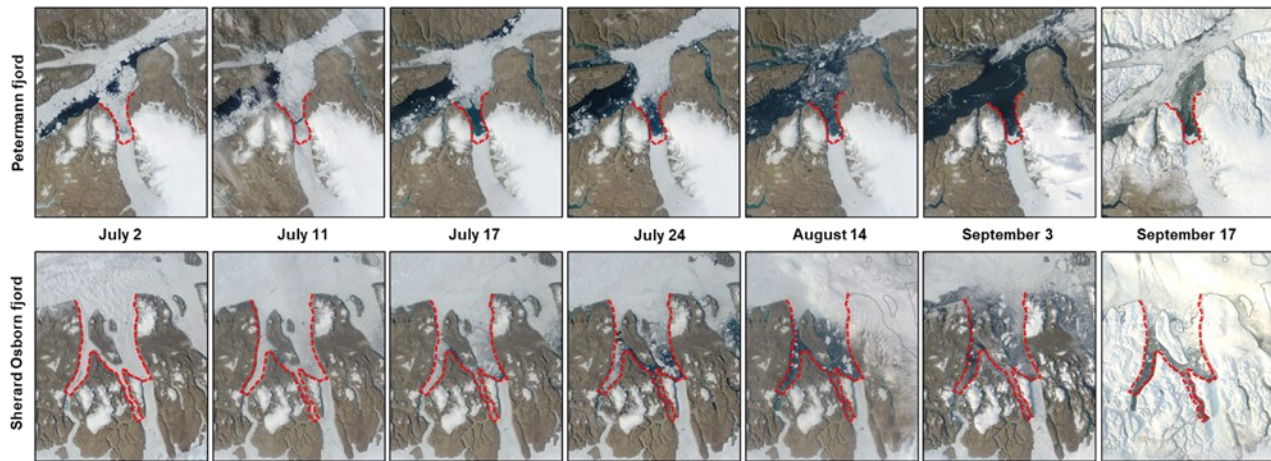
Figure 4.2 Satellite imagery showing the seasonal progression of ice-break up and formation in the region surrounding Petermann and Sherard Osborn Fjords during cloud-free days. Red-dashed lines indicate the fjord boundaries, with areas beyond the boundary covered by a floating ice tongue.

Based on these ice conditions, it was apparent that the waters of PF were exposed to ice-free, open water conditions for a longer period, and thus a higher level of continuous solar irradiance and increased susceptibility to wind-driven mixing. By late August the fjord was open to the surrounding waters, allowing for increased horizontal exchange with the Nares Strait. By contrast, Sherard Osborn Fjord remained ice-covered throughout the study period.

4.4.2 Oceanographic Conditions

In response to these differences in ice regime and fjord circulation, PF and SOF displayed strongly contrasting oceanographic conditions in the upper water column (0 - 100 m; Figure 4.3). Vertical temperature and salinity profiles in SOF revealed an 'amplified' stratification regime, whereby atmospherically warmed meltwater, reaching high temperatures of 3.5° C and low salinity of 15 PSU, overlaid cold intermediate waters with a maximum temperature of 0° C and low salinity of 30 PSU. Fluorescence and oxygen profiles, which can be indicative of both the level of primary productivity and the level of aerobic respiration, also show contrasting conditions amongst the two fjords: the magnitude of fluorescence was higher and coincided with a shallower peak in PF,

whereas oxygen saturation within the mixed layer above 75 m reached 115% and was consistently higher in SOF. (Figure 4.3).
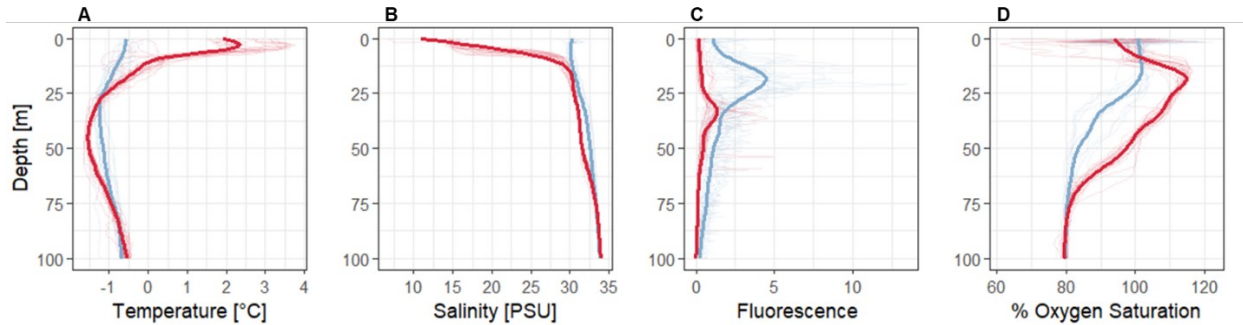
Figure 4.3 Oceanographic profiles of temperature (A), salinity (B), fluorescence (C) and oxygen saturation (D) in the upper 100 m of the water column at Petermann (blue line) and Sherard Osborn (red line) fjords. Bold trend lines were fitted using generalized additive models.

4.4.3 Marine Snow Morphology

Particles imaged by the UVP5 predominantly include detrital materials (~99%), including phytodetrital aggregates and fecal pellets, along with living organisms such as gelatinous and crustacean zooplankton (~1%). We combined all non-living particle images into a single group, which we refer to as 'marine snow.' Through quantitative analysis of marine snow morphology, we found four dominant cluster morphotypes (Figure 4.4) which varied in size (perimeter, area, length etc.), shape (circularity), brightness (mean/median grey level) and structure (homogeneity or heterogeneity). Type 1 consisted of large, 'fluffy' aggregate-like particles. Type 2 consisted of small, circular particles. Type 3 consisted of 'flake-like' medium sized, irregularly shaped particles. Type 4 consisted of large, circular particles, mostly distinguished by their darkness relative to other groups.
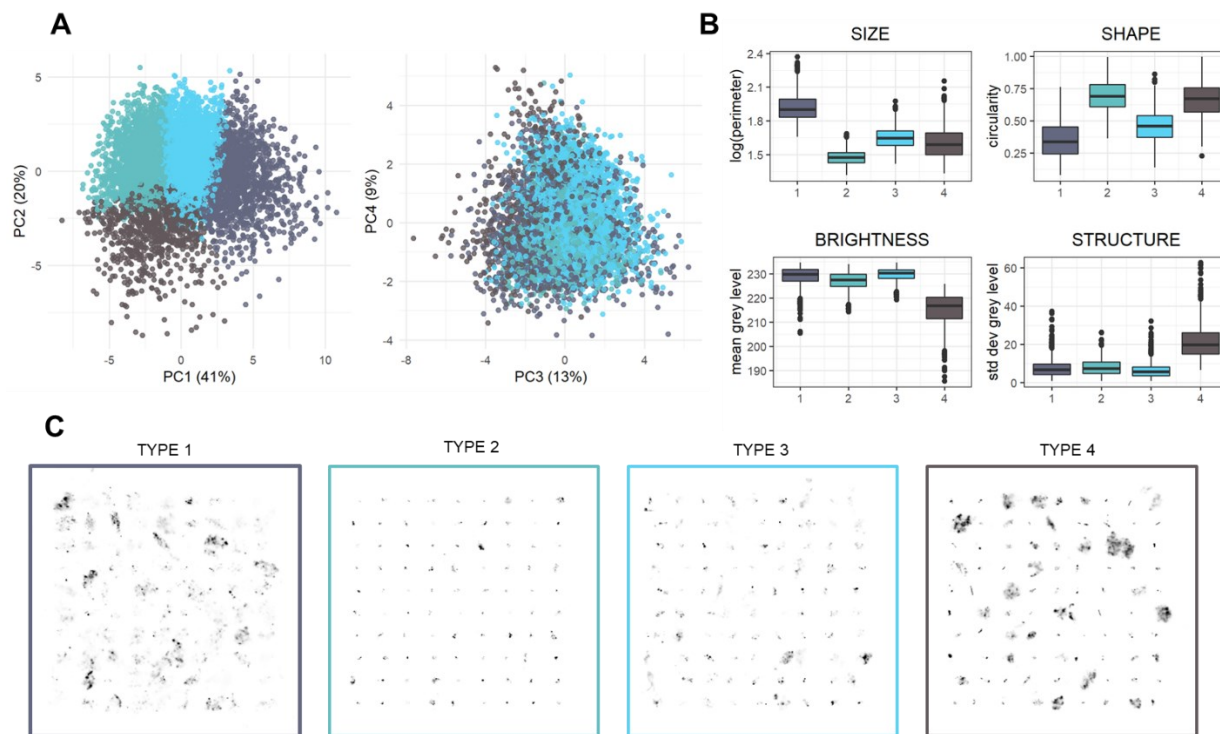
Figure 4.4 Marine snow morphotypes. A: Principal components analysis of 19 morphological descriptors and the results of k-means clustering (k=4) to identify morphotypes. B: Boxplots of exemplary morphological features used to describe morphotypes showing maximum, minimum, and median values and boxes with 25th and 75th quartiles range. C: Image mosaics containing 90 random images for each marine snow morphotype. Image contrast values were automatically adjusted in ImageJ software using a 0.10% pixel saturation value to improve visualization.

4.4.4 Marine Snow Quantity and Quality

Among regions, the highest particle concentrations in the upper 100 m were found in PF and the lowest particle concentrations were found in SOF (Figure 4.5A). Regional marine snow profiles were characterized by the proportion of each morphotype at 10 m depth intervals (Figure 4.5B). We observed varying patterns in particle production and attenuation with depth, that appeared consistent for each morphotype. Morphotype profiles of SOF were characterized by a high proportion of Type 4 particles. Type 4 (dark and round) particles were associated with stations sampled in heavy ice conditions and high volume of surface meltwater (LS and SOF) and their relative occurrence increased with depth. Type 1 particles (large and 'fluffy') were found in the

lowest abundance at SOF sites. Marine snow profiles at LS sites had similar composition to SOF; however, there was a higher occurrence of Type 2 particles (small, round) and Types 1 and 3 were absent in some depth horizons. At PF locations, we observed the highest proportion of Type 3 (medium sized, irregular shape) particles which attenuated with depth. PF locations had a high proportion of Type 2 (small, round) particles, which increased in abundance with depth. The KC-HB regional profile showed similar composition profiles as PF, despite hosting much lower concentrations than PF. Together these profiles indicate two distinct regimes (PF, KC-HB vs SOF, LS) in particle quality, with varying levels in particle concentrations among regions.
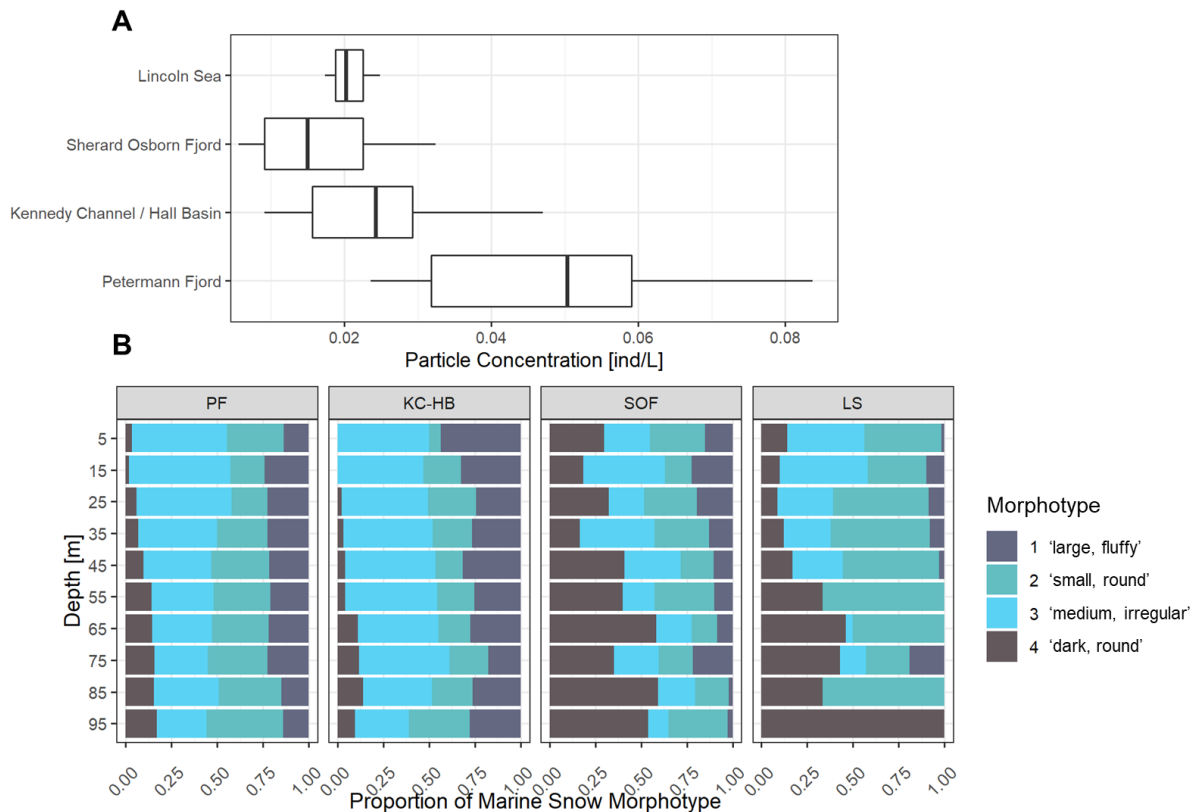
Figure 4.5 Marine snow particle concentration and morphotype depth profiles in the upper 100 m of the water column. **A**. Integrated water column (upper 100 m) particle concentrations for each sampling region. Boxplots show maximum, minimum, and median values and 25th and 75th percentile values for each location. **B**. Proportion of each marine snow morphotype across 10 m depth bins in each region.

4.4.4 Copepod community and size structure

Based on multinet sampling, copepods accounted for 97.7% of the total zooplankton abundance in the upper 100 m. An analysis of similarity (ANOSIM) showed statistically significant differences in the community structure of copepod size classes in the upper 100 m between fjords (R = 0.60, p < 0.005). SOF was characterized by consistently low nauplii abundance (< 10%) and high numbers of small copepods (~50%) (Figure 4.6). In contrast, PF had a more even distribution of size classes, with nauplii comprising approximately 30% of the total copepod abundance. Even though the relative abundances of copepods within each size class differed across the two fjords, the total number of copepods (summed across size classes) was similar between fjords.
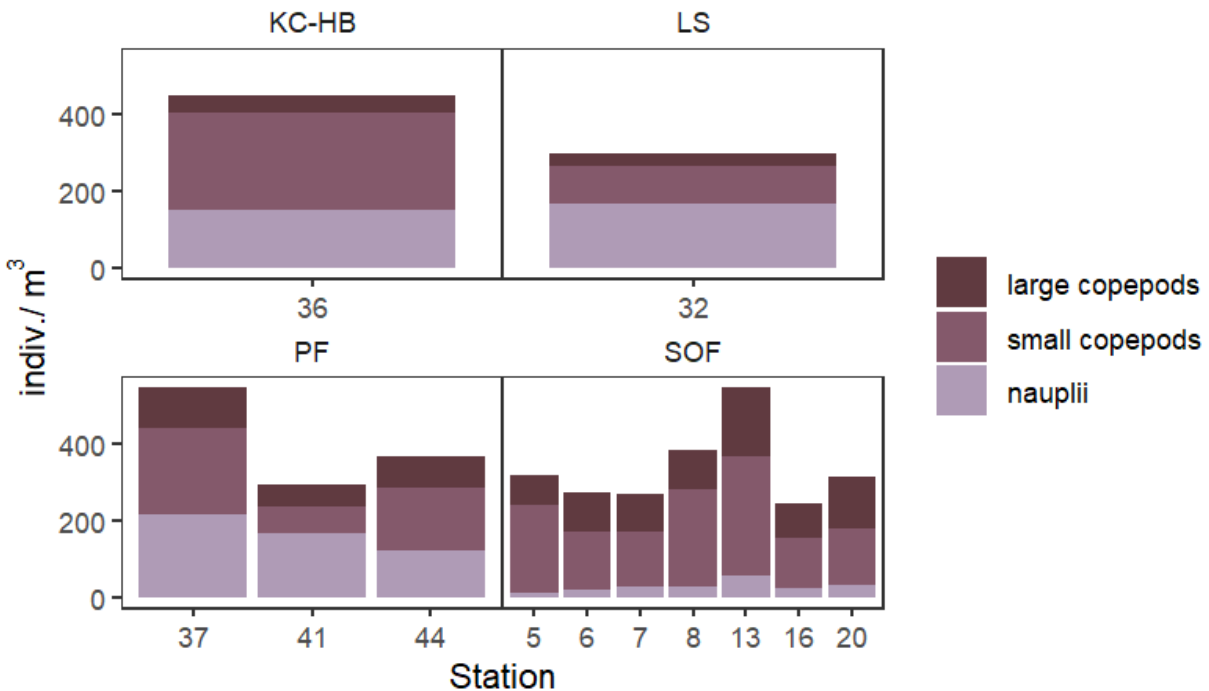
Figure 4.6 Abundance (count per m^3) of copepods sampled by multinet sites in the upper 100 m of the water column. Colors indicate abundance per size class. Numbers below each bar indicate the station number. Each panel represents a different sampling region in NW Greenland: KC-HB

= Kennedy Channel / Hall Basin, LS = Lincoln Sea, PF = Petermann Fjord, SOF = Sherard Osborn Fjord.

4.4.5 Vertical Distribution

Comparison of broadband acoustic profiles revealed distinct vertical distribution patterns among fjords (Figure 4.7). Overall, acoustic backscatter profiles showed a general trend of attenuation of copepod backscatter with depth. Profiles across SOF had lower variation compared than PF. Within profiles, SOF also showed a less even distribution of backscatter (Equivalent Area = 59.3 m vs 71.0 in PF) and a shallower centre of mass (COM) of backscatter (COM = 50.7 m vs 54.8m in PF). PF profiles were less stable in their pattern, showing a higher variation in the amplitude of backscatter. However, in PF there was a consistently higher proportion of copepod backscatter below 75 m. In all locations, backscatter was highest toward the surface. Low sampling effort precluded detailed analysis in LS and KC-HB. However, patterns in acoustic backscatter in outlying regions (LS and KC-HB) were similarly aligned to their neighboring fjords, but less coherent (Suppl. Figure 3).
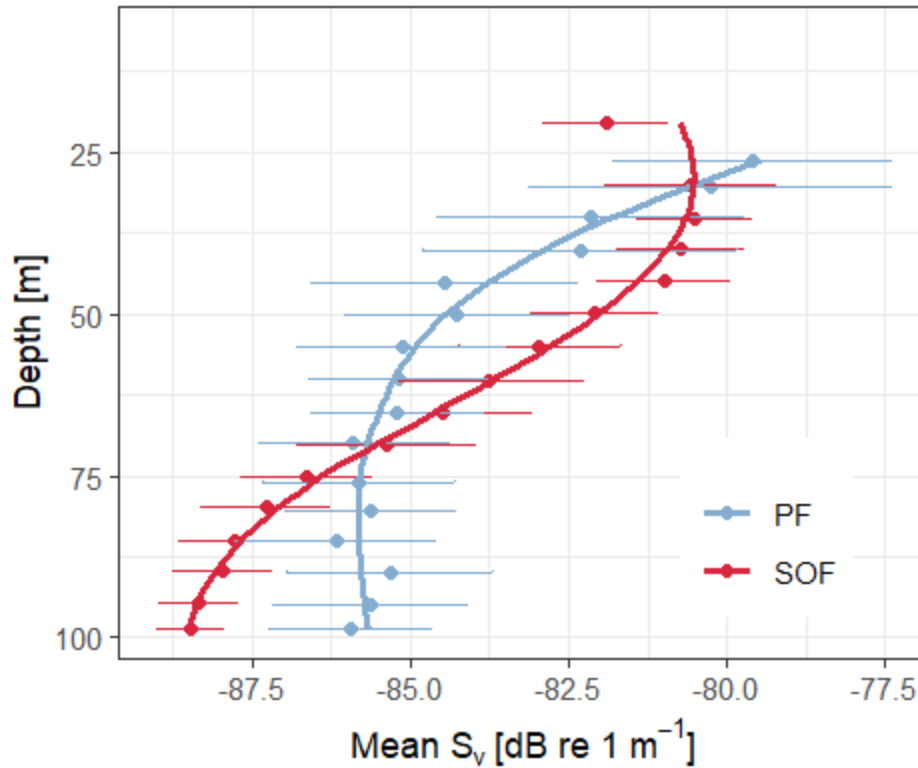
Figure 4.7 Vertical profiles of copepod acoustic backscatter in Sherard Osborn Fjord (SOF; red line and points) and Petermann Fjord (PF; blue line and points). Points indicate linear averages calculated for each 5 m interval and error bars indicate +/- the standard deviation. Trend lines are fitted using a locally estimated scatterplot smoothing (loess) function.

4.5 Discussion

Our study demonstrates that amplified fjord stratification creates distinct patterns in planktonic assemblages. In Sherard Osborn Fjord (SOF), reduced mixing and a shallow pycnocline at 8 m (Figure 4.3) were associated with low particle production and lower quality particles for zooplankton grazers. Under these conditions, copepods shift their vertical distribution toward the surface to presumably maximize their feeding opportunities while potentially incurring additional predation pressure. By using a morphological approach to quantify marine snow, we were able to characterize the types of particles associated with what we conclude were contrasting states of pelagic production.

In Petermann Fjord (PF), the well-mixed surface waters were associated with the highest particle concentrations relative to SOF and the outlying sampling sites. The high-resolution sampling of the UVP5 also allowed us to observe changes in particle composition, whereby patterns of both production and attenuation reflected distinct changes in the particle field with depth. The vertical profiles of zooplankton acoustic backscatter indicated a corresponding shift in the habitat use of copepods within the different particle fields of the euphotic zone. In particle depleted waters (amplified stratification), where small and dark particle types prevailed (Types 2 and 4), copepods were found concentrated toward the surface, where food abundance was likely highest. In contrast, the well-mixed waters of PF showed the highest particle concentrations, weaker changes in the vertical composition of marine snow, which were reflected by a more evenly distributed copepod community.

We believe the high diversity of particles and lowered attenuation of Types 1 and 3 ('fluffy','flakey', and irregular-shaped aggregates) reflects enhanced feeding opportunities for grazing copepods. Similarly, Trudnowska et al. (2022) found these types to be associated with late-stage blooms in open waters in their study. The largest particles in their study were associated with *Phaeocystis* blooms which contain high levels of polysaccharides, which may contribute to particle size via agglomerative properties. While pelagic diatoms are generally considered the preferred prey of Arctic copepods, *Phaeocystis* can provide sufficient nutrition for survival, despite inhibiting reproductive success (Turner et al., 2002; Cleary et al., 2017). Our comparisons among fjord environments revealed contrasting scenarios which may exemplify widespread conditions seen in future Arctic marine ecosystems.

4.5.1 Stratification limits food availability

Compared to land-terminating glacial fjords, marine-terminating fjords are generally considered more productive due to entrainment of nutrients in meltwater plumes (Meire et al., 2017). In open fjords, such as PF, thermal stratification can enhance primary production by trapping nutrients and algal cells in the euphotic zone (Tremblay et al., 2015). At times, strong winds can further enhance productivity by replenishing surface nutrients (Castro de la Guardia et al., 2019). Buoyant subglacial plumes can also enhance the nutrient load, creating upwelled regions of high productivity within fjords (Meire et al., 2017).

In semi-enclosed fjord systems, such as SOF, summertime discharge typically produces strong, near-surface stratification, resulting in a shallow nutrient-poor layer which thereby limits primary production and results in lower phytoplankton biomass distributed deeper in the water column (Hopwood et al., 2020). Increasing meltwater volume from sea-ice and ice-damming can further enhance this effect, creating thermohaline gradients requiring higher wind stress and turbulence to break down. Rather than topographical enhancement, such as upwelling or resuspension seen in other fjord systems, the lower productivity in SOF is a result of a topographic reduction in mixing (Stranne et al., 2021). This paradigm was consistent with satellite imagery, where virtually no open water days occurred (Figure 4.3). As a result, we observed a low fluorescence signal, low particle concentrations, and low-quality marine snow (Types 2 & 4) for grazing copepods. While these indices alone are not reflective of phytoplankton bloom stage (e.g., pre- or post-bloom) they do suggest a strong temporal coupling between primary production and particle formation (Szeligowska et al., 2022).

4.5.1 Vertical patterns in marine snow morphology

Phytoplankton blooms in seasonally ice-covered Arctic fjords are typically dominated by diatoms, either as senescent cells or algal aggregates (Hopwood et al., 2020). When combined with inorganic matter, living and dead organisms, through complex biochemical processes, they form sinking aggregates known as marine snow (Alldredge and Silver, 1988). Depending on the ratio of biomass-to-grazing pressure, sinking particles may be fragmented into small, slowly sinking materials or digested directly into dense fast-sinking fecal pellets (Wiedmann et al., 2016). The attenuation and production patterns of discrete particle types through the study areas suggests not only differences in the composition and production of marine snow, but also the result of complex interactions between copepod feeding and fragmentation, coagulation and sinking. In our study, we observed the strongest vertical gradients in particle types at SOF and LS (Figure 4.5), where fluorescence was low, which suggests a higher intensity of particle consumption and fragmentation (i.e., turnover rate). For instance, sharp vertical gradients in marine snow distributions and high sinking rates imply short timescales of production and loss (Lampitt et al., 1993). Adding to the complexity, the mechanisms behind particle shape formation are tied to species and context-specific factors. For example, in certain species of phytoplankton, aggregate/colonial formation can be impeded by intense chemical signals from grazing copepods (Long et al. 2007). Without data on phytoplankton species composition, we can only conclude that fragmentation/consumption of particulate was likely more efficient when food was limited (Briggs et al., 2020). This process is best exemplified by the comparison of particle type attenuation patterns, whereby steep morphological gradients were seen at the lowest particle quantities (SOF).

When comparing regions with similar particle concentrations but different morphology profiles patterns (SOF, KC-HB & LS), the interpretation becomes less clear. We would expect that the

multi-year sea ice of LS would yield the lowest particle concentrations due to reduced irradiance, however; the comparable particle concentrations may be supported by sinking ice algae aggregates. These results show that similar particle concentrations can exist among varying conditions of ice cover, only varying in their morphology. Therefore, our results highlight that particle morphology may play a larger role in ecosystem regulation than quantity alone (Cavan et al., 2017).

4.5.2 Linking particle quality to ecology

Low-latitude studies using sediment traps have suggested that particles in the upper 100 m are typically composed of algal-derived aggregates, non-descript aggregates and fecal pellets (Riser et al., 2001; Goldthwait and Alldredge, 2006). Based on the correspondence of vertical patterns between morphotype and copepod distribution, we conclude the highest quality food is exemplified by morphotypes 1 and 3. These types were both the largest and most irregular in shape, associated with previously described qualitative descriptors such as 'fluffy' and 'agglomerated' (Lombard et al., 2013; Trudnowska et al., 2021). Types 2 and 4 were both characterized by their smaller size, which could be associated with fecal pellets and partially consumed fragments. This observed reduction in quality of particulate could in part be due to low overall primary production, but also likely results from feeding and fragmentation by copepods (Briggs et al., 2020). Type 4 particles, which increased in abundance with depth, were characterized by their darkness and circularity. While difficult to assign the origin, similar particles described as 'dark' have been associated with ice-cover, sympagic algae, fecal pellets, and fragments of large aggregates (Trudnowska et al., 2021). These particles were found in the deeper portion of the upper water column, where copepod abundance was lowest. These results suggest that this particle morphotype represents poor-quality food for copepods. In Disko Bay, fecal pellets can comprise up 35% of the

total particulate flux (Riser et al., 2001; Juul-Pedersen et al., 2006). The increasing abundance of Type 4 with depth at all sites may indicate that they are key contributors to the particle-injection pump in these fjords (Boyd et al., 2019).

4.5.3 What caused the change in copepod distribution?

In response to differences in the particle field among fjords, we observed different vertical distribution of copepod backscatter in the upper water column. Despite the measurement limitations associated with the upper 25 m in many profiles, acoustic backscatter between 25-100 m allowed us to observe vertical patterns in copepod distribution at fine scales. Moreover, the distribution patterns were consistent within fjords across 5 weeks of temporally correspondent sampling, suggesting that copepods were responding to stable and localized oceanographic conditions within each fjord. In SOF oxygen saturation levels between 15-75 m (Figure 4.3) were lower than in PF, potentially reflecting consistently lower levels of aerobic respiration. Similarly, fluorescence levels were lower in SOF, suggesting either low primary production or a high consumer-to-biomass ratio in phytoplankton. While these measurements reflect consistency of ecosystem state among fjords, there are other potential factors, which we did not measure, that could explain the response of copepods.

Previous studies suggest that the vertical distribution of high-latitude copepods is driven primarily by biotic factors such as food availability (Herman, 1983; Longhurst et al., 1984; Basedow et al., 2010). Typically, flux feeding zooplankton will arrange themselves at the base of the euphotic zone, as a strategy to maximize feeding and avoid predation in the well-lit surface waters (Aksnes and Giske, 1993). As marine snow aggregates sink, they release chemical trails which copepods can detect and follow (Lombard et al., 2013). Our findings suggest that the variations in quantity and quality of sinking marine snow has a direct impact on the vertical distribution of copepods,

yet there are also a range of other factors to consider. For instance, density dependence through swarming can reduce individual predation risk in surface waters but can also force zooplankton deeper due to competition for food (Fortier and Harris, 1989), reduce their numbers through cannibalism (Basedow and Tande, 2006), or initiate a switch from herbivory to omnivory (Ohman and Runge, 1994). Vertical distribution could also be explained by spatio-temporal differences in seasonal development (Basedow et al., 2006). The higher relative abundance of large copepods and low nauplii in SOF may reflect a population in a later stage of development. Large copepods are expected to have a deeper distribution (Basedow et al., 2010), which contradicts the shallower distributional patterns observed in SOF. The ontogenetic adaptation for a given species likely depends on the persistence of the conditions, from year to year. Without multi-year data, it remains difficult to conclude if ice-damming is a recurrent seasonal process that drives adaptation in species or population structure. For instance, *Calanus* can modify nauplii emergence to match peaks in productivity or switch to particle feeding when phytoplankton is scarce (Søreide et al., 2010; Trudnowska et al., 2020). The higher proportion of small copepods (*Pseudocalanus, microcalanus*) in SOF may also suggest a community-wide shift toward species with more efficient particle feeding. Ultimately, without detailed taxonomic data, such conclusions remain speculative.

Compared to open ocean ecosystems, glacial fjords possess unique and complex physical characteristics that can also impact planktonic systems. For this reason, it is important to consider how additional abiotic factors such as light and lithogenic suspended particulate may impact copepod vertical distribution. Due to limited instrumentation, we were unable to account for variation in light within the upper water column. The attenuation of light in glacial fjords is often influenced by suspended particulate matter (Sagan and Darecki, 2018). According to a recent study

(Szeligowska et al., 2022), near surface turbidity layers can impact the distribution of copepods in similar patterns seen in our study. As the UVP5 is not suitable for measuring small particles in the size ranges associated with glacial discharge, we were unable to investigate the source of turbidity signals in our study.

Overall, our results showed that marine snow abundance, diversity and heterogeneity in the upper water column varied considerably between the fjords and regions. Homogenous morphotype profiles (Figure 4.5) were associated with a well-mixed surface layer and subsequently homogenous distribution of copepod backscatter (Figure 4.7). The contrary was seen in SOF and LS, where a stratified water column displayed heterogenous particle vertical structure and shallower copepod backscatter. As food provisioning in zooplankton typically involves tradeoffs between feeding success and predator avoidance, the shift in distribution of copepods toward the surface (Figure 4.7), may inadvertently lead to increased predation risk. Future studies including light measurements and in-situ optical particle measurements for both suspended sediments and marine snow could help elucidate which drivers have a larger influence on copepod vertical distribution.

4.6 Conclusion

Surface stratification processes common to Arctic environments are further enhanced in fjords where horizontal water exchange is inhibited by topography and ice damming. High Arctic fjords are mesocosms for glacial-ocean interactions that can lead to enhanced production relative to outlying waters. In this study, we compared two fjords with contrasting stratification regimes. We found that in the highly stratified waters of Sherard Osborn Fjord, marine snow particle production was low and associated with strong variation in the vertical patterns of morphotypes. These conditions were associated with a shallower distribution of copepods. In the well mixed waters of

Petermann Fjord, the marine snow production was higher, and the particle field included a higher proportion of detrital aggregates, creating better feeding opportunities for copepods at depth. While the summertime distribution of zooplankton in high Arctic environments is known to concentrate in the euphotic zone during periods when primary productivity is highest, little was known about their response to the particle field. We showed that at fine scales, copepods respond to the quantity and quality of marine snow, potentially exposing themselves to higher predation risks near well-lit surface waters. The rapid loss of glaciers in the high Arctic will dramatically increase the volume of meltwater flux into coastal ecosystems, leading to enhance thermohaline stratification. This study shows that under such conditions, the particulate available to copepods will be of lower quality and quantity, impacting the grazing behavior of copepods with consequences to benthic-pelagic coupling and higher trophic production.

4.6 References

Aagaard, K., Coachman, L. K., and Carmack, E. (1981). On the halocline of the Arctic Ocean. *Deep Sea Research Part A. Oceanographic Research Papers* 28, 529–545. doi: https://doi.org/10.1016/0198-0149(81)90115-1.

Aksnes, D. L., and Giske, J. (1993). A theoretical model of aquatic visual feeding. *Ecol Modell* 67, 233–250. doi: https://doi.org/10.1016/0304-3800(93)90007-F.

Alldredge, A. L., and Silver, M. W. (1988). Characteristics, dynamics and significance of marine snow. *Prog Oceanogr* 20, 41–82. doi: https://doi.org/10.1016/0079-6611(88)90053-5.

Basedow, S. L., Edvardsen, A., and Tande, K. S. (2006). Spatial patterns of surface blooms and recruitment dynamics of Calanus finmarchicus in the NE Norwegian Sea. *J Plankton Res* 28, 1181–1190. doi: 10.1093/plankt/fbl048.

Basedow, S. L., and Tande, K. S. (2006). Cannibalism by female Calanus finmarchicus on naupliar stages. *Mar Ecol Prog Ser* 327, 247–255. doi: 10.3354/meps327247.

Basedow, S. L., Tande, K. S., and Stige, L. C. (2010). Habitat selection by a marine copepod during the productive season in the Subarctic. *Mar Ecol Prog Ser* 416, 165–178. Available at: https://www.int-res.com/abstracts/meps/v416/p165-178/.

Blachowiak-Samolyk, K., Kwasniewski, S., Dmoch, K., Hop, H., and Falk-Petersen, S. (2007). Trophic structure of zooplankton in the Fram Strait in spring and autumn 2003. *Deep Sea*

Research Part II: Topical Studies in Oceanography 54, 2716–2728. doi: https://doi.org/10.1016/j.dsr2.2007.08.004.

Boyd, P. W., Claustre, H., Levy, M., Siegel, D. A., and Weber, T. (2019). Multi-faceted particle pumps drive carbon sequestration in the ocean. *Nature* 568, 327–335. doi: 10.1038/s41586-019-1098-2.

Briggs, N., Dall'Olmo, G., and Claustre, H. (2020). Major role of particle fragmentation in regulating biological sequestration of CO2 by the oceans. *Science (1979)* 367, 791–793. doi: 10.1126/science.aay1790.

Bruyant, F., Amiraux, R., Amyot, M.-P., Archambault, P., Artigue, L., de Freitas, L., et al. (2022). The Green Edge cruise: investigating the marginal ice zone processes during late spring and early summer to understand the fate of the Arctic phytoplankton bloom. *Earth Syst Sci Data* 14, 4607–4642. doi: 10.5194/essd-14-4607-2022.

Buesseler, K. O. (1998). The decoupling of production and particulate export in the surface ocean. *Global Biogeochem Cycles* 12, 297–310. doi: https://doi.org/10.1029/97GB03366.

Castro de la Guardia, L., Garcia-Quintana, Y., Claret, M., Hu, X., Galbraith, E. D., and Myers, P. G. (2019). Assessing the Role of High-Frequency Winds and Sea Ice Loss on Arctic Phytoplankton Blooms in an Ice-Ocean-Biogeochemical Model. *J Geophys Res Biogeosci* 124, 2728–2750. doi: 10.1029/2018JG004869.

Cleary, A. C., Søreide, J. E., Freese, D., Niehoff, B., and Gabrielsen, T. M. (2017). Feeding by Calanus glacialis in a high arctic fjord: potential seasonal importance of alternative prey. *ICES Journal of Marine Science* 74, 1937–1946. doi: 10.1093/icesjms/fsx106.

De La Rocha, C. L., and Passow, U. (2007). Factors influencing the sinking of POC and the efficiency of the biological carbon pump. *Deep Sea Research Part II: Topical Studies in Oceanography* 54, 639–658. doi: https://doi.org/10.1016/j.dsr2.2007.01.004.

Demer, D. A., Berger, L., Bernasconi, M., Bethke, E., Boswell, K. M., Chu, D., et al. (2015). Calibration of acoustic instruments. *ICES Cooperative Research Report* 326, 1–133. doi: http://dx.doi.org/10.25607/OBP-185.

Durkin, C. A., Buesseler, K. O., Cetinić, I., Estapa, M. L., Kelly, R. P., and Omand, M. (2021). A Visual Tour of Carbon Export by Sinking Particles. *Global Biogeochem Cycles* 35, 1–17. doi: 10.1029/2021GB006985.

Fortier, L., and Harris, R. P. (1989). Optimal foraging and density-dependent competition in marine fish larvae. *Mar Ecol Prog Ser* 51, 19–33. Available at: http://www.jstor.org/stable/24833823.

Fortier, M., Fortier, L., Hattori, H., Saito, H., and Legendre, L. (2001). Visual predators and the diel vertical migration of copepods under Arctic sea ice during the midnight sun. *J Plankton Res* 23, 1263–1278. doi: 10.1093/plankt/23.11.1263.

Goldthwait, S. A., and Alldredge, A. L. (2006). An investigation of diel synchronicity between water column marine snow concentration and the flux of organic matter in the Santa Barbara Channel, California. *Deep Sea Research Part I: Oceanographic Research Papers* 53, 485–505. doi: https://doi.org/10.1016/j.dsr.2005.05.011.

Hegseth, E. N., and Tverberg, V. (2013). Effect of Atlantic water inflow on timing of the phytoplankton spring bloom in a high Arctic fjord (Kongsfjorden, Svalbard). *Journal of Marine Systems* 113–114, 94–105. doi: https://doi.org/10.1016/j.jmarsys.2013.01.003.

Herman, A. W. (1983). Vertical distribution patterns of copepods, chlorophyll, and production in northeastern Baffin Bay. *Limnol Oceanogr* 28, 709–719. doi: https://doi.org/10.4319/lo.1983.28.4.0709.

Hopwood, M. J., Carroll, D., Dunse, T., Hodson, A., Holding, J. M., Iriarte, J. L., et al. (2020). Review article: How does glacier discharge affect marine biogeochemistry and primary production in the Arctic? *Cryosphere* 14, 1347–1383. doi: 10.5194/tc-14-1347-2020.

Jackson, G. A., and Checkley, D. M. (2011). Particle size distributions in the upper 100m water column and their implications for animal feeding in the plankton. *Deep Sea Res 1 Oceanogr Res Pap* 58, 283–297. doi: 10.1016/j.dsr.2010.12.008.

Jakobsson, M., Mayer, L. A., Farrell, J. F., and Ryder 2019 Scientific Party (2020a). Expedition report: SWEDARCTIC Ryder 2019.

Jakobsson, M., Mayer, L. A., Nilsson, J., Stranne, C., Calder, B., O'Regan, M., et al. (2020b). Ryder Glacier in northwest Greenland is shielded from warm Atlantic water by a bathymetric sill. *Commun Earth Environ* 1, 1–10. doi: 10.1038/s43247-020-00043-0.

Juul-Pedersen, T., Nielsen, T. G., Michel, C., MÃƒÂ¸ller, E. F., Tiselius, P., Thor, P., et al. (2006). Sedimentation following the spring bloom in Disko Bay, West Greenland, with special emphasis on the role of copepods. *Mar Ecol Prog Ser* 314, 239–255. Available at: https://www.int-res.com/abstracts/meps/v314/p239-255/.

Kalenitchenko, D., Joli, N., Potvin, M., Tremblay, J.-É., and Lovejoy, C. (2019). Biodiversity and Species Change in the Arctic Ocean: A View Through the Lens of Nares Strait. *Front Mar Sci* 6. doi: 10.3389/fmars.2019.00479.

Kosobokova, K., and Hirche, H.-J. (2000). Zooplankton distribution across the Lomonosov Ridge, Arctic Ocean: species inventory, biomass and vertical structure. *Deep Sea Research Part I: Oceanographic Research Papers* 47, 2029–2060. doi: 10.1016/S0967-0637(00)00015-7.

Lampitt, R. S., Hillier, W. R., and Challenor, P. G. (1993). Seasonal and diel variation in the open ocean concentration of marine snow aggregates. *Nature* 362, 737–739. doi: 10.1038/362737a0.

Lê, S., Josse, J., and Husson, F. (2008). FactoMineR : An R Package for Multivariate Analysis. *J Stat Softw* 25. doi: 10.18637/jss.v025.i01.

Lombard, F., Koski, M., and Kiørboe, T. (2013). Copepods use chemical trails to find sinking marine snow aggregates. *Limnol Oceanogr* 58, 185–192. doi: https://doi.org/10.4319/lo.2013.58.1.0185.

Long, J. D., Smalley, G. W., Barsby, T., Anderson, J. T., and Hay, M. E. (2007). Chemical cues induce consumer-specific defenses in a bloom-forming marine phytoplankton. *Proceedings of the National Academy of Sciences* 104, 10512–10517. doi: 10.1073/pnas.0611600104.

Longhurst, A. R. (1976). "Vertical Migration," in *The Ecology of the Seas*, eds. D. H. Cushing and J. J. Walsh (Philadelphia, PA: WB Saunders), 116–137.

Longhurst, A., Sameoto, D., and Herman, A. (1984). Vertical distribution of Arctic zooplankton in summer: eastern Canadian archipelago. *J Plankton Res* 6, 137–168. doi: 10.1093/plankt/6.1.137.

Meire, L., Mortensen, J., Meire, P., Juul-Pedersen, T., Sejr, M. K., Rysgaard, S., et al. (2017). Marine-terminating glaciers sustain high productivity in Greenland fjords. *Glob Chang Biol* 23, 5344–5357. doi: 10.1111/gcb.13801.

MODIS Characterization Support Team (MCST) (2017). MODIS 500m Calibrated Radiance Product. Goddard Space Flight Center, USA doi: 10.5067/MODIS/MYD02HKM.061.

Napp, J. M., Brooks, E. R., Matrai, P., and Mullin, M. M. (1988). Vertical distribution of marine particles and grazers. II. Relation of grazer distribution to food quality and quantity. *Mar Ecol Prog Ser* 50, 59–72. Available at: http://www.jstor.org/stable/24831618.

Ohman, M. D., and Runge, J. A. (1994). Sustained fecundity when phytoplankton resources are in short supply: Omnivory by Calanus finmarchicus in the Gulf of St. Lawrence. *Limnol Oceanogr* 39, 21–36. doi: https://doi.org/10.4319/lo.1994.39.1.0021.

Picheral, M., Guidi, L., Stemmann, L., Karl, D. M., Iddaoud, G., and Gorsky, G. (2010). The underwater vision profiler 5: An advanced instrument for high spatial resolution studies of particle size spectra and zooplankton. *Limnol Oceanogr Methods* 8, 462–473. doi: 10.4319/lom.2010.8.462.

Riser, C. W., Wassmann, P., Olli, K., and Arashkevich, E. (2001). Production, retention and export of zooplankton faecal pellets on and off the Iberian shelf, north-west Spain. *Prog Oceanogr* 51, 423–441. doi: https://doi.org/10.1016/S0079-6611(01)00078-7.

Sagan, S., and Darecki, M. (2018). Inherent optical properties and particulate matter distribution in summer season in waters of Hornsund and Kongsfjordenen, Spitsbergen. *Oceanologia* 60, 65–75. doi: https://doi.org/10.1016/j.oceano.2017.07.006.

Sameoto, D. D. (1984). Vertical distribution of zooplankton biomass and species in northeastern Baffin Bay related to temperature and salinity. *Polar Biol* 2, 213–224. doi: 10.1007/BF00263627.

Søreide, J. E., Leu, E., Berge, J., Graeve, M., and Falk-Petersen, S. (2010). Timing of blooms, algal food quality and Calanus glacialis reproduction and growth in a changing Arctic. *Glob Chang Biol* 16, 3154–3163. doi: https://doi.org/10.1111/j.1365-2486.2010.02175.x.

Stranne, C., Nilsson, J., Ulfsbo, A., O'Regan, M., Coxall, H. K., Meire, L., et al. (2021). The climate sensitivity of northern Greenland fjords is amplified through sea-ice damming. *Commun Earth Environ* 2, 4–11. doi: 10.1038/s43247-021-00140-8.

Stuart-Lee, A., Mortensen, J., Juul-Pedersen, T., Middelburg, J., Soetaert, K., Hopwood, M., et al. (2023). Influence of glacier type on bloom phenology in two Southwest Greenland fjords. *Estuar Coast Shelf Sci*, 108271. doi: 10.1016/j.ecss.2023.108271.

Szeligowska, M., Trudnowska, E., Boehnke, R., and Błachowiak-Samołyk, K. (2022). Dark plumes of glacial meltwater affect vertical distribution of zooplankton in the Arctic. *Sci Rep* 12, 17953. doi: 10.1038/s41598-022-22475-8.

Szeligowska, M., Trudnowska, E., Boehnke, R., Dąbrowska, A. M., Dragańska-Deja, K., Deja, K., et al. (2021). The interplay between plankton and particles in the Isfjorden waters influenced by marine- and land-terminating glaciers. *Science of the Total Environment* 780. doi: 10.1016/j.scitotenv.2021.146491.

Thorndike, R. L. (1953). Who belongs in the family? *Psychometrika* 18, 267–276. doi: 10.1007/BF02289263.

Toullec, J., Vincent, D., Frohn, L., Miner, P., Le Goff, M., Devesa, J., et al. (2019). Copepod Grazing Influences Diatom Aggregation and Particle Dynamics. *Front Mar Sci* 6. doi: 10.3389/fmars.2019.00751.

Tremblay, J.-É., Anderson, L. G., Matrai, P., Coupel, P., Bélanger, S., Michel, C., et al. (2015). Global and regional drivers of nutrient supply, primary production and CO2 drawdown in the changing Arctic Ocean. *Prog Oceanogr* 139, 171–196. doi: https://doi.org/10.1016/j.pocean.2015.08.009.

Trudnowska, E., Balazy, K., Stoń-Egiert, J., Smolina, I., Brown, T., and Gluchowska, M. (2020). In a comfort zone and beyond—Ecological plasticity of key marine mediators. *Ecol Evol* 10, 14067–14081. doi: https://doi.org/10.1002/ece3.6997.

Trudnowska, E., Lacour, L., Ardyna, M., Rogge, A., Irisson, J. O., Waite, A. M., et al. (2021). Marine snow morphology illuminates the evolution of phytoplankton blooms and determines their subsequent vertical export. *Nat Commun* 12, 1–13. doi: 10.1038/s41467-021-22994-4.

Trudnowska, E., Sagan, S., Kwasniewski, S., Darecki, M., and Blachowiak-Samolyk, K. (2015). Fine-scale zooplankton vertical distribution in relation to hydrographic and optical characteristics of the surface waters on the Arctic shelf. *J Plankton Res* 37, 120–133. doi: 10.1093/plankt/fbu087.

Turner, J. T., Ianora, A., Esposito, F., Carotenuto, Y., and Miralto, A. (2002). Zooplankton feeding ecology: does a diet of Phaeocystis support good copepod grazing, survival, egg production and egg hatching success? *J Plankton Res* 24, 1185–1195. doi: 10.1093/plankt/24.11.1185.

Urmy, S. S., Horne, J. K., and Barbee, D. H. (2012). Measuring the vertical distributional variability of pelagic fauna in Monterey Bay. *ICES Journal of Marine Science* 69, 184–196. doi: 10.1093/icesjms/fsr205.

Vinogradov, M. E. (1962). Feeding of the Deep-Sea Zooplankton. *Rapp. Proc.-Verb.* 153, 114–120.

Vinogradov, M. E. (1997). "Some Problems of Vertical Distribution of Meso- and Macroplankton in the Ocean," in *Advances in Marine Biology*, eds. J. H. S. Blaxter, A. J. Southward, A. V Gebruk, E. C. Southward, and P. A. Tyler (Academic Press), 1–92. doi: https://doi.org/10.1016/S0065-2881(08)60015-2.

von Appen, W.-J., Waite, A. M., Bergmann, M., Bienhold, C., Boebel, O., Bracher, A., et al. (2021). Sea-ice derived meltwater stratification slows the biological carbon pump: results from continuous observations. *Nat Commun* 12, 7309. doi: 10.1038/s41467-021-26943-z.

Wassman, P., and Reigstad, M. (2011). Future Arctic Ocean seasonal ice zones and implications for pelagic-benthic coupling. *Oceanography* 24, 220–231.

Weydmann-Zwolicka, A., Prątnicka, P., Łącka, M., Majaneva, S., Cottier, F., and Berge, J. (2021). Zooplankton and sediment fluxes in two contrasting fjords reveal Atlantification of the Arctic. *Science of The Total Environment* 773, 145599. doi: https://doi.org/10.1016/j.scitotenv.2021.145599.

Wickham, H., Averick, M., Bryan, J., Chang, W., McGowan, L., François, R., et al. (2019). Welcome to the Tidyverse. *J Open Source Softw* 4, 1686. doi: 10.21105/joss.01686.

Wiedmann, I., Reigstad, M., Marquardt, M., Vader, A., and Gabrielsen, T. M. (2016). Seasonality of vertical flux and sinking particle characteristics in an ice-free high arctic fjord—Different from subarctic fjords? *Journal of Marine Systems* 154, 192–205. doi: https://doi.org/10.1016/j.jmarsys.2015.10.003.
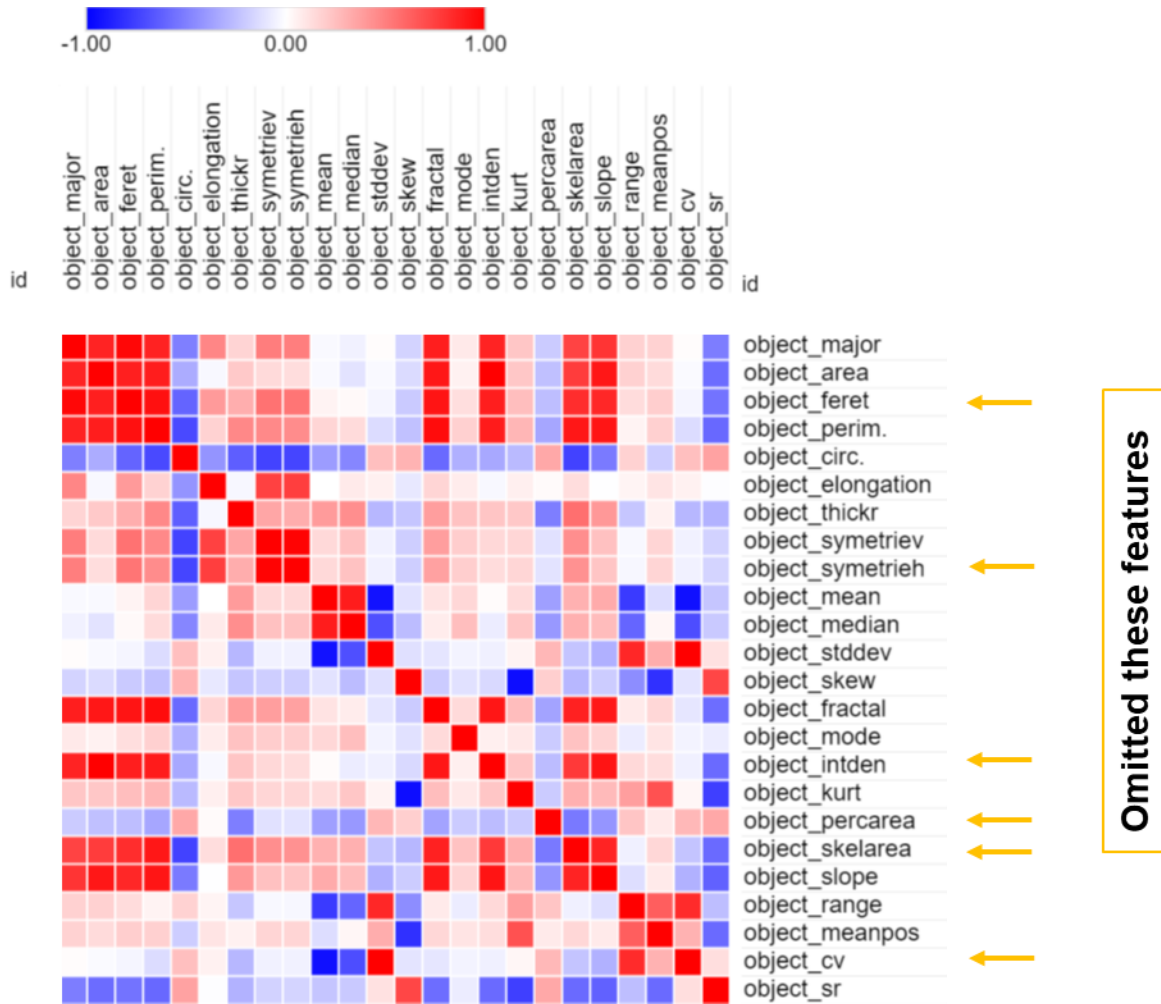
4.7 Supplementary Figures & Tables

Site	Ryder19_05_MN	Ryder19_06_MN	Ryder19_07_MN	Ryder19_08_MN	Ryder19_13_MN	Ryder19_16_MN	Ryder19_20_MN	Ryder19_32_MN	Ryder19_36_MN	Ryder19_37_MN	Ryder19_41_MN	Ryder19_44_MN
Lat	82 11.45 N	82 01.40 N	81 58.72 N	82 00.66 N	81 53.01 N	81 50.03 N	81 53.17 N	82 09.91 N	81 38.94 N	81 00.11 N	81 05.51 N	81 11.5059 N
Lon	51 49.74 W	52 04.33 W	52 07.11 W	51 44.97 W	51 06.92 W	51 01.57 W	51 00.46 W	59 50.49 W	64 12.90 W	60 58.49 W	61 36.14 W	62 04.168 W
Depth	706	837	826	622	260	678	253	412	623	1027	1100	933
Time (Surface)	0:26:31	19:42:15	15:13:47	13:49:27	13:31:45	17:08:50	14:23:00	14:11:25	17:07:00	19:51:55	6:29:05	21:30
Begin Descent	0:27:49	19:43:08	15:14:26	13:50:48	13:32:22	17:10:16	14:23:12	14:12:10	17:08:30	19:53:36	6:29:51	21:32:27
Descent Rate	40 m / min	40 m / min	40 m / min	40 m / min	40 m / min	40 m / min	40 m / min	40 m / min	40 m / min	60 m / min	60 m / min	60 m / min
Arrive Bottom	0:44:00	20:02:00	15:33:50	14:04:41	13:38:44	17:25:35	14:29:00	14:21:24	17:18:20	20:10:13	6:42:57	21:45:00
Begin Ascent	0:44:44	20:03	15:34:10	14:05:32	13:39:34	17:26:28	14:29:40	14:22:16	17:19:05	20:11:27	6:43:56	21:45:23

Depth	05_MN	06_MN	07_MN	08_MN	13_MN	16_MN	20_MN	32_MN	36_MN	37_MN	41_MN	44_MN
0	1:09:16	20:30:07	16:01:12	14:26:23	13:48:00	17:48:19	14:37:00-14:37:50	14:36:28- 14:37:46	17:38:42-17:40:05	20:43:07	7:18:49	22:15:06
25	1:07:50	20:28:36	15:59:00	14:24:51	13:47:02	17:46:36	14:36:00-14:36:47	14:34:52-14:35:37	17:37:14-17:38:10	20:41:41	7:16:45	22:13:40
50	1:06:34	20:28:00	15:58:11	14:24:14	13:46:49	17:46:18	14:35:00 - 14:35:55	14:33:54	17:37:07	20:41:02	7:15:55	22:13:00
75	1:04:51	20:26:21	15:56:38	14:22:36	13:45:04	17:44:43	14:34:00-14:34:50	14:32:24	17:35:17	20:39:32	7:13:34	22:11:13
100	1:04:20	20:26:00	15:56:08	14:22:10	13:44:58	17:44:20	14:33:50	14:32:01	17:35:00	20:39:14	7:13:10	22:10:43
125					13:43:20							
150					13:43:12							
175					13:41:26							
200					13:41:15							
225	0:59:44		15:51:50	14:17:40	13:39:34	17:39:35	14:29:40	14:27:16	17:30:30	20:34:46	7:07:45	22:05:29
250	0:59:00		15:51:23	14:16:47	Max = 250	17:39:25	Max = 240	14:26:48	17:30:00	20:34:18	7:07:16	22:04:52
375	0:54:28	20:16:28	15:47:00	14:12:16		17:35:00		14:22:16		20:29:48	7:02:24	21:59:30
400	0:53:50	20:16:00	15:46:20	14:11:13		17:34:41		Max = 400		20:29:36	7:01:54	21:58:55
575				14:05:32					17:19:05			
600				Max = 610					Max = 590			
625	0:44:44											
650	Max = 665											
675						17:26:28						
700						Max = 660						
825		20:03:07	15:34:10									
850		Max = 820	Max = 810									
875												21:45:23
900												Max = 880
1000										20:11:27		
1025										Max = 980	6:43:56	Max =1000

Supplementary Figure 1. Multinet sampling metadata and depth intervals. Each color represents a distinct depth interval sampled by the five (5) nets during vertical tows.

Supplemental Table 1. Morphometric features as grouped into key ecological descriptors of marine snow particle shape.

UVP5 Morphometric feature	Key ecological descriptor (Trudnowska et al 2022)
object_mean	brightness
object_median	brightness
object_mode	brightness
object_range	brightness
object_stddev	brightness
object_circ.	shape
object_elongation	shape
object_symetriev	shape
object_thickr	shape
object_area	size

object_fractal	size
object_major	size
object_perim.	size
object_skelarea	size
object_kurt	structure
object_meanpos	structure
object_skew	structure
object_slope	structure
object_sr	structure

Supplementary Figure 2. Similarity Matrix of morphological features of marine snow using Pearson correlation coefficients. Features with Pearson correlation value below/above ±0.97 were omitted from the analysis.
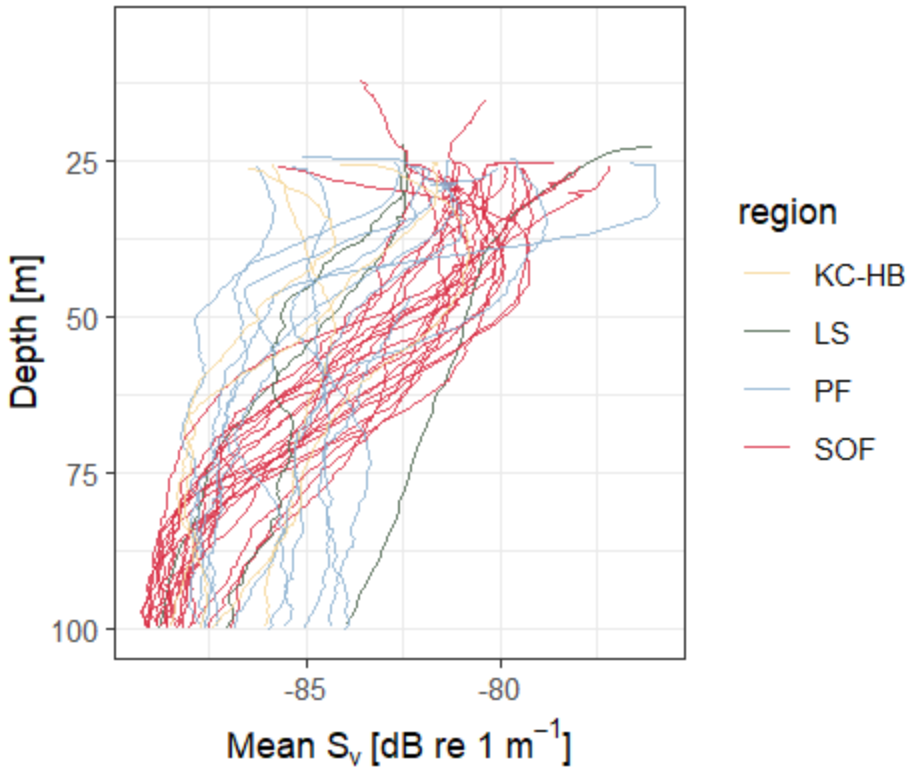
Supplementary Figure 3. De-noised and filtered broadband acoustic profiles from all sampling stations.

Chapter 5.   Conclusion – Overview, Synthesis, and Future Directions

5.1 Overview

In the waters between Canada and Greenland's Arctic, species distributions and seasonal distribution dynamics are poorly resolved. As the Arctic warms rapidly due to Anthropogenic climate change, shifting conditions present an even greater challenge to establishing ecosystem baselines. Typically, the conditions observed in the Arctic represent mere snapshots of the ecosystem; in ice-covered seas, comprehensive monitoring programs typically employed in lower latitudes are often unfeasible. Thus, innovative methodologies are needed to improve our understanding of ecological states and dynamics in Arctic seas. Fisheries research employs a broad range of multi-disciplinary tools. Among them, hydroacoustics is a powerful tool that enables both broad (e.g., stock distribution) and fine-scale (e.g., individuals) measurements of fish and their prey across space and time. The aim of this thesis is to integrate hydroacoustics with oceanography, data science, and biology to gain a better and more comprehensive understanding of pelagic fish and zooplankton distribution patterns.

In each chapter of this thesis, I applied an innovative hydroacoustic approach to better understand the distributional patterns of small sound scattering organisms, such as lanternfish and their zooplankton prey. I explored how environmental factors like temperature, light, and stratification influence the distribution of pelagic organisms. Furthermore, this thesis advances methodological approaches in broadband acoustics, including deep-sea profiling and improved precision in target measurements. Overall, this thesis lays the groundwork for an improved understanding of the potential sensitivities of the deep-sea Arctic ecosystems to future environmental change.

5.2 Chapter Summaries & Future Directions

Chapter 2 addresses one of the challenges in using broadband acoustic target measurements in the mesopelagic zone: how to get precise hydroacoustic measurements of individual organisms within a sound-scattering layer. In this chapter, we learned that a variety of physical and biological processes in high density scattering layers can create anomalous signals in the data. We found these anomalous signals can skew estimates when calculating mean target strengths of a distinct volume of scatterers. Using an informed machine learning approach, we automatically detected outliers, thereby filtering out anomalous, signals in the data. Our results were then used to document the vertical distribution patterns of lanternfish in the Labrador Sea and demonstrated the improvement to the precision of our target strength and density measurements. By doing so, we avoided an up to 25% bias in density estimation and laid the groundwork for future automated approaches to broadband data processing. Such improvements in density estimation will be critical in management of future mesopelagic harvests.

Chapter 2 addressed arising challenges with the use of broadband acoustics in target measurement. We identified measurement errors associated with the signal processing of target data. Dealing with such errors adds additional steps in the already cumbersome signal processing pipeline. Our research demonstrates that unsupervised machine learning can facilitate more rapid analyses by automatically identifying anomalous, or erroneous signals in the data. Similar approaches can be applied to regional stock assessment surveys for forage species such as capelin, herring, and Arctic cod.

Recently, lowered acoustic devices (i.e., acoustic probes) have become more accessible and easier to operate. For instance, acoustic probes can be mounted to lowered instrument packages such as CTD rosettes. Our research demonstrates how to use echosounders or ADCPs mounted on a CTD-

Rosette to measure the vertical distribution of individual organisms at close range. Our precise methods to estimate target strength and density can now be used to investigate cross basin differences in mesopelagic abundances and their relationship to the major circulation patterns across ocean basins. Finally, our density estimates (up to 2.6 ind / 1000 m^3) in the DSL compare favorably with other studies (Dias Bernardes et al., 2020; Klevjer et al., 2020; Sameoto, 1989) and should be applied to global studies of the mesopelagic zone.

In Chapter 3 (Chawarski et al., 2022), I began by asking how far the deep-scattering layer (DSL) extends into the Canadian Arctic. During a 1200 km journey crossing from SW Greenland to Baffin Bay, I observed a stark boundary in the DSL as we crossed the Davis Strait. This finding initiated a research project to investigate what the potential drivers of such boundaries were and how they may manifest in the community and ecosystem structure of the deep ocean. In sharing these findings with my colleague Thor Klevjer at the Institute for Marine Research (IMR), I found that a similar boundary occurred in the Southern Ocean. In both locations, the boundary was associated with a drop in backscatter equating to approximately an order of magnitude reduction in acoustic biomass (S_v). We took these findings even further and found that this boundary was associated with a vertical dispersion of deeper organisms, mostly within the size ranges of mesozooplankton. We then compared data from mid-water trawl sampling on either side of the Davis Strait, both in Baffin Bay and the Labrador Sea, and found that the fish communities differed in their composition, representing distinct Atlantic (southern) and Arctic (northern) pelagic communities. The most important finding from this study was that these boundaries occurred directly along frontal zones, where deep water mass boundaries intersect.

Our results demonstrated that distinct mesopelagic communities are distinguished by water masses with different temperature signatures. When we compared these findings to the Southern Ocean,

we found similar patterns and a similar magnitude of backscatter reduction toward the South Pole. The boundaries in each hemisphere occurred at different latitudes, lending further support to the hypothesis that temperature, not just light, plays a role in regulating mesopelagic community structure at high latitudes. As a result, these community boundaries are likely sensitive to shifting ocean temperature regimes with climate change.

Chapter 3 contributed to the broader field of fisheries science by identifying two important and distinct biogeographic boundaries. Both the Davis Strait and the Polar Frontal Zone of the Southern Ocean are regions deserving more attention, both in the context of ongoing changes due to climate warming and as unique regions for understanding biological adaptations to oceanographic conditions. There are growing, publicly available datasets such as Myctobase (Woods et al., 2022), which contain trait information for dozens of mesopelagic species from 72 circumpolar cruises spanning 37 years. Such rich datasets could be used to address one of the ecological principles mentioned in the discussion of Chapter 3, known as Bergmann's rule. Bergmann's rule is defined as the geographic tendency within a clade of organisms for size to decrease as temperature increases or latitude decreases. Empirical evidence for this rule was found for mesopelagic fish species in the Scotia Sea (Saunders & Tarling, 2018), but could be more broadly applied to the entirety of the Southern Ocean with greater focus on other linked traits, such as trophic position or diel migration behavior. Furthermore, there is a general dearth of knowledge regarding the life-history of lanternfishes (Catul et al., 2011; St. John et al., 2016), therefore any studies investigating reproductive and ontogenetic environmental constraints could shed light on the physiological mechanisms that likely govern distributional patterns described in my thesis.

The work in Chapter 3 also contributes to our understanding of the vertical distribution of metazoan life through the bathypelagic zone. We demonstrated the utility of lowered acoustic

Doppler current profilers (LADCPs) to document relative changes in the distribution of backscatter across these boundaries, which we believe is linked to the efficiency of the biological carbon pump. This concept has sparked interesting research (Klevjer et al. in preparation), which addresses how the dispersion of deep-water organisms is related to global primary production patterns.

Chapter 4 was borne from a 2019 expedition to Ryder Glacier in NW Greenland (Jakobsson et al., 2020). The expedition goal was to characterize the biogeophysical conditions of Sherard Osborn fjord, an unmapped fjord on Greenland's northwest coast facing the Lincoln Sea. The data for this chapter were collected using methodologies developed during earlier cruises: we opted to mount an autonomous echosounder to the CTD-rosette alongside the Underwater Vision Profiler (UVP5). We developed a study to collect unbiased estimates of mesozooplankton distribution in the fjord to compare with the outlying regions. The UVP5 was used to identify and quantify zooplankton and detrital particles.

Following the analysis of both Petermann and Sherard Osborn fjord CTD data, we found highly contrasting oceanographic conditions present in each fjord (Stranne et al., 2021). We took this opportunity to refine our study to investigate the impact of stratification on marine snow production and copepod vertical distribution. We found that by taking a morphological approach to the particles captured by the UVP5, we were able to observe distinct differences in the size, shape, structure, and brightness of marine snow. Based on our findings, lower quantities of particles were associated with highly stratified waters, suggesting either low particle production, or high turnover or remineralization of carbon. Second, particle morphological features reflected difference in phytodetrital aggregates, which are an important food source for copepods. We found that low quantities of particles were also associated with low morphological diversity. These

conditions were reflected in a shift in the vertical distribution of copepods toward the surface, suggestive of a behavioral response to poorer feeding opportunities.

Chapter 4 contributed to the broader field of fisheries science as it provided a snapshot into the potential conditions facing Arctic production under climate warming. Glacial meltwater from the Greenland ice sheet is anticipated to increase water column stratification in coastal Arctic regions (Hopwood et al., 2020). Should vertical thermohaline gradients become strong enough to inhibit mixing of nutrients, phytoplankton blooms and their subsequent particle transport pathways will likely decrease in amplitude, impacting the overall productivity of marine systems (Hopwood et al., 2018). The shift in copepods towards surface waters documented in chapter 4 is an indicator of them entering sub-optimal habitat; exposure to high irradiance conditions increases their predation risk (Möller et al., 2020). In the short term this may benefit high trophic organisms such as small pelagic fish; however, suboptimal feeding conditions for copepods can often manifest as reduced fecundity with long term implications for overall production (Peterson & Bellantoni, 1987).

Chapter 4 also contributes to future research by demonstrating the application of combined optical-acoustical autonomous sampling. Through developing a morphological approach to the study of marine snow, the authors of Trudnowska et al. (2021) laid a solid groundwork for quantifying relationships between low-trophic organisms and the ocean's particle pump. Future studies on the biological pump should leverage a morphological approach to particles using the massive UVP5 collected image database that is available in EcoTaxa (Picheral et al., 2022). In general, comparisons between optical and hydroacoustic data would strengthen our understanding of the drivers of vertical distribution in the various pelagic zones of the ocean. As future sensor packages become miniaturized and autonomous, requiring less field effort or intervention, they can be

mounted to scalable low-power platforms such as Argo floats. Globally distributed data streams would provide invaluable data for modelling efforts to understand the impacts of climate change on ocean productivity.

5.3 Limitations

One of the weaknesses of these studies remains pervasive in the field of hydroacoustics - validation of acoustic signals is immensely challenging in the deep ocean. A general rule of thumb in hydroacoustics is that a 3 dB change in backscatter equates to a ten-fold change in the acoustic energy, or biomass (Simmonds & MacLennan, 2005). In a single species system, it can therefore be assumed that the standard measure of acoustic energy, S_v is correlated with biomass. Lanternfishes (family Myctophidae), which co-occur with diverse groups of mesopelagic fishes, can display cryptic backscattering properties, whereby the material properties of their swim-bladder can change from gas-filled to lipid-filled (Butler & Pearcy, 1972; Dornan et al., 2019). Because lipid-filled swim-bladders have a lower backscatter strength, this can impact biomass interpretations considerably. Furthermore, the particularly small swim-bladders in these fishes are at or near resonance with lower frequencies (Ariza et al., 2016; Godø et al., 2009; Scoulding et al., 2015). Therefore, resonance peaks along narrow low frequency bandwidths can amplify the S_v, or TS, creating the illusion of large targets or high biomass. Others have suggested that gelatinous plankton, which are typically under-sampled by trawl-netting, contribute to an unknown portion of the backscatter, creating considerable uncertainty in biomass estimates (Proud et al., 2018).

 There is a concerted and growing effort within the hydroacoustic community to account for all the complex scattering properties of species within the mesopelagic zone (Agersted et al., 2021; Cotter et al., 2021; Khodabandeloo et al., 2021). For these reasons, we avoided estimations of biomass in our work and instead focused on distributional patterns. Apart from the limitations of acoustic

instrumentation, there are inherent challenges to using net-collected sampling, particularly in the mesopelagic zone. Nets lowered to the mesopelagic zone collect samples during ascent and descent, making it difficult to interpret from which depth zones samples were captured. Also, individual organisms of different sizes and taxonomy display differential avoidance behavior (Kaartvedt et al., 2012), which can lead to biased sampling of the true population or community. Furthermore, gelatinous plankton is typically damaged by nets, creating a challenge to enumeration and identification. Finally, mesopelagic fish identification is challenging. For instance, morphological taxonomy of lanternfishes relies on photophore patterns which are often damaged during trawling. In some cases, identification may be enabled via genomic sequencing; however, such approaches are available to standardized fisheries surveys. Thus, net sampling provides a tool which enables spatial comparison of communities but should be cautiously interpreted, particularly regarding deep ocean communities. In each chapter, I provide a snapshot of the conditions at each sampling region, as they occurred during ideal summer sampling conditions. From our data, it is not clear how stable these conditions are across seasons or years.

Broadband acoustics has been touted as a promising tool for species discrimination based on the assumption that the frequency content of the returned signal contains clues about the anatomical features and sizes of organisms (Chu & Stanton, 1998; Ehrenberg & Torkelson, 2000). This premise has been the focus of several recent papers, showing promise in distinguishing co-occurring taxa (Agersted et al., 2021; Bassett et al., 2018, 2020; Cotter et al., 2021; Kubilius et al., 2020). However, these studies make use of relatively wide bandwidths, including multiple transducers. In our study, we used a relatively narrow bandwidth and a single 38 kHz transducer, which carries low discriminatory power. Therefore, in Chapter 3 we did not focus on distinguishing functional groups or taxa, but rather dealt with the nature of the measurements themselves.

In recent years, the working group on fisheries acoustic science and technology (WGFAST) has released several seminal cooperative reports sharing standardized techniques for acoustic methods such as calibrations and target measurements (Demer et al., 2015; Korneliussen et al., 2018). At the writing of this thesis, standardized procedures for the implementation of broadband methodologies are not clearly expressed in the literature. Furthermore, common software packages, such as Echoview ©, contain disclaimers that the applications of methods such as target detection remain 'Experimental.' As a result, the development of our research required several consultations with acoustic experts. Many of them agree that the implementation of broadband acoustics, from instrumentation to software, is still in the early stages of development. For example, methods such as echo-counting are confounded by frequency-dependent beam formation. The coming years will require broadband acoustic expert contributions in the form of instrumentation and software improvements, as well as improved efficiency of the signal processing pipeline.

When working in the fjords of northwest Greenland (Chapter 4), I collected data in a complex and challenging environment. Acoustic data collection typically works well in open water with few boundaries. Near the sea-ice and icebergs of Sherard Osborn fjord, we found that multipath scattering from ice keels created substantial sidelobe interference, which masked biological signals near water-ice or water-air boundaries. Signal processing techniques such as signal tapering (Lavery et al., 2017), or the use of narrower beamwidth or shaded transducers (Polonichko & Romeo, 2007) could facilitate the detection of organisms closer to such boundaries. Furthermore, marine-terminating glaciers are often associated with subglacial plumes carrying mineralogical suspended sediments (Hopwood et al., 2020; Stuart-Lee et al., 2023; Szeligowska et al., 2022). We found that these turbidity currents can create distinct scattering layers in our data. Future efforts to

quantify the suspended sediments through acoustic inversions could resolve differences between biological and physical backscatter where such currents occur. Another limitation of Chapter 4 was the limited scope of taxonomic resolution in our zooplankton dataset; we were unable to achieve detailed taxonomic and ontogenetic resolution on our samples. Doing so would have helped answer whether the conditions we observed during the Ryder 2019 Expedition (Chapter 4) led to not only a behavioral response in zooplankton, but also a shift in population dynamics under persistently stratified conditions. In persistent conditions, copepods would likely adapt the effort and timing of their reproduction to match the food availability (Cleary et al., 2017; Daase et al., 2013; Falk-Petersen et al., 2009).

5.4 Final Remarks

In this thesis, I have addressed knowledge gaps in how small polar and subpolar pelagic fish and zooplankton are horizontally and vertically distributed in Arctic ecosystems. I collected data during several icebreaker expeditions to the Arctic and applied innovative techniques to quantify patterns I observed in the data. I demonstrated that across large spatial scales, the mesopelagic zone is structured by water masses with distinct temperature signatures (Chapter 2). I developed methodology for improving the precision of target measurements in the mesopelagic zone (Chapter 3). I also found linkages between upper ocean mixing, marine snow production, and copepod distribution (Chapter 4). Each study contributed to a better understanding of pelagic ecosystems in two distinct biogeographic regions, the Labrador Sea and northwest Greenland.

5.5 References

Agersted, M. D., Khodabandeloo, B., Liu, Y., Melle, W., & Klevjer, T. A. (2021). Application of an unsupervised clustering algorithm on in situ broadband acoustic data to identify different mesopelagic target types. *ICES Journal of Marine Science*, *78*(8), 2907–2921. https://doi.org/10.1093/icesjms/fsab167

Ariza, A., Landeira, J. M., Escánez, A., Wienerroither, R., Aguilar de Soto, N., Røstad, A., Kaartvedt, S., & Hernández-León, S. (2016). Vertical distribution, composition and migratory patterns of acoustic scattering layers in the Canary Islands. *Journal of Marine Systems*, *157*, 82–91. https://doi.org/10.1016/j.jmarsys.2016.01.004

Bassett, C., De Robertis, A., & Wilson, C. D. (2018). Broadband echosounder measurements of the frequency response of fishes and euphausiids in the Gulf of Alaska. *ICES Journal of Marine Science*, *75*(3), 1131–1142. https://doi.org/10.1093/icesjms/fsx204

Bassett, C., Lavery, A. C., Stanton, T. K., & Cotter, E. D. (2020). Frequency- and depth-dependent target strength measurements of individual mesopelagic scatterers. *The Journal of the Acoustical Society of America*, *148*(2), EL153–EL158. https://doi.org/10.1121/10.0001745

Butler, J. L., & Pearcy, W. G. (1972). Swimbladder Morphology and Specific Gravity of Myctophids off Oregon. *Journal of the Fisheries Research Board of Canada*, *29*(8), 1145–1150. https://doi.org/10.1139/f72-170

Catul, V., Gauns, M., & Karuppasamy, P. K. (2011). A review on mesopelagic fishes belonging to family Myctophidae. *Reviews in Fish Biology and Fisheries*, *21*(3), 339–354. https://doi.org/10.1007/s11160-010-9176-4

Chawarski, J., Klevjer, T. A., Coté, D., & Geoffroy, M. (2022). Evidence of temperature control on mesopelagic fish and zooplankton communities at high latitudes. *Frontiers in Marine Science*, *9*. https://doi.org/10.3389/fmars.2022.917985

Chu, D., & Stanton, T. K. (1998). Application of pulse compression techniques to broadband acoustic scattering by live individual zooplankton. *Journal of the Acoustical Society of America*, *104*, 39–55.

Cleary, A. C., Søreide, J. E., Freese, D., Niehoff, B., & Gabrielsen, T. M. (2017). Feeding by Calanus glacialis in a high arctic fjord: potential seasonal importance of alternative prey. *ICES Journal of Marine Science*, *74*(7), 1937–1946. https://doi.org/10.1093/icesjms/fsx106

Cotter, E., Bassett, C., & Lavery, A. (2021). Classification of broadband target spectra in the mesopelagic using physics-informed machine learning. *The Journal of the Acoustical Society of America*, *149*(6), 3889–3901. https://doi.org/10.1121/10.0005114

Daase, M., Falk-Petersen, S., Varpe, Ø., Darnis, G., Søreide, J. E., Wold, A., Leu, E., Berge, J., Philippe, B., & Fortier, L. (2013). Timing of reproductive events in the marine copepod Calanus glacialis: A pan-Arctic perspective. *Canadian Journal of Fisheries and Aquatic Sciences*, *70*(6), 871–884. https://doi.org/10.1139/cjfas-2012-0401

Demer, D. A., Berger, L., Bernasconi, M., Bethke, E., Boswell, K. M., Chu, D., Domokos, R., Dunford, A., Fassler, S., Gauthier, S., Hufnagle, L. T., Jech, J. M., Bouffant, N., Lebourges-Dhaussy, A., Lurton, X., Macaulay, G. J., Perrot, Y., Ryan, T., Parker-Stetter, S., … Williamson, N. (2015). Calibration of acoustic instruments. In *ICES Cooperative Research Report* (Vol. 326, Issue 32, pp. 1–133). https://doi.org/http://dx.doi.org/10.25607/OBP-185

Dias Bernardes, I., Ona, E., & Gjøsæter, H. (2020). Study of the Arctic mesopelagic layer with vessel and profiling multifrequency acoustics. *Progress in Oceanography*, *182*(January). https://doi.org/10.1016/j.pocean.2019.102260

Dornan, T., Fielding, S., Saunders, R. A., & Genner, M. J. (2019). Swimbladder morphology masks Southern Ocean mesopelagic fish biomass. *Proceedings of the Royal Society B: Biological Sciences*, *286*(1903), 1–8. https://doi.org/10.1098/rspb.2019.0353

Ehrenberg, J. E., & Torkelson, T. C. (2000). FM slide (chirp) signals: a technique for significantly improving the signal-to-noise performance in hydroacoustic assessment systems. *Fisheries Research*, *47*(2), 193–199. https://doi.org/https://doi.org/10.1016/S0165-7836(00)00169-7

Falk-Petersen, S., Mayzaud, P., Kattner, G., & Sargent, J. R. (2009). Lipids and life strategy of Arctic Calanus. *Marine Biology Research*, *5*(1), 18–39. https://doi.org/10.1080/17451000802512267

Godø, O. R., Patel, R., & Pedersen, G. (2009). Diel migration and swimbladder resonance of small fish: Some implications for analyses of multifrequency echo data. *ICES Journal of Marine Science*, *66*(6), 1143–1148. https://doi.org/10.1093/icesjms/fsp098

Hopwood, M. J., Carroll, D., Browning, T. J., Meire, L., Mortensen, J., Krisch, S., & Achterberg, E. P. (2018). Non-linear response of summertime marine productivity to increased meltwater discharge around Greenland. *Nature Communications*, *9*(1). https://doi.org/10.1038/s41467-018-05488-8

Hopwood, M. J., Carroll, D., Dunse, T., Hodson, A., Holding, J. M., Iriarte, J. L., Ribeiro, S., Achterberg, E. P., Cantoni, C., Carlson, D. F., Chierici, M., Clarke, J. S., Cozzi, S., Fransson, A., Juul-Pedersen, T., Winding, M. H. S., & Meire, L. (2020). Review article: How does glacier discharge affect marine biogeochemistry and primary production in the Arctic? *Cryosphere*, *14*(4), 1347–1383. https://doi.org/10.5194/tc-14-1347-2020

Jakobsson, M., Mayer, L. A., Farrell, J. F., & Ryder 2019 Scientific Party. (2020). *Expedition report: SWEDARCTIC Ryder 2019*.

Kaartvedt, S., Staby, A., & Aksnes, D. L. (2012). Efficient trawl avoidance by mesopelagic fishes causes large underestimation of their biomass. *Marine Ecology Progress Series*, *456*, 1–6. https://doi.org/10.3354/meps09785

Khodabandeloo, B., Agersted, M. D., Klevjer, T. A., Pedersen, G., & Melle, W. (2021). Mesopelagic flesh shear viscosity estimation from in situ broadband backscattering measurements by a viscous–elastic model inversion. *ICES Journal of Marine Science*, *78*(9), 3147–3161. https://doi.org/10.1093/icesjms/fsab183

Klevjer, T. A., Melle, W., Knutsen, T., & Aksnes, D. L. (2020). Vertical distribution and migration of mesopelagic scatterers in four north Atlantic basins. *Deep Sea Research Part II: Topical Studies in Oceanography*, *180*(104811), 1–11. https://doi.org/10.1016/j.dsr2.2020.104811

Korneliussen, R. J., Berger, L., Campanella, F., Chu, D., Demer, D., Fielding, S., Fassler, S., Gauthier, S., Hutton, B., Iriarte, F., Jech, J. M., Kloser, R., Lawson, G. L., Lebourges-

Dhaussy, A., McQuinn, I., Pena, M., Scoulding, B., Sakinan, S., Schaber, M., … Thompson, C. H. (2018). Acoustic target classification. In *ICES Cooperative Research Report, No. 344*. https://doi.org/http://doi.org/10.17895/ices.pub.4567

Kubilius, R., Macaulay, G. J., & Ona, E. (2020). Remote sizing of fish-like targets using broadband acoustics. *Fisheries Research*, *228*(April). https://doi.org/10.1016/j.fishres.2020.105568

Lavery, A. C., Bassett, C., Lawson, G. L., & Jech, J. M. (2017). Exploiting signal processing approaches for Broadband echosounders. *ICES Journal of Marine Science*, *74*(8), 2262–2275. https://doi.org/10.1093/icesjms/fsx155

Möller, K. O. V. E., John, M. S. T., Temming, A., Diekmann, R., Peters, J., & Floeter, J. (2020). *Predation risk triggers copepod small-scale behavior in the Baltic Sea*. *044*, 1–12. https://doi.org/10.1093/plankt/fbaa044

Peterson, W. T., & Bellantoni, D. C. (1987). Relationships between water-column stratification, phytoplankton cell size and copepod fecundity in Long Island Sound and off central Chile. *South African Journal of Marine Science*, *5*(1), 411–421. https://doi.org/10.2989/025776187784522748

Picheral, M., Colin, S., & Irisson, J.-O. (2022). *EcoTaxa, a tool for the taxonomic classification of images*. http://ecotaxa.obs-vlfr.fr

Polonichko, V., & Romeo, J. (2007). *Effects of transducer geometry and beam spreading on acoustic Doppler velocity measurements near boundaries*. https://doi.org/10.1109/OCEANS.2007.4449128

Proud, R., Handegard, N. O., Kloser, R. J., Cox, M. J., & Brierley, A. S. (2018). From siphonophores to deep scattering layers: uncertainty ranges for the estimation of global mesopelagic fish biomass. *ICES Journal of Marine Science*. https://doi.org/10.1093/icesjms/fsy037

Sameoto, D. (1989). Feeding Ecology of the Lantern Fish Benthosema Glaciale in a Subarctic Region. *Polar Biology*, *9*(9), 167–178. https://doi.org/10.1007/BF00297172

Saunders, R. A., & Tarling, G. A. (2018). Southern Ocean mesopelagic fish comply with Bergmann's rule. *American Naturalist*, *191*(3), 343–351. https://doi.org/10.1086/695767

Scoulding, B., Chu, D., Ona, E., & Fernandes, Paul. G. (2015). Target strengths of two abundant mesopelagic fish species. *The Journal of the Acoustical Society of America*, *137*(2), 989–1000. https://doi.org/10.1121/1.4906177

Simmonds, E. J., & MacLennan, D. N. (2005). *Fisheries acoustics, 2nd edition*. Chapman and Hall.

St. John, M. A., Borja, A., Chust, G., Heath, M., Grigorov, I., Mariani, P., Martin, A. P., & Santos, R. S. (2016). A dark hole in our understanding of marine ecosystems and their services: Perspectives from the mesopelagic community. *Frontiers in Marine Science*, *3*(MAR), 1–6. https://doi.org/10.3389/fmars.2016.00031

Stranne, C., Nilsson, J., Ulfsbo, A., O'Regan, M., Coxall, H. K., Meire, L., Muchowski, J., Mayer, L. A., Brüchert, V., Fredriksson, J., Thornton, B., Chawarski, J., West, G., Weidner, E., & Jakobsson, M. (2021). The climate sensitivity of northern Greenland fjords is amplified through sea-ice damming. *Communications Earth & Environment*, *2*(1), 4–11. https://doi.org/10.1038/s43247-021-00140-8

Stuart-Lee, A., Mortensen, J., Juul-Pedersen, T., Middelburg, J., Soetaert, K., Hopwood, M., Engel, A., & Meire, L. (2023). Influence of glacier type on bloom phenology in two Southwest Greenland fjords. *Estuarine, Coastal and Shelf Science*, 108271. https://doi.org/10.1016/j.ecss.2023.108271

Szeligowska, M., Trudnowska, E., Boehnke, R., & Błachowiak-Samołyk, K. (2022). Dark plumes of glacial meltwater affect vertical distribution of zooplankton in the Arctic. *Scientific Reports*, *12*(1), 17953. https://doi.org/10.1038/s41598-022-22475-8

Trudnowska, E., Lacour, L., Ardyna, M., Rogge, A., Irisson, J. O., Waite, A. M., Babin, M., & Stemmann, L. (2021). Marine snow morphology illuminates the evolution of phytoplankton blooms and determines their subsequent vertical export. *Nature Communications*, *12*(1), 1–13. https://doi.org/10.1038/s41467-021-22994-4

Woods, B., Trebilco, R., Walters, A., Hindell, M., Duhamel, G., Flores, H., Moteki, M., Pruvost, P., Reiss, C., Saunders, R. A., Sutton, C., Gan, Y.-M., & Van de Putte, A. (2022). Myctobase, a circumpolar database of mesopelagic fishes for new insights into deep pelagic prey fields. *Scientific Data*, *9*(1), 404. https://doi.org/10.1038/s41597-022-01496-y